An Introduction to the Mechanics of Tensegrity Structures

TO APPEAR IN 2001 AS A BOOK CHAPTER IN HANDBOOK ON MECHANICAL SYSTEMS DESIGN:
TO ORDER CONTACT: Nora Konopka Acquisitions Editor, Electrical Engineering CRC Press LLC 2000 Corporate Blvd. NW Boca Raton, FL 33431 561-998-2531 (phone) 561-997-7249 (fax) nkonopka@crcpress.com

Robert E. Skelton [1]
bobskelton@ucsd.edu

J. William Helton [2]
helton@math.ucsd.edu

Rajesh Adhikari [1]
rajesh.Adhikari@sdrc.com

Jean-Paul Pinaud [1]
jpinaud@mae.ucsd.edu

Waileung Chan [1]
waileung@mae.ucsd.edu

April 19, 2001

[1]Mechanical and Aerospace Engineering Department
Structural Systems and Control Lab
University of California San Diego, La Jolla, CA 92093-0411, USA.
[2]Department of Mathematics
University of California San Diego, LA Jolla, CA 92093-0112, USA.

Table of Contents

List of Figures

Abstract

Tensegrity structures consist of strings (in tension) and bars (in compression). Strings are strong, light, and foldable, so tensegrity structures have the potential to be light but strong and deployable. Pulleys, NiTi wire, or other actuators to selectively tighten some strings on a tensegrity structure can be used to control its shape. This article describes some principles we have found to be true in a detailed study of mathematical models of several tensegrity structures. We describe properties of these structures which appear to have a good chance of holding quite generally. We describe how pretensing all strings of a tensegrity makes its shape robust to various loading forces. Another property (proven analytically) asserts that the shape of a tensegrity structure can be changed substantially with little change in the potential energy of the structure. Thus shape control should be inexpensive. This is in contrast to the control of classical structures which require substantial energy to change their shape. A different aspect of the article is presentation of several tensegrities which are light but extremely strong. The concept of self-similar structures is used to find minimal mass subject to a specified buckling constraint. The stiffness and strength of these structures is determined.

Chapter 1

Introduction

Tensegrity structures are built of bars and strings attached to the ends of the bars. The bars can resist compressive force and the strings cannot. Most bar-string configurations which one might conceive are not in equilibrium, and if actually constructed will collapse to a different shape. Only bar-string configurations in a stable equilibrium will be called **tensegrity structures**.

If well designed, the application of forces to a tensegrity structure will deform it into a slightly different shape in a way which supports the applied forces. Tensegrity structures are very special cases of trusses, where members are assigned special functions. Some members are always in tension and others are always in compression. We will adopt the words "strings" for the tensile members, and "bars" for compressive members. (The difference between the choice of words to describe the tensile members "strings", "tendons" or "cables" is a choice motivated only by the scale of applications.) A tensegrity structure's bars cannot be attached to each other through joints that impart torques. The end of a bar can be attached to strings or ball jointed to other bars.

The artist Kenneth Snelson [1] built the first tensegrity structure and his artwork was the inspiration for the first author's interest in tensegrity. Buck-

minster Fuller [2] coined the word tensegrity from two words, tension and integrity.

Fig. 1.1: Snelson's Tensegrity Structure

1.1 The Benefits of Tensegrity

There exists a large literature on the geometry, artform, and architectural appeal of tensegrity structures, but there exists little on the dynamics and mechanics of these structures [2–19]. Form-finding results appear in [10, 20–24] for simple symmetric structures, and [14] shows an array of stable tensegrity units connected to yield a large stable system, which can be deployable. Tensegrity structures for civil engineering purposes have been built and described in [25–27]. Several reasons are given below why tensegrity structures should receive new attention from mathematicians and engineers, even though the concepts are fifty years old.

Tension Stabilizes:
A compressive member looses stiffness as it is loaded, whereas a tensile member gains stiffness as it is loaded. Stiffness is lost in two ways in a compressive

member. In the absence of any bending moments in the axially-loaded members, the forces act exactly through the mass center, the material spreads, increasing the diameter of the center cross section, whereas the tensile member reduces its cross section under load. In the presence of bending moments due to offsets in the line of force application and the center of mass, the bar becomes softer due to the bending motion. For most materials, the tensile strength of a longitudinal member is larger than its buckling (compressive) strength. (obviously, sand, masonary, and unreinforced concrete are exceptions to this rule). Hence a large stiffness to mass ratio can be achieved by increasing the use of tensile members. This notion will be made more precise in the sequel.

Tensegrity Structures are Efficient:
It has been known since the middle of the 20th century that continua cannot explain the strength of materials. The geometry of the material layout is critical to strength at all scales, from nanoscale biological systems to megascale civil structures. Traditionally, man has conceived and built structures in rectilinear fashion. Civil structures tend to be made with orthogonal beams, plates and columns. Orthogonal members are also used in aircraft wings with longerons and spars. However, evidence suggests that this "orthogonal" architecture does not usually yield the minimal mass design for a given set of stiffness properties [28]. Bendsoe and Kikuchi [29], Jarre [30], and others have shown that the optimal distribution of mass for specific stiffness objectives tends to be neither a solid mass of material with a fixed external geometry, nor material laid out in orthogonal components. Material is needed only in the essential load paths, not the orthogonal paths of traditional man-made structures. *Tensegrity structures* use longitudinal members arranged in very unusual (and non–orthogonal) patterns to achieve strength with small mass. Another way in which tensegrity systems become mass-efficient is with self-similar constructions replacing one tensegrity member by yet another tensegrity structure.

Tensegrity Structures are Deployable:
Materials of high strength tend to have very limited displacement capability. Piezoelectric materials are capable of only small displacement and "smart"

structures using such sensors and actuators have only small displacement capability. Since the compressive members of tensegrity structures are either disjoint, or connected with ball joints, large displacement, deployability and stowage in a compact volume will be immediate virtues of tensegrity structures [8, 11]. This feature offers operational and portability advantages. A portable bridge, or a power transmission tower made as a tensegrity structure could be manufactured in the factory, stowed on a truck or helicopter in a small volume, transported to the construction site, and deployed using only winches for erection through cable tension. Erectable temporary shelters could be manufactured, transported and deployed in a similar manner. Deployable structures in space (complex mechanical structures combined with active control technology) can save launch costs by reducing the mass required, or by eliminating the requirement for assembly by man.

Tensegrity Structures are Easily Tunable:
The same deployment technique can also make small adjustments for fine tuning of the loaded structures, or adjustment of a damaged structure. Structures that are designed to allow tuning will be an important feature of next generation mechanical structures, including civil engineering structures.

Tensegrity Structures Can be More Reliably Modeled:
All members of a tensegrity structure are axially loaded. Perhaps the most promising scientific feature of tensegrity structures is that while the *global* structure bends with external static loads, none of the *individual* members of the tensegrity structure experience bending moments. (In this report, we design all compressive members to experience loads well below their Euler buckling loads.) Generally, members that experience deformation in two or three dimensions are much harder to model than members that experience deformation in only one dimension. The Euler buckling load of a compressive member is from a bending instability calculation, and it is known in practice to be very unreliable. That is, the actual buckling load measured from the test data has a larger variation and is not as predictable as the tensile strength. Hence, increased use of tensile members is expected to yield more robust models and more efficient structures. More reliable models can be expected for axially loaded members compared to models for members in

bending [31].

Tensegrity Structures Facilitate High Precision Control:
Structures that can be more precisely modeled can be more preciously controlled. Hence, tensegrity structures might open the door to quantum leaps in the precision of controlled structures. The architecture (geometry) dictates the mathematical properties and hence these mathematical results easily scale to both large and small scales, from the nanoscale to the megascale, from applications in microsurgery to antennas, to aircraft wings, to robotic manipulators.

Tensegrity is a Paradigm that Promotes the Integration of Structure and Control Disciplines:
A given tensile or compressive member of a tensegrity structure can serve multiple functions. It can simultaneously be a load-carrying member of the structure, a sensor (measuring tension or length), an actuator (such as nickel-titanium wire), thermal insulator, or electrical conductor. In other words, by proper choice of *materials and geometry*, a grand challenge awaits the tensegrity designer: How to control the electrical, thermal, and mechanical energy in a material or structure? For example, smart tensegrity wings could use shape control to maneuver the aircraft or to optimize the air foil as a function of flight condition, without the use of hinged surfaces. Tensegrity structures provide a promising paradigm for integrating structure and control design.

Tensegrity Structures are Motivated from Biology:
Figure 1.2 shows a rendition of spider fiber, where amino acids of two types have formed hard β–pleated sheets that can take compression, and thin strands that take tension [32, 33]. The β–pleated sheets are discontinuous and the tension members form a continuous network. Hence, the nanostructure of the spider fiber is a Tensegrity Structure. Nature's endorsement of tensegrity structures warrants our attention because per unit mass, the spider fiber is the strongest natural fiber.

A recent article by Ingber [7, 34, 35] argues that tensegrity is the fundamental building architecture of life. His observations come from experiments in

cell biology, where prestressed truss structures of the tensegrity type have been observed in cells. It is encouraging to see the similarities in structural building blocks over a wide range of scales. If tensegrity is nature's preferred building architecture, modern analytical and computational capabilities of tensegrity could make the same incredible efficiency possessed by natural systems transferrable to man-made systems, from the nano- to the megascale. This is a grand design challenge, to develop scientific procedures to create smart tensegrity structures that can regulate the flow of thermal, mechanical, and electrical energy in a material system by proper choice of materials, geometry, and controls. This report contributes to this cause by exploring the mechanical properties of simple tensegrity structures.

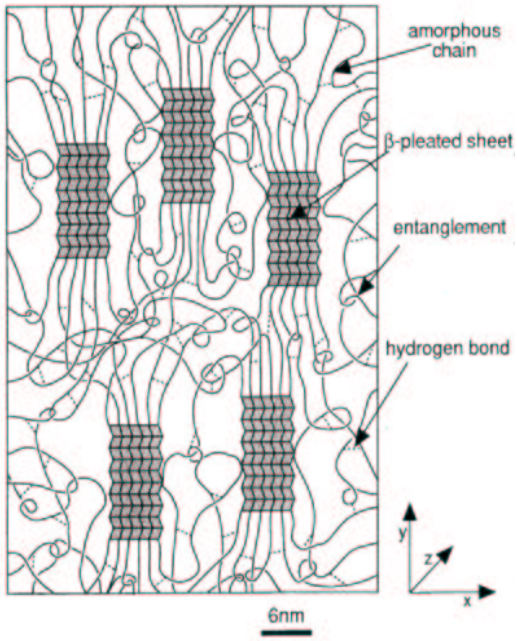

Fig. 1.2: Structure of the Spider Fiber.

The remainder of the introduction describes the main results of this paper. We start with formal definitions and then turn to results.

1.2 Definitions and Examples

This is an introduction to the mechanics of a class of prestressed structural systems that are composed only of axially-loaded members. We need a couple of definitions to describe tensegrity scientifically.

Definition 1 *We say that the geometry of a material system is in a* stable *equilibrium if all particles in the material system return to this geometry, as time goes to infinity, starting from any initial position arbitrarily close to this geometry.*

In general, a variety of boundary conditions may be imposed, to distinguish, for example, between bridges and space structures. But, for the purposes of this paper we characterize only the material system with free-free boundary conditions, as for a space structure. We will herein characterize the bars as rigid bodies and the strings as one-dimensional elastic bodies. Hence, a material system is in equilibrium if the nodal points of the bars in the system are in equilibrium.

Definition 2 *A* Class k Tensegrity Structure *is a stable equilibrium of axially-loaded elements, with a maximum of k compressive members connected at the node(s).*

Fact 1 Class k Tensegrity Structures *must have tension members.*

Fact 1 follows from the requirement to have a stable equilibrium.

Fact 2 *Kenneth Snelson's structures of which Fig. 1.1 is an example are all* Class 1 Tensegrity Structures*, using Definition 1. Buckminster Fuller coined the word tensegrity to imply a connected set of tension members and a disconnected set of compression members. This fits our "Class 1" definition.*

A *Class 1 Tensegrity Structure* has a connected network of members in tension, while the network of compressive members is disconnected. To illustrate these various definitions, Fig. 1.3(a) illustrates the simplest tensegrity structure, composed of one bar and one string in tension. Thin lines are strings and shaded bars are compressive members. Figure 1.3(b) describes the next simplest arrangement, with two bars. Figure 1.3(c) is a Class 2 Tensegrity Structure because 2 bars are connected at the nodes. Figure 1.3(c) represents a Class 2 Tensegrity in the plane. However, as a three-dimensional structure, it is not a tensegrity structure because the equilibrium is unstable (the tensegrity definition requires a stable equilibrium).

From these definitions, the existence of a tensegrity structure having a specified geometry reduces to the question of whether there exist finite tensions that can be applied to the tensile members to hold the system in that geometry, in a stable equilibrium.

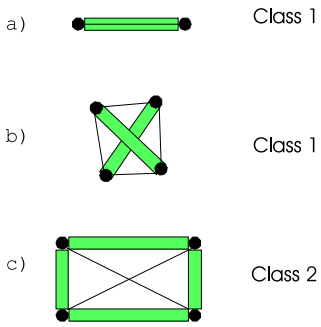

Fig. 1.3: Tensegrity Stuctures.

We have illustrated that the geometry of the nodal points, and the connections cannot be arbitrarily specified. The role that geometry plays in the mechanical properties of tensegrity structures is the focus of this paper.

The planar tensegrity examples that will be shown follow a naming convention that describes the number of compressive members and tension members. The number of compressive members is associated with the letter C, while the number of tensile members is associated with T. For example, a structure

that contains 2 compressive members and four tension members is called a C2T4 tensegrity.

1.3 The Structures Analyzed in this Paper

The basic examples we analyzed are the structures shown in Fig. 1.4, where thin lines are the strings and the thick lines are bars. Also we analyzed various structures built from these basic structural units. Each structure was analyzed under several types of loading. In particular, the top and bottom loads indicated on the C2T4 structure point in opposite directions, thereby resulting in bending. We also analyzed a C2T4 structure with top and bottom loads pointing the same direction, that is, a compressive situation. The $C4T2$ structure of Fig. 1.4(b) reduces to a $C4T1$ structure when the horizontal string is absent. The mass and stiffness properties of such structures will be of interest under compressive loads, F, as shown. The 3-bar SVD was studied under two types of loading, axial and lateral. Axial loading is compressive while lateral loading results in bending.

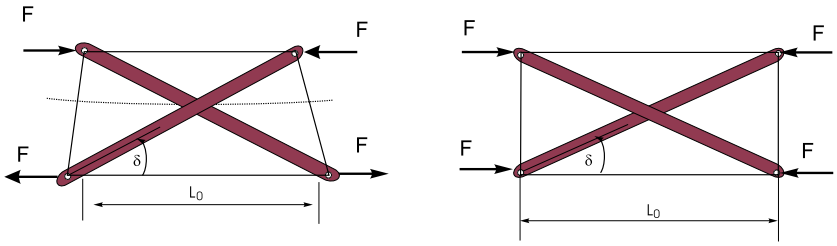

(a) C2T4 bending loads (left) and compressive loads (right)

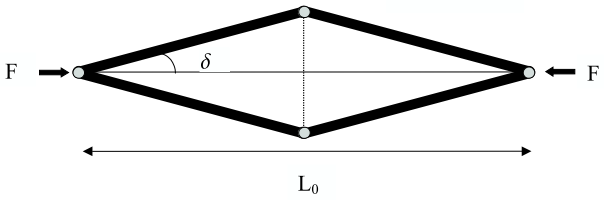

(b) C4T2

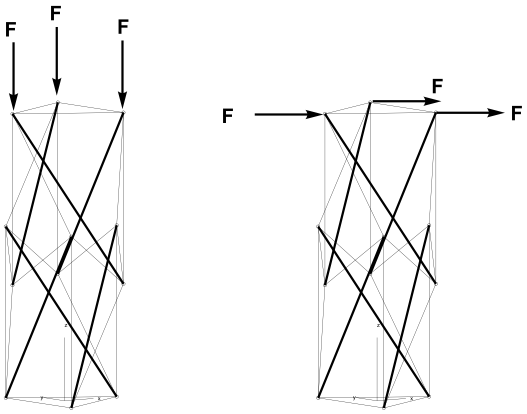

(c) 3-bar SVD - axial loads (left) and lateral loads (right)

Fig. 1.4: Tensegrities studied in this paper(Not to scale).

1.4 Main Results on Tensegrity Stiffness

A reasonable test of any tensegrity structure is to apply several forces each of magnitude F at several places and plot how some measure of its shape changes. We call the plot of $\frac{dF}{dshape}$ versus F a stiffness profile of the structure. The paper analyzes stiffness profiles of a variety of tensegrity structures. We paid special attention to the role of pretension set in the strings of the tensegrity. While we have not done an exhaustive study there are properties common to these examples which we now describe. How well these properties extend to all tensegrity structures remains to be seen. However, laying out the principles here is an essential first step to discovering those universal properties which do exist.

The following example with masses and springs prepare us for two basic principles which we have observed in the tensegrity paradigm.

1.4.1 Basic Principle 1: Robustness from Pretension

As a parable to illustrate this phenonmenon we resort to the simple example of a mass attached to two bungy cords. See Fig. 1.5.

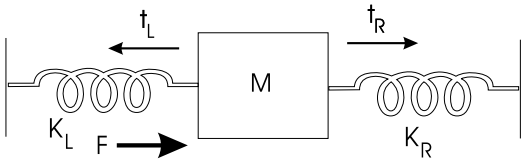

Fig. 1.5: Mass-Spring System

Here K_L, K_R are the spring constants, F is an external force pushing right on the mass, and t_L, t_R are tensions in the bungy cords when $F = 0$. The bungy cords have the property that when they are shorter than their rest length they become inactive. If we set any positive *pretensions* t_L, t_R, there is a corresponding equilibrium configuration and we shall be concerned with

how the shape of this configuration changes as force F is applied. Shape is a peculiar word to use here when we mean position of the mass, but it forshadows discussions about very general tensegrity structures. The effect of the stiffness of the structure is seen in Fig. 1.6.

There are two key quantities in this graph which we see repeatedly in tensegrity structures. The first is the critical value F_1 where the stiffness drops. It is easy to see that F_1 equals the value of F at which the right cord goes slack. Thus F_1 increases with the pretension in the right cord.

The second key parameter in this figure is the size of the jump as measured by the ratio

$$r := \frac{S_{\text{tens}}}{S_{\text{slack}}}.$$

When $r = 1$, the stiffness plot is a straight horizontal line with no discontinuity. Therefore the amount of pretension, affects the value of F_1, but has no influence on the stiffness. One can also notice that increasing the value of r increases the size of the jump. What determines the size of r is just the ratio κ of the spring constants $\kappa := \frac{K_R}{K_L}$, since $r = 1 + \kappa$, indeed

$$r \text{ is an increasing function of } \kappa$$

$$r \not\cong \infty \quad \text{if} \quad \kappa \cong \infty.$$

Of course pretension is impossible if $K_R = 0$. Pretension increases F_1 and hence allows us to stay in the high stiffness regime given by S_{tens}, over a larger range of applied external force F.

1.4.2 The Robustness from Pretension Principle for Tensegrity Structures

Pretension is known in the structures community as a method of increasing the load bearing capacity of a structure through the use of strings that are

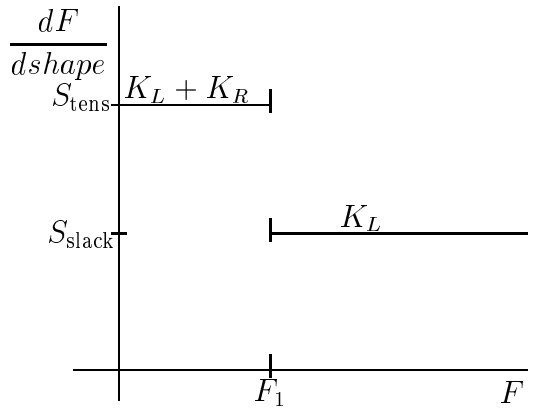

Fig. 1.6: Mass-Spring System Stiffness Profile

stretched to a desired tension. This allows for the structure to support greater loads without as much deflection as compared to a structure without any pretension.

For a tensegrity structure, the role of pretension is monumental. For example, in the analysis of the planar tensegrity structure, the slackening of a string results in dramatic nonlinear changes in the bending rigidity. Increasing the pretension allows for greater bending loads to be carried by the structure while still exhibiting near constant bending rigidity. In other words, the slackening of a string occurs for a larger external load. We can loosely describe this as a *robustness* property, in that the structure can be designed with a certain pretension to accomodate uncertainties in the loading (bending) environment. Not only does pretension have consequence for these mechanical properties, but also for the so-called prestressable problem, which is left for the statics problem. The prestressable problem involves finding a geometry which can sustain its shape without external forces applied and with all strings in tension [12, 20].

Tensegrity Structures in Bending

What we find is that bending stiffness profiles for all examples we study have levels S_{tens} when all strings are in tension, S_{slack_1} when one string is slack and then other levels as other strings go slack or as strong forces push the structure into radically different shapes, see Fig. 1.7. These very high force regimes can be very complicated and so we do not analyze them. Loose motivation for the form of a bending stiffness profile curve was given in the mass and two bungy cord example, in which case we had two stiffness levels.

One can imagine a more complicated tensegrity geometry that will possibly yield many stiffness levels. This intuition arises from the possibility that multiple strings can become slack depending on the directions and magnitudes of the loading environment. One hypothetical situation is shown in Fig. 1.7 where three levels are obtained. All tensegrity examples in the paper have bending stiffness profiles of this form, at least until the force F radically distorts the figure. The specific profile is heavily influenced by geometry of the tensegrity structure as well as of the stiffness of the strings, K_{string}, and bars, K_{bar}. In particular, the ratio

$$K := \frac{K_{\text{string}}}{K_{\text{bar}}}$$

is an informative parameter.

General Properties common to our bending examples are:

I. When no string is slack, the geometry of a tensegrity and the materials used have much more effect on its stiffness than the amount of pretension in its strings.

II. As long as all strings are in tension (that is, $F < F_1$) stiffness has little dependence on F or on the amount of pretension in the strings.

III. A larger pretension in the strings produces a larger F_1.

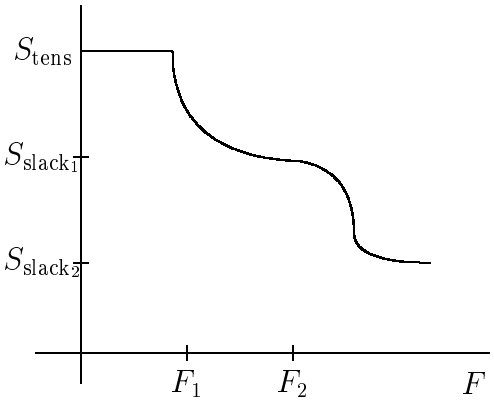

Fig. 1.7: Gedanken Stiffness Profile

IV. As F exceeds F_1 the stiffness quickly drops.

V. The ratio

$$r_1 := \frac{S_{\text{tens}}}{S_{\text{slack}}}$$

is an increasing function of K. Moreover, $r_1 \to \infty$ as $K \to \infty$ (if the bars are flabby the structure is flabby once a string goes slack). Similar parameters, r_2 can be defined for each change of stiffness.

examples in this paper which substantiate these principles are the stiffness profile of C2T4 under bending loads as shown in Fig. 2.2. Also, the "laterally loaded" 3-bar SVD tensegrity shows the same behavior with respect to the above principles, Figure 4.12 and Fig. 4.13.

Tensegrity Structures in Compression

For compressive loads, the relationships between stiffness, pretension and force do not always obey the simple Principles listed above. In fact, we see three qualitatively different stiffness profiles in our compression loading studies. We now summarize these three behavior patterns.

The C2T4 planar tensegrity exhibits the pretension robustness properties of Principles I, II, III, as shown in Fig. 1.6. The pretension tends to prevent slack strings.

The $C4T2$ structure has a stiffness profile of the form in Fig. 1.8. Only in the $C4T1$ and $C4T2$ examples does stiffness immediately start to fall as we begin to apply a load.

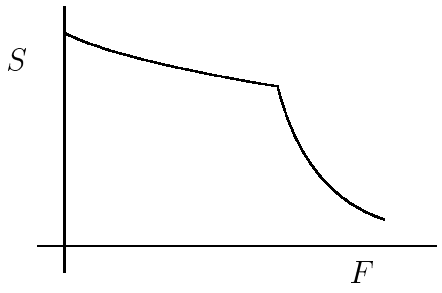

Fig. 1.8: Stiffness profile for $C4T2$ in compression

The axially loaded 3-bar-SVD, the stiffness profile even for small forces is seriously effected by the amount of pretension in the structure. Rather than stiffness being constant for $F < F_1$ as is the case with bending, we see in Fig. 4.9 that stiffness increases with F for small and moderate forces. The qualitative form of the stiffness profile is shown in Fig. 1.9. We have not systematically analyzed the role of the stiffness ratio K in compression situations.

Summary on Stiffness and Pretension

Now we summarize all situations we have seen except for the $C4T2$ compression situation.

> **When a load is applied to a tensegrity structure the stiffness is essentially constant as the loading force increases**

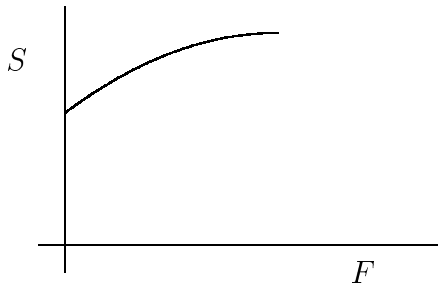

Fig. 1.9: Stiffness profile of 3-bar SVD in compression

unless a string goes slack.

1.5 Basic Principle 2: Changing Shape with Small Control Energy

We begin our discussion not with a tensegrity structure, but with an analogy. Imagine, as in Fig. 1.10, that the rigid boundary conditions of Fig. 1.5 become frictionless pulleys. Suppose we are able to actuate the pulleys and we wish to move the mass to the right, we can turn each pulley clockwise. The pretension can be large and yet very small control torques are needed to change the position of the nodal mass.

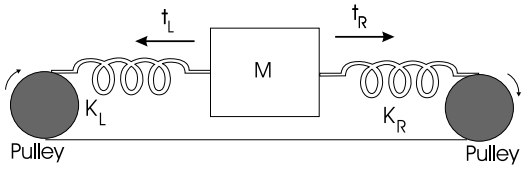

Fig. 1.10: Mass-Spring Control System

Tensegrity structures, even very complicated ones, can be actuated by placing pulleys at the nodes (ends of bars) and running the end of each string thru

a pulley. Thus we think of two pulleys being associated with each string and rotation of the pulleys can be used to shorten or loosen the string. The mass-spring example foreshadows the fact that even *in tensegrity structures, shape changes (moving nodes changes the shape) can be achieved with little change in the potential energy of the system.*

1.6 Mass vs. Strength

The paper also considers the issue of strength vs. mass of tensegrity structures. We find our planar examples to be very informative. We shall consider two types of strength. They are the size of bending forces and the size of compressive forces required to break the object.

Bending Strength vs. Mass First in Chapter 2 we study the ratio of **bending strength to mass**. We compare this for our $C2T4$ unit to a solid rectangular beam of the same mass. As expected reasonably constructed $C2T4$ units will be stronger. We do this comparison to a rectangular beam by way of illustrating the mass vs. strength question, since a thorough study would compare tensegrity structures to various kinds of trusses and would require a very long paper.

Compression Strength vs. Mass We analyze **compression stiffness** of the C2T4 tensegrity. The $C2T4$ has worse strength under compression than a solid rectangular bar. We analyze *compression stiffness* of $C4T2$ and $C4T1$ structures and use self-similar concepts to reduce mass, while constraining stiffness to a desired value. The $C4T1$ structure has better compression strength to mass ratio than a solid bar when $\delta < 29°$. The $C4T1$, while strong (not easily broken) the stiffness might not be extremely high.

1.6.1 A 2D Beam Composed of Tensegrity Units

After analyzing one $C2T4$ tensegrity unit, we lay n of them side by side to form a beam. We derive in Section 2.3 that the Euler Buckling formula for a beam adapts directly to this case. From this we conclude that the strength of the beam under compression is determined primarily by the bending rigidity $(EI)_n$ of each of its units. In principle, one can build beams with arbitrarily great bending strength. In practice this requires more study. Thus the favorable bending properties found for $C2T4$ bode well for beams made with tensegrity units.

1.6.2 A 2D Tensegrity Column

In Chapter 3 we take the $C4T2$ structure in Fig. 1.4(b) and replace each bar with a smaller $C4T2$ structure, then we replace each bar of this new structure by a yet smaller $C4T2$ structure. In principle such a self similar construction can be repeated to any level. Assuming that the strings do not fail and have significantly less mass than the bars, we find that the compression strength increases without bound if we keep the mass of the total bars constant. This completely ignores the geometrical fact that as we go to finer and finer levels in the fractal construction, the bars increasingly overlap. Thus, at least in theory, we have **a class of tensegrity structures with unlimited compression strength to mass ratio**. Further issues of robustness to lateral and bending forces would have to be investigated to insure practicality of such structures. However, our dramatic findings based on a pure compression analysis are intriguing. The self-similar concept can be extended to the third dimension in order to design a realistic structure that could be implemented in a column.

The report is arranged as follows. Chapter 2 analyzes a very simple planar tensegrity structure to show an efficient structure in bending. Chapter 3 analyzes a planar tensegrity structure efficient in compression. Chapter 4 defines a shell class of tensegrity structures and examines several members of

this class. Chapter 5 offers conclusions and future work. Appendices explain nonlinear and linear analysis of planar tensegrity.

Chapter 2

Planar Tensegrity Structures Efficient in Bending

In this chapter, we examine the bending rigidity of a single tensegrity unit, a planar tensegrity model under pure bending as shown in Fig. 2.1, where thin lines are the four strings and the two thick lines are bars. Since the structure in Fig. 2.1 has 2 compressive and 4 tensile members, we will refer to it as a $C2T4$ structure.

2.1 Bending Rigidity of A Single Tensegrity Unit

To arrive at a definition of bending stiffness suitable to C2T4, note that the moment M acting on the section is given by

$$M = FL_{bar} \sin \delta, \tag{2.1}$$

where F is the magnitude of the external force, L_{bar} is the length of the bar and δ is the angle that the bars make with strings in the deformed state, as shown in Fig. 2.1.

In Fig. 2.1, ρ is the radius of curvature of the tensegrity unit under bending deformation. It can be shown from Fig. 2.1 that,

$$\rho = \left(\frac{L_{bar}}{2}\right)^2 \cos\delta \sin\delta \frac{1}{u}, \quad u = \frac{1}{2} L_{bar} \sin\delta \tan\theta. \tag{2.2}$$

The *bending rigidity* is defined by $EI = M\rho$. Hence,

$$EI = FL_{bar} \sin\delta\rho = FL_{bar} \sin^2\delta \left(\frac{L_{bar}}{2}\right)^2 \cos\delta \frac{1}{u}. \tag{2.3}$$

where EI is the equivalent bending rigidity of the planar one–stage tensegrity unit and u is the nodal displacement. The evaluation of the bending rigidity of the planar unit requires the evaluation of u, which will follow in the sequel under various hypotheses. The bending rigidity will later be obtained by substituting u in (2.3).

2.1.1 Effective Bending Rigidity with Pretension

In the absence of external forces $\mathbf{f}$, let $\mathbf{A}_0$ be the matrix defined in Appendix A in terms of the initial prestressed geometry, and let $\mathbf{t}_0$ be the initial pre-

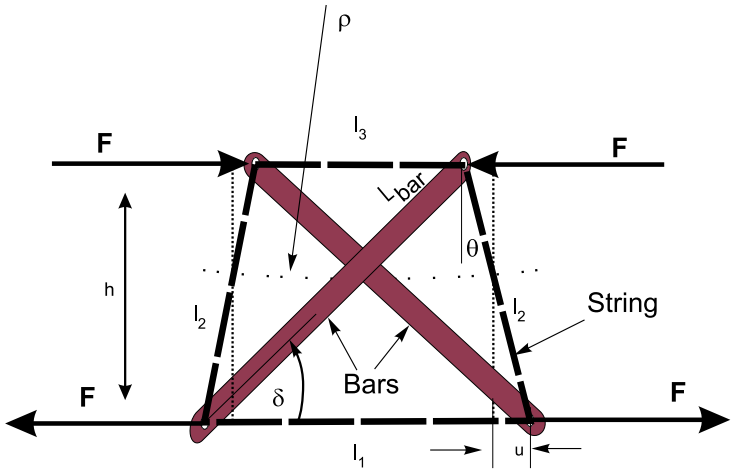

Fig. 2.1: Planar one–stage tensegrity unit under pure bending.

tension applied on the members of the tensegrity. Then,

$$\mathbf{A}_0\mathbf{t}_0 = \mathbf{0}, \qquad \mathbf{t}_0^T = [\mathbf{t}_{0\_bars} \quad \mathbf{t}_{0\_strings}], \qquad \mathbf{t}_{0\_strings} \geq 0. \tag{2.4}$$

For a nontrivial solution of (2.4), $\mathbf{A}_0$ must have a right null space. Furthermore, the elements of $\mathbf{t}_0$ obtained by solving (2.4) must be such that the strings are always in tension, where $\mathbf{t}_{0\_strings} \geq 0$ will be used to denote that each element of the vector is non negative. For this particular example of planar tensegrity, the null space of $\mathbf{A}_0$ is only one dimensional. $\mathbf{t}_0$ always exists, satisfiying (2.4), and $\mathbf{t}_0$ can be scaled by any arbitrary positive scalar multiplier. However, the requirement of a *stable* equilibrium in the tensegrity definition, places one additional constraint to the conditions (2.4); the geometry from which A_0 is constructed must be a stable equilibrium.

In the following discussions, E_s, $(EA)_s$, and A_s denote the Young's modulus of elasticity, the axial rigidity and the cross–sectional area of the strings, respectively, whereas E_b, $(EA)_b$ and A_b, denote those of the bars, respectively. $(EI)_b$ denotes the bending rigidity of the bars.

The equations of the static equilibrium and the bending rigidity of the tensegrity unit is a nonlinear function of the geometry δ, the pretension $\mathbf{t}_0$, the external force $\mathbf{F}$ and the stiffnesses of the strings and bars. In this case, the nodal displacement u is obtained by solving nonlinear equations of the static equilibrium, (see Appendix A for the underlying assumptions and for a detailed derivation)

$$\mathbf{A}(\mathbf{u})\mathbf{K}\mathbf{A}(\mathbf{u})^T\mathbf{u} = \mathbf{F} - \mathbf{A}(\mathbf{u})\mathbf{t}_0 \tag{2.5}$$

Also, $\mathbf{t}_0$ is the pretension applied in the strings, $\mathbf{K}$ is a diagonal matrix containing axial stiffness of each member, i.e. $K_{ii} = (EA)_i/L_i$, where L_i is the length of the i–th member. $\mathbf{u}$ represents small nodal displacements in the neighborhood of equilibrium caused by small increment in the external forces. The standard Newton–Raphson method is applied to solve (2.5) at each incremental load step $\mathbf{F}_k = \mathbf{F}_{k-1} + \Delta\mathbf{F}$. Matrix $\mathbf{A}(\mathbf{u}_k)$ is updated at each iteration until a convergent solution for $\mathbf{u}_k$ is found.

Figure 2.2 depicts EI as a function of the angle δ, pretension of the top string, and the rigidity ratio K which is defined as the ratio of the axial rigidity of the strings to the axial rigidity of the bars, i.e. $K = (EA)_s/(EA)_b$. The pretension is measured as a function of the prestrain in the top string ϵ_0. In obtaining Fig. 2.2, the bars were assumed to be equal in diameter and the strings were also assumed to be of equal diameter. Both the bars as well as the strings were assumed to be made of steel for which Young's modulus of elasticity E was taken to be $2.06 \times 10^{11} N/m^2$, and the yield strength of the steel σ_y was taken to be $6.90 \times 10^8 N/m^2$. In Fig. 2.2, EI is plotted against the ratio of the external load F to the yield force of the string. The yield force of the string is defined as the force that causes the strings to reach the elastic limit. The yield force for the strings is computed as,

$$\text{Yield force of string} = \sigma_y A_s,$$

where σ_y is the yield strength and A_s is the cross-sectional area of the string. The external force F was gradually increased till at least one of the strings yielded.

The following conclusions can be drawn from Fig. 2.2:

1. Fig. 2.2(a) suggests that the bending rigidity EI of a tensegrity unit with all taut strings increases with increase in the angle δ, up to a maximum at $\delta = 90^0$.

2. Maximum bending rigidity EI is obtained when none of the strings are slack, and the EI is approximately constant for any external force until one of the strings go slack.

3. Fig. 2.2(b) shows that the pretension does not have much effect on the magnitude of EI of a planar tensegrity unit. However, pretension does play a remarkable role in preventing the string from going slack which, in turn, increases the range of the constant EI against external loading. This provides robustness of EI predictions against uncertain external forces. This feature provides robustness against uncertainties in external forces.

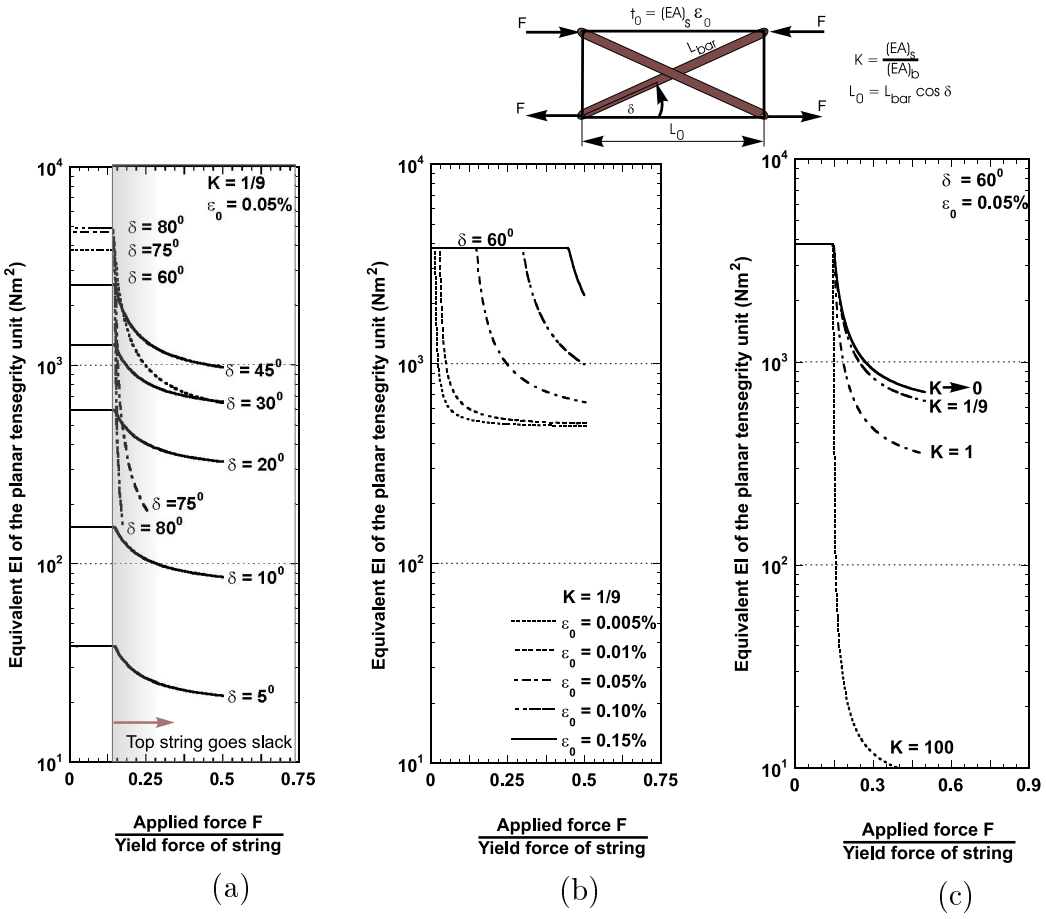

Fig. 2.2: Bending rigidity EI of the planar tensegrity unit for (a) different initial angle δ with rigidity ratio $K = 1/9$ and prestrain in the top string $\epsilon_0 = 0.05\%$, (b) different ϵ_0 with $K = 1/9$, (c) different K with $\delta = 60^0$ and $\epsilon_0 = 0.05\%$. L_{bar} for all cases is 0.25m.

4. In Fig. 2.2(c) we chose structures having the same geometry and the same total stiffness, but different K, where K is the ratio of the axial rigidity of the bars to the axial rigidity of the strings. We then see that K has little influence on EI as long as none of the strings are slack. However, the bending rigidity of the tensegrity unit with slack string is influenced K, with maximum EI occuring at $K = 0$ (rigid bars).

It was also observed that as the angle δ is increased or as the stiffness of the bar is decreased, the force sharing mechanism of the members of the tensegrity unit changes quite noticeably. This phenomena is seen only in the case when the top string is slack. For example, for $K = 1/9$ and $\epsilon_0 = 0.05\%$, for small values of δ, the major portion of the external force is carried by the bottom string, whereas after some value of δ (greater than 45^0), the major portion of the external force is carried by the vertical side strings rather than the bottom string. In such cases, the vertical side strings could reach their elastic limit prior to the bottom string. Similar phenomena was also observed for a case of $K = 100$, $\delta = 60^0$ and $\epsilon_0 = 0.05\%$. In such cases, as shown in Fig. 2.2(a) for $\delta = 70^0$ and $\delta = 75^0$, the EI drops drastically once the top string goes slack. Fig. 2.3 summarizes the conclusions on bending rigidity, where the arrows indicate increasing directions of δ or $\mathbf{t}_0$ or K.

Note that when t_0 is the pretension applied to the top string, the pretension in the vertical side strings is equal to $t_0/\tan\delta$. The cases of $\delta > 80^0$ were not computed, but it is clear that the bending rigidity is a step function as δ approaches 90^0, with EI constant until the top string becomes slack, then the EI goes to zero as the external load increases further.

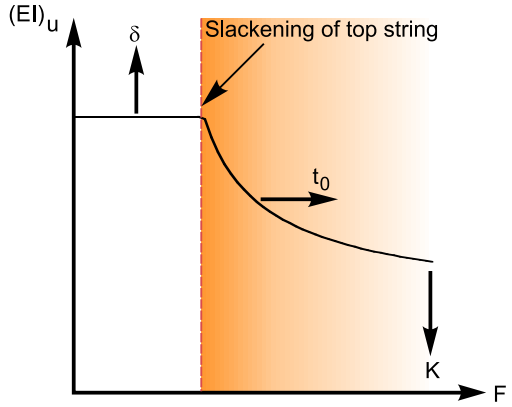

Fig. 2.3: Trends relating geometry δ, prestress $\mathbf{t}_0$, and material K.

2.1.2 Bending Rigidity of the Planar Tensegrity for the Rigid Bar Case ($K = 0$)

The previous section briefly describes the basis of the calculations for Fig. 2.1. The following sections considers the special case $K = 0$ to show more analytical insight. The *nonslack case* describes the structure when all strings exert force. The *slack case* describes the structure when string 3 exerts zero force, due to the deformation of the structure. Therefore, the force in string 3 must be computed in order to determine when to switch between the slack and nonslack equations.

Some Relations From Geometry and Statics

Nonslack Case: Summing forces at each node we obtain the equilibrium conditions

$$f_c \cos\delta = F + t_3 - t_2 \sin\theta \tag{2.6}$$

$$f_c \cos\delta = t_1 + t_2 \sin\theta - F \tag{2.7}$$

$$f_c \sin\delta = t_2 \cos\theta, \tag{2.8}$$

where f_c is the compressive load in a bar, F is the external load applied to the structure, and t_i is the force exerted by string i defined as

$$t_i = k_i(l_i - l_{i0}). \tag{2.9}$$

The following relations are defined from the geometry of Fig. 2.1:

$$\begin{aligned} l_1 &= L_{bar}\cos\delta + L_{bar}\tan\theta\sin\delta \\ l_2 &= L_{bar}\sin\delta\sec\theta \\ l_3 &= L_{bar}\cos\delta - L_{bar}\sin\delta\tan\theta \\ h &= L_{bar}\sin\delta, \end{aligned} \tag{2.10}$$

where l_i denote the geometric length of the strings. We will find the relation between δ and θ by eliminating f_c and F from (2.6) - (2.8)

$$\cos\theta = \frac{t_1 + t_3}{2t_2}\tan\delta. \tag{2.11}$$

Substitution of relations (2.10) and (2.9) into (2.11) yields

(2.12)
$$\cos\theta = \frac{k_1(L_{bar}\cos\delta + L_{bar}\tan\theta\sin\delta - l_{10}) + k_3(L_{bar}\cos\delta - L_{bar}\tan\theta\sin\delta - l_{30})}{2k_2(L_{bar}\sin\delta\sec\theta - l_{20})}\tan\delta.$$

If $k_i = k$, then (2.12) simplifies to

$$\tan\delta = \frac{2l_{20}}{l_{10}+l_{30}}\cos\theta = \beta\cos\theta. \tag{2.13}$$

Slack Case: In order to find a relation between δ and θ for the slack case when t_3 has zero tension, we use (2.12) and set k_3 to zero. With the simplification that we use the same material properties, we obtain

$$0 = L_{bar}\tan\theta\sin\delta\tan\delta + 2l_{20}\cos\theta - l_{10}\tan\delta - L_{bar}\sin\delta. \tag{2.14}$$

This relationship between δ and θ will be used in (2.22) to describe bending rigidity.

Bending Rigidity Equations

The *bending rigidity* is defined in (2.3) in terms of ρ and F. Now we will solve the geometric and static equations for ρ and F in terms of the parameters θ, δ of the structure. For the nonslack case, we will use (2.13) to get an analytical formula for the EI. For the slack case we do not have analytical formula. Hence, this must be done numerically.

From geometry we can obtain ρ,

$$\tan\theta = \frac{l_1}{2(\rho + \frac{h}{2})}.$$

Solving for ρ we obtain

$$\begin{aligned}\rho &= \frac{l_1}{2\tan\theta} - \frac{h}{2} \\ &= \frac{L_{bar}\cos\delta + L_{bar}\tan\theta\sin\delta}{2\tan\theta} - \frac{L_{bar}\sin\delta}{2} \\ &= \frac{L_{bar}}{2}\frac{\cos\delta}{\tan\theta}. \end{aligned} \tag{2.15}$$

Nonslack Case: In the nonslack case, we now apply the relation in (2.13) to simplify (2.15)

$$\rho = \frac{L_{bar}}{2}\frac{1}{\tan\theta\sqrt{1+\beta^2\cos^2\theta}}. \tag{2.16}$$

From (2.6) - (2.8) we can solve for the equilibrium external F

$$\begin{aligned} F &= \frac{1}{2}\left(t_1 + 2t_2\sin\theta - t_3\right) \\ &= \frac{1}{2}\left(k_1 L_{bar}\cos\delta + k_1 L_{bar}\tan\theta\sin\delta - k_1 l_{10}\right. \\ &\quad + 2k_2 L_{bar}\sin\delta\tan\theta - 2k_2 l_{20}\sin\theta \\ &\quad \left. - k_3 L_{bar}\cos\delta + k_3 L_{bar}\sin\delta\tan\theta + k_3 l_{30}\right). \end{aligned} \tag{2.17}$$

Again, using (2.13) and $k_i = k$, equation (2.17) simplifies to

$$F = \frac{2kL_{bar}\beta\sin\theta}{\sqrt{1+\beta^2\cos^2\theta}} - \frac{k}{2}(l_{10} - l_{30} + 2l_{20}\sin\theta). \tag{2.18}$$

We can substitute (2.18) and (2.16) into (2.3)

(2.19)

$$EI = \frac{L_{bar}^2\beta\cos^2\theta}{2(1+\beta^2\cos^2\theta)(\sin\theta)}\left(\frac{2kL_{bar}\beta\sin\theta}{\sqrt{1+\beta^2\cos^2\theta}} - \frac{k}{2}(l_{10} - l_{30} + 2l_{20}\sin\theta)\right),$$

and we obtain the bending rigidity of the planar structure with no slack strings present. The expression for string length l_3 in the nonslack case reduces to

$$l_3 = L_{bar}\frac{1-\beta\sin\theta}{\sqrt{1+\beta^2\cos^2\theta}}. \tag{2.20}$$

This expression can be used to determine the angle which causes l_3 to become slack.

Slack Case: Similarly, for the case when string 3 goes slack we set $k_3 = 0$ and $k_i = k$ in (2.17), which yields simply

$$\begin{aligned} F_{slack} &= \frac{1}{2}\left(t_1 + 2t_2\sin\theta\right) \\ &= \frac{1}{2}\left(kL_{bar}\cos\delta + 3kL_{bar}\tan\theta\sin\delta - kl_{10} - 2kl_{20}\sin\theta\right) \end{aligned} \tag{2.21}$$

and

(2.22)
$$EI_{slack} = \frac{L_{bar}^2 \sin\delta\cos\delta}{4\tan\theta}(kL_{bar}\cos\delta + 3kL_{bar}\tan\theta\sin\delta - kl_{10} - 2kl_{20}\sin\theta).$$

See Fig. 2.2(c) for a plot of EI for the $K = 0$ (rigid bar) case.

Constants and Conversions: All plots shown are generated with the following data which can then be converted as follows if necessary.

$$\begin{aligned} Young's\ Modulus,\ E &= 2.06 \text{ x } 10^{11}\ N/m^2 \\ Yield\ Stress,\ \sigma &= 6.9 \text{ x } 10^{8}\ N/m^2 \\ Diameter\ of\ Tendons &= 1\ mm \\ Cross\ Sectional\ Area\ of\ Tendon &= 7.8540 \text{ x } 10^{-7}\ m^2 \\ Length\ of\ Bar,\ L_{bar} &= .25\ m \\ Prestress &= e_0 \\ Initial\ Angle &= \delta_0 \end{aligned}$$

The spring constant of a string is

(2.23)
$$k = \frac{EA}{L_{bar}\cos(\delta_0)}.$$

The following equation can be used to compute the equivalent rest length given some measure of prestress t_0

$$\begin{aligned} t_0 &= (EA)_s e_0 = k(l - l_0) \\ l_0 &= L_{bar}\cos(\delta_0) - \frac{EAe_0}{k}. \end{aligned} \quad (2.24)$$

2.1.3 Effective Bending Rigidity with Slack String ($K > 0$)

As noted earlier, the tensegrity unit is a statically indeterminate structure (meaning that matrix **A** is not full column rank) as long as the strings remain

taut during the application of the external load. However, as soon as one of the strings goes slack, the tensegrity unit becomes statically determinate. In the following, an expression for bending rigidity of the tensegrity unit with an initially slack top string is derived. Even in the case of a statically determinate tensegrity unit with slack string, the problem is still a large displacement and nonlinear problem. However, a linear solution, valid for small displacements only, resulting in a quite simple and analytical form can be found. Based on the assumptions of small displacements, an analytical expression for EI of the tensegrity unit with slack top string has been derived in Appendix B and is given below.

$$EI \approx \frac{1}{2}\frac{{L_{bar}}^2 (EA)_s \sin^2\delta \cos^3\delta}{(\sin^3\delta + 2\cos^3\delta + K)}. \tag{2.25}$$

The EI obtained from nonlinear analysis, i.e. from (2.3) together with (2.5), is compared with the EI obtained from linear analysis, i.e. from (2.25), and is shown in Fig. 2.4. Figure 2.4 shows that the linear analysis provides a lower bound to the actual bending rigidity. The linear estimation of EI, i.e. (2.25), is plotted in Fig. 2.5 as a function of the initial angle δ for different values of the stiffness ratio K. Both bars and the strings are assumed to be made of steel, as before. It is seen in Fig. 2.5 that the EI of the tensegrity unit with slack top string attains a maximum value for some value of δ. The decrease of EI (after the maximum) is due to the change in the force sharing mechanism of the members of the tensegrity unit, as discussed earlier. For small values of δ, the major portion of the external force is carried by the bottom string, whereas for larger values of δ, the vertical side strings start to share the external force. As δ is further increased, the major portion of the external force is carried by the vertical side strings rather than the bottom string. This explains the decrease in the EI with increase in δ after some value of δ for which EI is maximum. The locus of the maximum EI is also shown in Fig. 2.5. The maximum value of EI and the δ for which EI is maximum, depends on the relative stiffness of the string and the bars, i.e. it depends on K. From Fig. 2.5 note that the maximum EI is obtained when the bars are much stiffer than the strings. EI is maximum when the bars are perfectly rigid, i.e. $K \to 0$. It is seen in Fig. 2.5 and it can also be

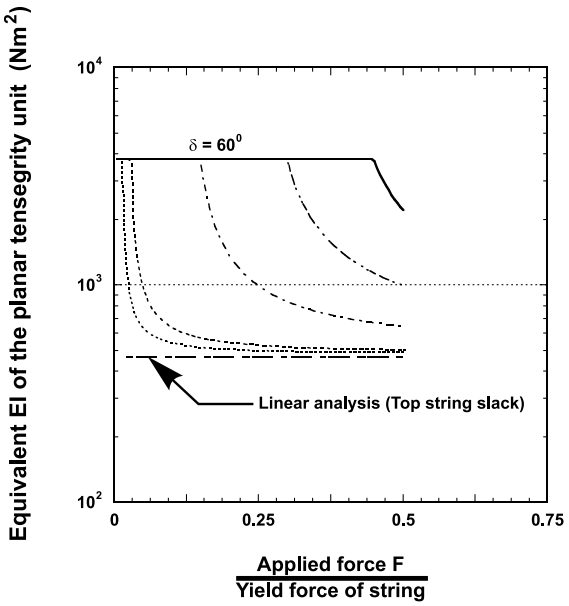

Fig. 2.4: Comparison of EI from nonlinear analysis with the EI from linear analysis with slack top string. ($L_{bar} = 0.25$**m,** $\delta = 60^0$ **and** $K = 1/9$**).**

shown analytically from (2.25), that for the case of bars much stiffer than the strings, $K \longrightarrow 0$, the maximum EI of the tensegrity unit with slack top string is obtained when $\delta = 45^0$. In constrast, note from Fig. 2.2(a) that, when no strings are slack, the maximum bending rigidity occurs with $\delta = 90^0$.

2.2 Mass Efficiency of a $C2T4$ Class 1 Tensegrity in Bending

This section demonstrates that beams composed of tensegrity units can be more efficient than continua beams. We make this point with a very specific example of a single unit C2T4 structure. In a later section we allow the number of unit cells to approach infinity to describe a long beam. Let Fig. 2.6

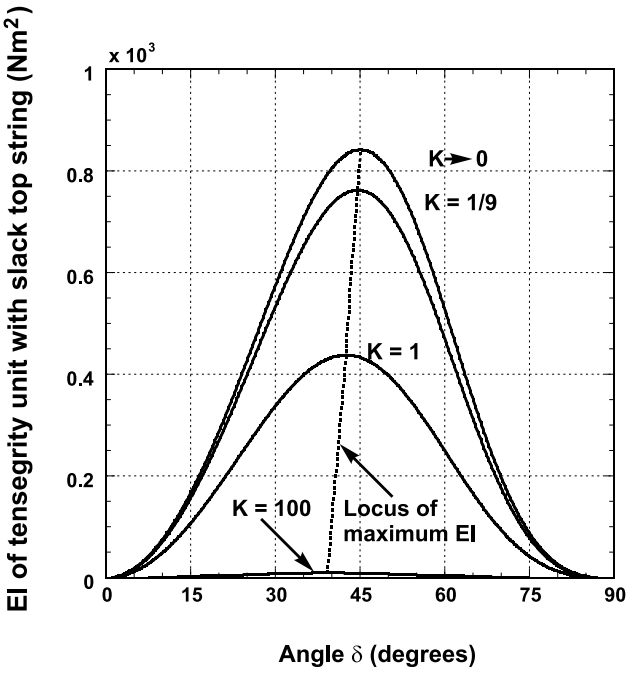

Fig. 2.5: EI **with slack top string with respect to the initial angle** δ **for** $L_{bar} = 0.25$**m.**

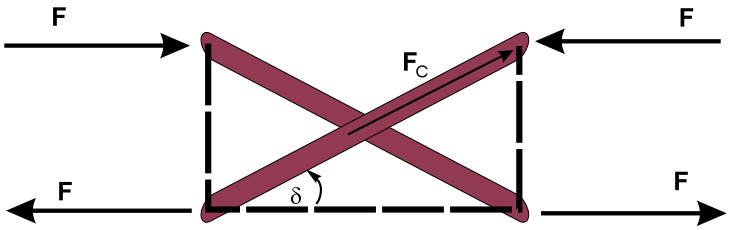

Fig. 2.6: C2T4 Tensegrity with slack top string

describe the configuration of interest. Note that the top string is slack (because the analysis is easier), even though the stiffness will be greater before the string is slack. The compressive load in the bar, F_c, is

$$F_c = F/\cos\delta$$

Designing the bar to buckle at this force yields

$$F_c = \frac{\pi^2\ E_1\ r_{bar}^4}{L_{bar}^2}, \quad (L_{bar},\ r_{bar}) = \text{length, radius of bar}$$

where the mass of the two bars is (ρ_1 = bar mass density)

$$m_b = 2m_1 = 2\pi\ \rho_1\ L_{bar}\ r_{bar}^2 \Rightarrow r_{bar}^2 = \frac{m_b}{2\pi\rho_1 L_{bar}}.$$

Hence, eliminating r_{bar} gives for the force

$$F_c = \frac{\pi^2\ E_1}{L_{bar}^2}\left(\frac{m_b^2}{4\pi^2\ \rho_1^2\ L_{bar}^2}\right) = \left(\frac{E_1}{4\rho_1^2\ L_{bar}^4}\right) m_b^2.$$

The moment applied to the unit is

$$M = F\ L_{bar}\ \sin\delta = \frac{E_1}{4\rho_1^2\ L_{bar}^3}\ m_b^2\ \cos\delta\ \sin\delta. \tag{2.30}$$

To compare this structure with a simple classical structure, suppose the same moment is applied to a single bar of rectangular cross-section with b units high and a units wide and yield strength σ_y such that

$$M = \frac{\sigma_y I}{C},\ I = \frac{1}{12}\ ab^3,\ C = \frac{b}{2},\ m_o = \rho_0\ L_0\ ab,$$

then, for the rectangular bar

$$M = \frac{\sigma_y\ m_0^2}{6a\ \rho_0^2\ L_0^2}. \tag{2.32}$$

Equating (2.30) and (2.32), using $L_0 = L_{bar}\cos\delta$, yields the material/geometry conservation law ($\bar{\sigma}$ is a material property and g is a property of the geometry)

$$\mu^2 \triangleq \left(\frac{m_b}{m_0}\right)^2 = \frac{2}{3}\ \bar{\sigma} g,\ \bar{\sigma} \triangleq \frac{\sigma_y}{E_1},\ g \triangleq \frac{L_0}{a\cos^4\delta\sin\delta} \tag{2.33}$$

The mass ratio μ is infinity if $\delta = 0^o,\ 90^o$, and the lower bound on the mass ratio is achieved when $\delta = \sin^{-1}(\frac{1}{\sqrt{5}}) = 26.565^o$.

Lemma 1 *Let σ_y denote the yield stress of a bar with modulus of elasticity E_1 and dimension $a \times b \times L_0$. Let M denote the bending moment about an axis perpendicular to the b dimension. M is the moment at which the bar fails in bending. Then, the $C2T4$ tensegrity fails at the same M but has less mass if $\bar{\sigma}g < \frac{3}{2}$, and minimal mass is achieved at $\delta = \tan^{-1}(\frac{1}{2})$.*

Proof: From (2.33),

$$\mu^2 = \frac{2}{3}\,\bar{\sigma}g \geq \frac{2}{3}\,\bar{\sigma}\underline{g},\ \underline{g} = 3.493856\frac{L_0}{a} \tag{2.34}$$

where the lower bound $\frac{2}{3}\,\bar{\sigma}\underline{g}$ is achieved at $\delta = \sin^{-1}(\frac{1}{\sqrt{5}})$, by setting $\frac{\partial g}{\partial \delta} = 0$ and solving $\cos^2\delta = 4\sin^2\delta$, or $\tan\delta = \frac{1}{2}$. □

For steel with $(\sigma_y,\ E_1) = (6.9 \times 10^8,\ 2 \times 10^{11})\frac{N}{m^2}$,

$$\mu^2 = \frac{2}{3}\,\bar{\sigma}g\ \geq 0.008035869\frac{L_0}{a} \tag{2.35}$$

where the lower bound is achieved for $\delta = 26.565^o$. Hence, for geometry of the steel comparison bar given by $\{\frac{L_0}{a} = 100$, and $\delta = \sin^{-1}(\frac{1}{\sqrt{5}}) = 26.565^o\}$, then $m_b = 0.8m_0$, showing 20% improvement in mass for a given yield moment. For the geometry $\{\frac{L_0}{a} = 20$ and $\delta = 26.565^o\}$, $m_b = 0.16m_0$, showing 84% improvement in mass for a given yield moment, M. The main point here is that strength and mass efficiency is achieved by *geometry* ($\delta = 26.565^o$), not materials.

It can be shown that the compressive force in a bar when the system C2T4 is under a pure bending load exhibits a similar robustness property that was shown with the bending rigidity. The force in a bar is constant until a string becomes slack, which is shown in Fig. 2.7.

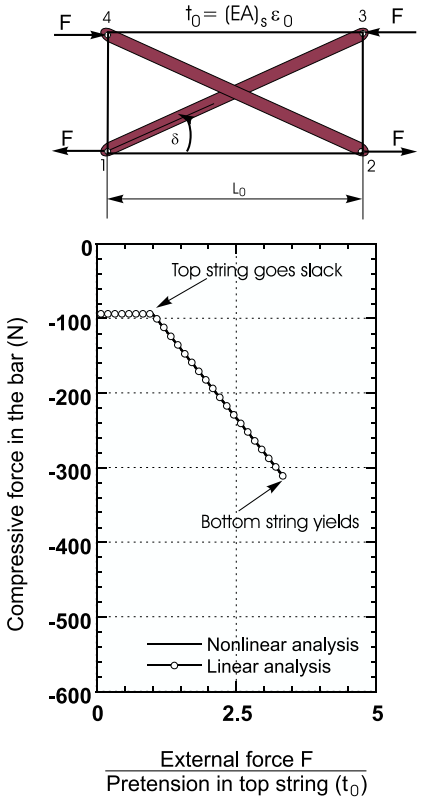

Fig. 2.7: Comparison of force in the bar obtained from linear and nonlinear analysis for pure bending loading. (Strings and bars are made of steel, Young's modulus $E = 2.06 \times 10^{11}$ N/m^2, yield stress $\sigma_y = 6.90 \times 10^8$ N/m^2, diameter of string = 1mm, diameter of bar = 3mm, $K = 1/9$, $\delta = 30^0$, $\epsilon_0 = 0.05\%$ and $L_0 = 1.0$m.)

2.3 Global Bending of a Beam Made From $C2T4$ Units

The question naturally arises "what is the bending rigidity of a beam made from many tensegrity cells?" Section 2.3.2 answers that question. First, in section 2.3.1 we review the standard beam theory.

2.3.1 Buckling Loads

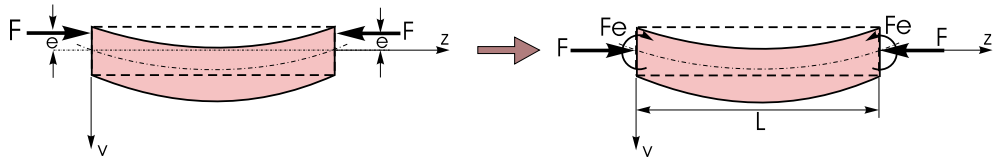

Fig. 2.8: Bending of a beam with eccentric load at the ends.

For a beam loaded as shown in Fig. 2.8, we have

$$EI\frac{d^2v}{dz^2} = -Fv - Fe \tag{2.36}$$

equivalently,

$$\frac{d^2v}{dz^2} + p^2v = -p^2e \tag{2.37}$$

where

$$p^2 = F/EI, \tag{2.38}$$

where EI is the bending rigidity of the beam, v is the transverse displacement measured from the neutral axis (denoted by the dotted line in Fig. 2.8), z represents the longitudinal axis, L is the length of the beam, e is the eccentricity of the external load F. The eccentricity of the external load is defined as the distance between the point of action of the force and the neutral axis of the beam.

The solution of the above equation is,

$$v = A\sin pz + B\cos pz - e \tag{2.39}$$

where constants A and B depend on the boundary conditions. For a pin–pin boundary condition, A and B are evaluated to be

$$A = e\tan\frac{pL}{2}, \qquad \text{and} \qquad B = e \tag{2.40}$$

Therefore, the deflection is given by

$$v = e\left[\tan\frac{pL}{2}\sin pz + \cos pz - 1\right] \tag{2.41}$$

2.3.2 Buckling of Beam with Many C2T4 Tensegrity Cells

Assume that the beam as shown in Fig. 2.8 is made of n small tensegrity units similar to the one shown in Fig. 2.1, such that $L = nL_0$, and the bending rigidity EI appearing in (2.36) and (2.38) is replaced by EI given by (2.25). Also, since we are analyzing a case when the beam breaks, we shall assume that the applied force is large compared to the pretension. The beam buckles at the unit receiving the greatest moment. Since the moment varies linearly with the bending and the bending is greatest at the center of the beam, the tensegrity unit at the center buckles. The maximum moment M_{max} leading to the worst case scenario is related to the maximum deflection at the center v_{max}. From (2.41),

$$v_{max} = e\left[\tan\frac{pL}{2}\sin\frac{pL}{2} + \cos\frac{pL}{2} - 1\right]. \tag{2.42}$$

Simple algebra converts this to

$$v_{max} = e\left(\frac{1}{\cos\frac{pL}{2}} - 1\right) \tag{2.43}$$

The worst case M_{max} is equal to $Fv_{max} + Fe$ and is given by

$$M_{max} = \frac{F}{\cos\left(\frac{nL_0}{2}\sqrt{\frac{F}{EI}}\right)}e \tag{2.44}$$

Now we combine this with the buckling formula for one tensegrity unit to get its breaking moment

$$M_{break} = eF_B = e\frac{\pi^2(EI)_b}{L_0^2}\cos^3\delta \tag{2.45}$$

Thus, from Eqn. (2.44) and (2.45), if F exceeds F_{gB} given by

$$\frac{F_{gB}}{\cos\left(\frac{nL_0}{2}\sqrt{\frac{F_{gB}}{EI}}\right)} = \frac{\pi^2(EI)_b}{L_0^2}\cos^3\delta \tag{2.46}$$

the central unit buckles, and F_{gB} is called the global buckling load.

Multiplying both sides of (2.46) by $(nL_0)^2$ and introducing three new variables,

$$\mathcal{F} = F_{gB}(nL_0)^2, \qquad \mathcal{P} = \frac{\pi^2(EI)_b}{L_0^2}\cos^3\delta, \qquad \mathcal{K} = \frac{1}{2}\sqrt{\frac{1}{EI}}, \tag{2.47}$$

we rewrite (2.46) as

$$\frac{\mathcal{F}}{\cos\left(\mathcal{K}\sqrt{\mathcal{F}}\right)} = \mathcal{P}n^2L_0^2 \tag{2.48}$$

Equivalently,

$$\eta(\mathcal{F}) = \mathcal{P}n^2L_0^2, \tag{2.49}$$

where η is a function defined as

$$\eta(\mathcal{F}) = \frac{\mathcal{F}}{\cos\left(\mathcal{K}\sqrt{\mathcal{F}}\right)}. \tag{2.50}$$

η is a monotonically increasing function in

$$0 \le \mathcal{F} \le \left(\frac{\pi}{2}\right)^2\frac{1}{\mathcal{K}^2}, \tag{2.51}$$

satisfying

$$\eta \ge \mathcal{F}. \tag{2.52}$$

It is interesting to know the buckling properties of the "beam" as the number of the tensegrity elements become large. As $n \to \infty, (nL_0)^2 \to \infty$, and from (2.49) and (2.51)

$$\mathcal{F} = \eta^{-1}\left[\mathcal{P}n^2L_0^2\right] \to \left(\frac{\pi}{2}\right)^2 \frac{1}{\mathcal{K}^2} \tag{2.53}$$

and $\mathcal{F}$ approaches the limit from below. From Eqs. (2.47) and (2.49),

$$F_{gB} = \frac{1}{n^2}\frac{1}{L_0^2}\left[\eta^{-1}\left(\mathcal{P}n^2L_0^2\right)\right] \tag{2.54}$$

Thus for large n, using (2.53), we get

$$\begin{aligned} F_{gB} &\approx \frac{1}{n^2}\frac{1}{L_0^2}\left(\frac{\pi}{2}\right)^2 \frac{1}{\mathcal{K}^2} \\ &\approx \frac{1}{n^2}\frac{1}{L_0^2}\left(\frac{\pi}{2}\right)^2 \frac{1}{\frac{1}{4}\frac{1}{EI}} \\ &\approx \frac{1}{n^2}\frac{\pi^2 EI}{L_0^2} \end{aligned} \tag{2.55}$$

The global buckling load as given by (2.55) is exactly the same as the classical Euler's buckling equation evaluated for the bending rigidity EI of the tensegrity unit. Therefore, asymptotically the buckling performance of the beam depends only on the characteristics of EI and L_o^2 just as a classical beam.

Note, for each n

$$F_{gB} \leq \frac{1}{n^2}\frac{\pi^2 EI}{L_0^2}.$$

The implication here is that the standard Euler buckling formula applies where EI is a function of the geometrical properties of the tensegrity unit. Fig. 2.2(a) shows that EI can be assigned any finite value. Hence the beam can be arbitrarily stiff if the tensegrity unit has horizontal length arbitrarily small. This is achieved by using an arbitrarily large number of tensegrity units with large δ (arbitrarily close to 90^0). More work is needed to define practical limits on stiffness.

2.4 A Class 1 C2T4 Planar Tensegrity In Compression

In this section we derive equations that describe the stiffness of the Class 1 $C2T4$ planar tensegrity under compressive loads. The *nonslack case* describes the structure when all strings exert force. The *slack case* describes the structure when string 3 and string 1 exert zero force, due to the deformation of the structure. Therefore, the force in string 3 and string 1 must be computed in order to determine when to switch between the slack and nonslack equations. We make the assumption that bars are rigid, that is $K = 0$.

Compressive Stiffness Derivation

Nonslack Case: Summing forces at each node we obtain the equilibrium conditions

$$f_c \cos\delta = F + t_3 \tag{2.56}$$

$$f_c \cos\delta = F + t_1 \tag{2.57}$$

$$f_c \sin\delta = t_2, \tag{2.58}$$

where f_c is the compressive load in a bar, F is the external load applied to the structure, and t_i is the force exerted by string i defined as

$$t_i = k_i(l_i - l_{i0}).$$

The following relations are defined from the geometry of Fig. 2.9:

$$\begin{aligned} l_1 &= L_{bar}\cos\delta \\ l_2 &= L_{bar}\sin\delta \\ l_3 &= L_{bar}\cos\delta \end{aligned} \tag{2.59}$$

Solving for F we obtain

$$F = k(l_{10} - \frac{l_{20}}{\tan\delta}). \tag{2.60}$$

Using the relation $L_0 = L_{bar}\cos\delta$ and $\tan\delta = \frac{\sqrt{L_{bar}^2 - L_0^2}}{L_0}$ results in

$$F = kl_{10} - \frac{kl_{20}L_0}{\sqrt{L_{bar}^2 - L_0^2}}. \tag{2.61}$$

We will also make the assumption now that all strings have the same material properties, specifically, $l_{i0} = l_0$. Now, the stiffness can be computed as

$$K \triangleq -\frac{dF}{dL_0} = \frac{kl_0}{\sqrt{L_{bar}^2 - L_0^2}} + \frac{kl_0L_0^2}{(L_{bar}^2 - L_0^2)^{\frac{3}{2}}} = \frac{kl_0L_{bar}^2}{(L_{bar}^2 - L_0^2)^{\frac{3}{2}}}. \tag{2.62}$$

Similarly for the *slack* case, when t_1 and t_3 are slack, we follow the same derivation setting $t_1 = t_3 = 0$ in (2.56)-(2.58)

$$F_{slack} = kL_{bar}\cos\delta - \frac{kl_0}{\tan\delta}. \tag{2.63}$$

Substitution of $L_0 = L_{bar}\cos\delta$ yields

$$F_{slack} = kL_0 - \frac{kl_0L_0}{\sqrt{L_{bar}^2 - L_0^2}}. \tag{2.64}$$

Taking the derivative with respect to L_0 gives

$$\begin{aligned} K_{slack} = -\frac{dF_{slack}}{dL_0} &= -k + \frac{kl_0}{\sqrt{L_{bar}^2 - L_0^2}} + \frac{kl_0L_0^2}{(L_{bar}^2 - L_0^2)^{\frac{3}{2}}} \\ &= k\left(\frac{l_0L_{bar}^2}{(L_{bar}^2 - L_0^2)^{\frac{3}{2}}} - 1\right). \end{aligned} \tag{2.65}$$

A plot of stiffness for the nonslack and slack case vs applied force is given in Fig. 2.10, where $k = 9.1523 \times 10^5\ N/m$, $\delta = 45°$, $L_{bar} = 0.25\ m$, and the force, F, ranges between 0 and $600N$.

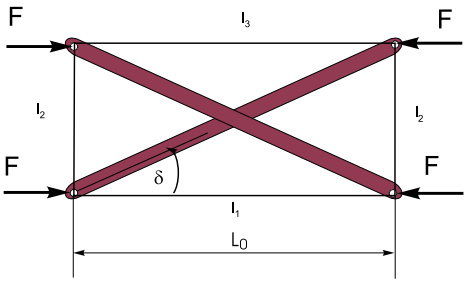

Fig. 2.9: $C2T4$ **in compression.**

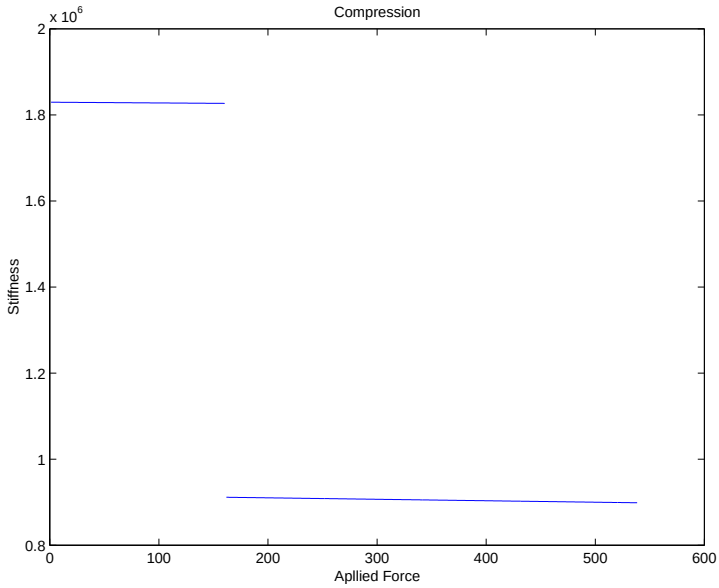

Fig. 2.10: Stiffness of $C2T4$ **vs applied load, plotted until strings yield.**

2.5 Summary of Chapter 2

Tensegrity structures have geometric structure that can be designed to achieve desirable mechanical properties. First, this paper demonstrates how bending rigidity varies with the geometrical parameters. The bending rigidity is reduced when a string goes slack, and pretension delays the onset of slack strings. The important conclusions made in this section are

- Beams made from tensegrity units can be stiffer than their continuous beam counterparts.
- Pretension can be used to maintain a constant bending rigidity over a wider range of external loads. This can be important to robustness, when the range of external loads can be uncertain.
- For larger loads the bending stiffness is dominated by geometry, not pretension. This explains the mass efficiency of tensegrity structures since one can achieve high stiffness by choosing the right geometry.
- The ratio of mass to bending rigidity of the $C2T4$ tensegrity is shown to be smaller than for a rectangular cross section bar, provided the geometry is chosen properly (angle between bars must be less than 53^o). Comparisons to a conventional truss would be instructive. There are many possibilities.

Chapter 3

Planar Class K Tensegrity Structures Efficient in Compression

It is not hard to show that the *Class 1 C2T4 Tensegrity* of Fig. 2.9 is not as mass efficient as a single rigid bar. That is, the mass of the structure in Fig. 2.9 is greater than the mass of a single bar which buckles at the same load $2F$. This motivates the examination of *Class 2 Tensegrity* structures which have the potential of greater strength and stiffness due to ball joints that can efficiently transfer loads from one bar to another. Compressive members are disconnected in the traditional definition [2] of tensegrity structures, which we call Class 1 Tensegrity. However, if stiff tendons connecting two nodes are very short, then for all practical purposes, the nodes behave as though they are connected. Hence *Class 1 Tensegrity generates Class k Tensegrity Structures as special cases* when certain tendons become relatively short. "Class k Tensegrity" describes a network of axially loaded members in which the ends of not more than k compressive members are connected (by ball joints, of course, since torques are not permitted) at nodes of the network.

In this section, we examine one basic structure which is efficient under com-

pressive loads. In order to design a structure that can carry a compressive load with small mass we will employ Class k Tensegrity together with the concept of self-similarity. Self-similar structures involve replacing a compressive member with a more efficient compressive system. This algorithm, or "fractal", can be repeated for each member in the structure. The basic principle responsible for the efficiency in compression of this structure is geometrical advantage, combined with the use of tensile members which have been shown to exhibit large load to mass ratios. We begin the derivation by starting with a single bar and its Euler Buckling conditions. Then this bar is replaced by four smaller bars and one tensile member. This process can be generalized and the formulae are given in the following sections. The objective is to characterize the mass of the structure in terms of strength and stiffness. This will allow one to design for minimal mass while bounding stiffness. In designing this structure there are trade-offs, for example, geometrical complexity poses manufacturing difficulties.

The materials of the bars and strings used for all calculations in this chapter are steel, which has the mass density $\rho = 7.862\frac{g}{cm^3}$, Young's modulus $E = 2.06^{11}\frac{N}{m^2}$ and Yield strength $\sigma = 6.9^{8}\frac{N}{m^2}$.

3.1 Compressive Properties of the $C4T2$ Class 2 Tensegrity

Suppose a bar of radius r_0 and length L_0, as shown in Fig. 3.1 buckles at load F. Then,

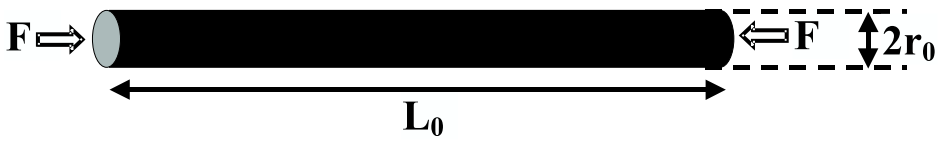

Fig. 3.1: A bar under compression.

$$F = \frac{E_0 \pi r_0^4}{L_0^2}, \tag{3.1}$$

where E_0 is the Young's Modulus of the bar material.
The mass of the bar is

$$m_0 = \rho_0 \pi r_0^2 L_0, \tag{3.2}$$

where ρ_0 is the mass density of the bar.
Equations (3.1) and (3.2) yield the force-mass relationship

$$F = \frac{E_0 m_0^2}{\rho_0^2 L_0^4}. \tag{3.3}$$

Now consider the four-bar pinned configuration in Fig. 3.2, which is designed

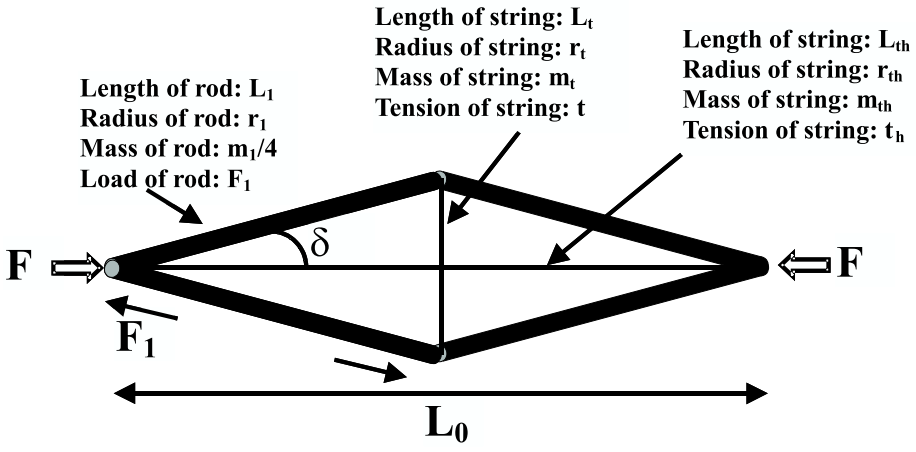

Fig. 3.2: A $C4T2$ Planar Class 2 Tensegrity Structure.

to buckle at the same load F. Notice that the Class 2 Tensegrity of Fig. 3.2 is in the dual (where bars are replaced by strings and vice versa) of the Class 1 Tensegrity of Fig. 1.3(b), and is of the same type as the Class 2 Tensegrity in Fig. 1.3(c).

We first examine the case when tendon t_h is slack. The four identical bars buckle at the bar compressive load F_1 and the mass of each of the four bars is $\frac{1}{4}m_1$. Hence,

$$F_1 = \frac{E_1 \pi r_1^4}{L_1^2}, \quad m_1 = 4\rho_1 \pi r_1^2 L_1, \quad F_1 = \frac{E_1 m_1^2}{16\rho_1^2 L_1^4}, \tag{3.4}$$

where (r_1, L_1, E_1, ρ_1) is resepectively, the radius, length, Young's Modulus and mass density of each bar, and the mass of the system $C4T1$ in Fig. 3.2 is

$$m_1 = 4\rho_1 \pi r_1^2 L_1.$$

Since from the Fig. 3.2, the length of each bar is L_1 and the compressive load in each bar is F_1 given by,

$$L_1 = \frac{L_0}{2\cos\delta}, \quad F_1 = \frac{F + t_h}{2\cos\delta}, \tag{3.5}$$

then, from (3.3)- (3.5)

$$F_1 = \frac{E_1 m_1^2}{16\rho_1^2 L_1^4} = \frac{F + t_h}{2\cos\delta}. \tag{3.6}$$

Note from (3.5) that the $C4T2$ structure with no external force F and tension $t_h = F_x$ in the horizontal string, places every member of the structure under the same load as a $C4T1$ structure (which has no horizontal string) with an external load $F = F_x$. In both cases $F_1 = \frac{F_x}{2\cos\delta}$.

Solving for the mass ratio, from (3.6)

$$\mu_1 \triangleq \left(\frac{m_1}{m_0}\right) = \frac{\rho_1}{\rho_0}\sqrt{\frac{E_0}{E_1}}\left(\frac{1 + \frac{t_h}{F}}{2\cos^5\delta}\right)^{\frac{1}{2}} \tag{3.7}$$

For slack tendon $t_h = 0$, note that $\mu_1 < 1$ if $\delta < \cos^{-1}(\frac{1}{2})^{\frac{1}{5}} = 29.477^o$. Of course, in the slack case (when $t_h = 0$), one might refer to Fig. 3.2 as a $C4T1$ structure, and we will use this designation to describe the system of Fig. 3.2 when t_h is slack. Increasing pretension in t_h to generate the non-slack case can be examined later. The results are summarized as follows:

Proposition 1 *With slack horizontal string $t_h = 0$, assume that strings are massless, and that the $C4T1$ system in Fig. 3.2 is designed to buckle at the same load F as the original bar of mass m_0 in Fig.(3.1). Then, the total mass m_1 of the $C4T1$ system is $m_1 = m_0(2\cos^5\delta)^{-\frac{1}{2}}$, which is less than m_0 whenever $\delta < 29.477$ degrees.*

Proof: This follows by setting $\mu_1 = 1$ in (3.7).

Some illustrative data that reflects the geometrical properties of the $C4T1$ in comparison with a bar which buckles with the same force F are shown in the table below.

	$\delta = 10^0$	$\delta = 20^0$
r_1	$.602r_0$	$.623r_0$
m_1	$.735m_0$	$.826m_0$
L_1	$.508L_0$	$.532L_0$
$\frac{L_1}{r_1}$	$.844\frac{L_0}{r_0}$	$.854\frac{L_0}{r_0}$

Table 1. Properties of the $C4T1$ Structure

For example, when $\delta = 10°$, the $C4T1$ requires only 73.5% of the mass of the bar to resist the same compressive force.

The data in Table 1 are computed from the following relationships for the $C4T1$ structure. The radius of each bar in the $C4T1$ system is r_1

$$r_1^2 = \frac{m_1}{4\rho_1 \pi L_1} = \frac{m_0 2\cos\delta}{4\rho_0 \pi L_0 \sqrt{2\cos^5\delta}},$$

and

$$r_0^2 = \frac{m_0}{\rho_0 \pi L_0}.$$

From this point forward we will assume the same material for all bars. Hence,

$$\left(\frac{r_1}{r_0}\right)^4 = \frac{1}{8\cos^3\delta}.$$

Likewise,

$$\left(\frac{L_1}{L_0}\right) = \frac{1}{2\cos\delta},$$

and

$$\left(\frac{r_1}{r_0}\right)^4 = \left(\frac{L_1}{L_0}\right)^3.$$

Also

$$\frac{L_1}{r_1} = \frac{L_0(8\cos^3\delta)^{\frac{1}{4}}}{2r_0\cos\delta} = \frac{L_0}{r_0}\left(\frac{1}{2cos\delta}\right)^{\frac{1}{4}}.$$

3.2 $C4T2$ Planar Tensegrity In Compression

In this section we derive equations that describe the stiffness of the $C4T2$ Planar Tensegrity under compressive loads. Pretension would serve to increase the restoring force in the string, allowing greater loads to be applied with smaller deformations. This is clearly shown in the force balance equation (3.5), where pretension can be applied through the use of the rest length l_{h0} of the string, and $t_h = k_h(L_0 - l_{h0})$, where k_h is the stiffness of the horizontal string.

Compressive Stiffness Derivation

From Fig. 3.2, the equilibrium configuration can be expressed as

$$F = t\cot\delta - t_h = k_t\,(L_t - l_0)\,\frac{L_0}{L_t} - t_h = k_t\left(1 - \frac{l_0}{L_t}\right)L_0 - t_h, \tag{3.8}$$

where t, L_0, L_t and l_0 are the tension, length of the structure, length of the string and the rest length of the vertical string, respectively. The length of the string can be written as

$$L_t^2 = 4L_1^2 - L_0^2,$$

where L_1 denotes the length of one bar. This relation simplifies the force balance equation to

$$F = k_t\left(1 - \frac{l_0}{\sqrt{4L_1^2 - L_0^2}}\right)L_0 - k_h(L_0 - l_{h0}). \tag{3.9}$$

Fig. 3.3 shows the plot of the load deflection curve of $C4T2$ structure with different δ_0. The compressive stiffness can be calculated by taking the derivative of (3.9) with respect to L_0 as follows,

$$\begin{aligned}\frac{dF}{dL_0} &= k_t\left(1-\frac{l_0}{\sqrt{4L_1^2-L_0^2}}\right)-k_t\frac{l_0L_0^2}{(4L_1^2-L_0^2)^{\frac{3}{2}}}-k_h\\ &= k_t\left(1-\frac{4l_0L_1^2}{(4L_1^2-L_0^2)^{\frac{3}{2}}}\right)-k_h. \qquad (3.10)\end{aligned}$$

Therefore, the stiffness is defined to be

$$K \triangleq -\frac{dF}{dL_0} = k_t\left(\frac{4l_0L_1^2}{(4L_1^2-L_0^2)^{\frac{3}{2}}}-1\right)+k_h = k_t\left(\frac{l_0\cos\delta}{L_0\sin^3\delta}-1\right)+k_h. \qquad (3.11)$$

Figure 3.4 shows the plot of stiffness versus the length of the structure and Fig. 3.5 shows the plot of stiffness versus the applied load F on the structure. Figures 3.3 - 3.5 demonstrate a step change in stiffness when tendon t_h goes slack. Note also that the $C4T1$ structure (t_h slack) demonstrates the property described in Fig. 1.8. Structures which demonstrate robustness to external forces (that is, they maintain stiffness until strings go slack) do not preserve strength very well, whereas, structures which demonstrate strength robustness have poor stiffness properties.

3.3 Self-Similar Structures of the type $C4T1$

Now let *each* of the four bars of the $C4T1$ system (that is, the $C4T2$ system with $t_h = 0$) in Fig. 3.2 be replaced by another $C4T1$ system. The new 16 bar structure of Fig. 3.6 is called $C4T1^2$, and is designed to buckle at the same load F. Hence if F_2 represents the force in each of the 16 bars, with length L_2 and radius r_2, and mass $m_2/16$, then, the relations below are obtained.

$$F_2 = \frac{E_0\pi r_2^4}{L_2^2}, \quad m_2 = 16\rho_0\pi r_2^2L_2, \quad F_2 = \frac{E_0m_2^2}{16\rho_0^2L_2^4} \qquad (3.12)$$

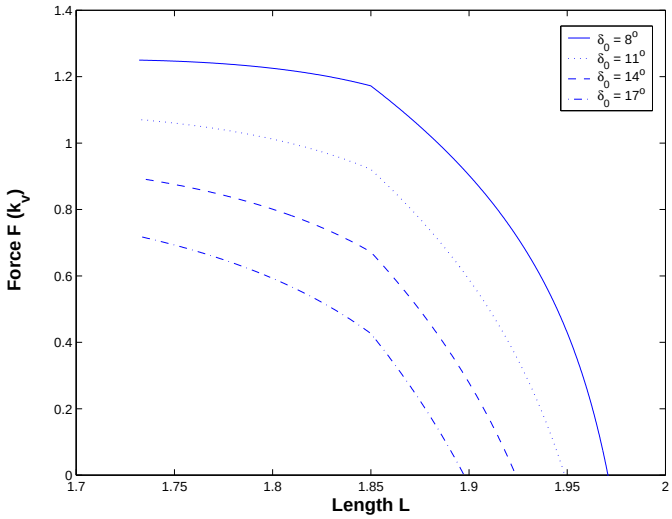

Fig. 3.3: Load Deflection curve of $C4T2$ structure with different δ. $k_h = 3k_t$

$$L_2 = \frac{L_1}{2\cos\delta}, \quad F_2 = \frac{F_1}{2\cos\delta} \tag{3.13}$$

$$m_2^2 = \frac{m_1^2}{2\cos^5\delta} = \frac{m_0^2}{(2\cos^5\delta)^2} \tag{3.14}$$

$$\left(\frac{r_2}{r_1}\right)^4 = (2\cos\delta)^{-3} \tag{3.15}$$

$$\left(\frac{r_2}{r_0}\right)^4 = (2\cos\delta)^{-6} \tag{3.16}$$

$$\frac{L_2}{L_1} = (2\cos\delta)^{-1} \tag{3.17}$$

$$\frac{L_2}{L_0} = (2\cos\delta)^{-2} \tag{3.18}$$

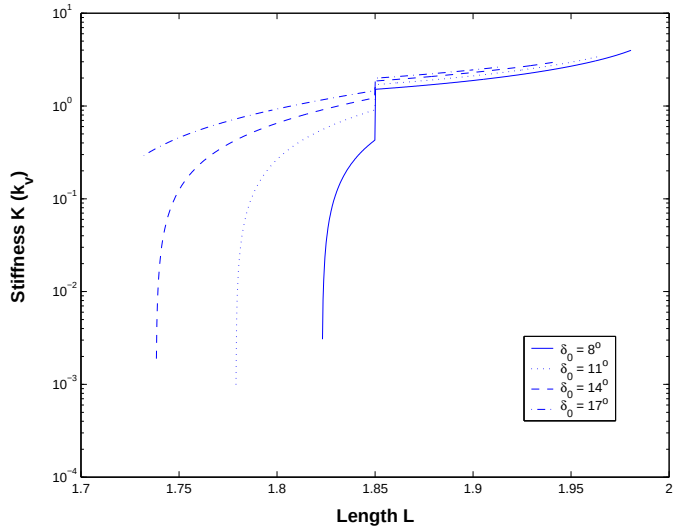

Fig. 3.4: Stiffness versus Length of $C4T2$ structure with different δ. $k_h = 3k_t$

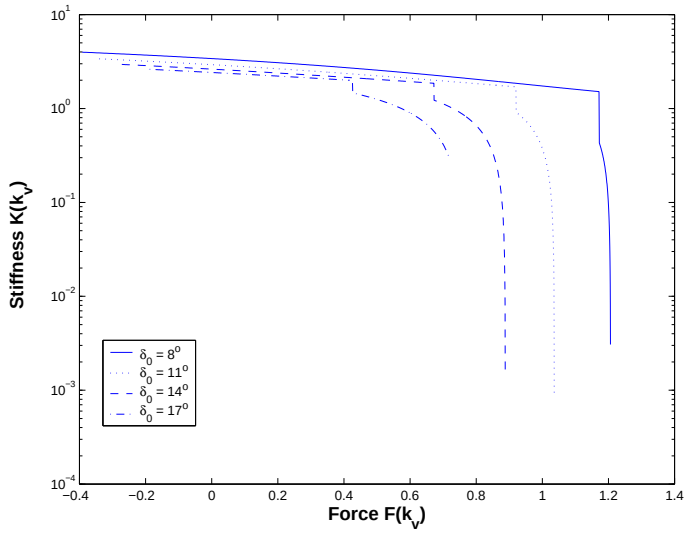

Fig. 3.5: Stiffness versus Force of $C4T1$ structure with different δ. $k_h = 3k_t$

$$\left(\frac{r_2}{r_1}\right)^4 = \left(\frac{L_2}{L_1}\right)^3 \tag{3.19}$$

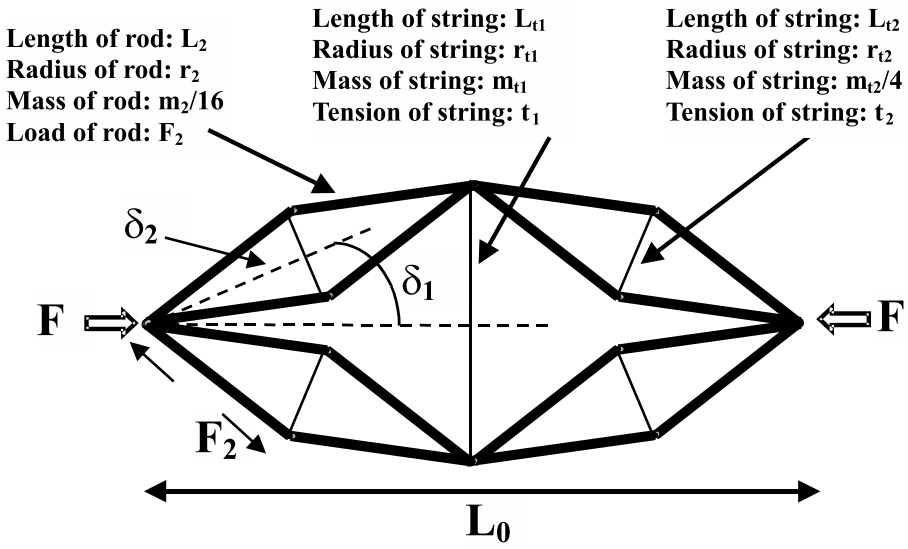

Fig. 3.6: A C16T5 Planar Tensegrity Structure. Points A are the same, and points B are the same, to illustrate that two identical bars overlap.

$$\left(\frac{r_2}{r_0}\right)^4 = \left(\frac{L_2}{L_0}\right)^3 \tag{3.20}$$

$$\frac{L_2}{r_2} = \frac{L_1}{r_1}(2\cos\delta)^{-\frac{1}{4}} = \frac{L_0}{r_0}(2\cos\delta)^{-\frac{1}{2}} \tag{3.21}$$

Now let us replace each bar in the structure of Fig. 3.6 by yet another $C4T1$ structure and continue this process indefinitely. In order to simplify language for these instructions, we coin some names that will simplify the description of the process we will later consider.

Definition 3 *Let the operation which replaces the bar of length L_0 with the design of Fig. 3.2 be called the "$C4T1$ operator." This replaces one compressive member with 4 compressive members plus one tension member, where the bar radii obey (3.23). Let δ be the same for any i. Let the operation which replaces the design of the bar Fig. 3.1 with the design of Fig. 3.6 be*

called the "$C4T1^2$ operator." If this $C4T1$ operation is repeated i times, then call it the "$C4T1^i$ operator," yielding the $C4T1^i$ system.

Lemma 2 *Let the $C4T1^i$ operator be applied to the initial bar, always using the same material and preserving buckling strength. Then the mass m_i, bar radius r_i, bar length L_i of the $C4T1^i$ system satisfy:*

$$\frac{m_i}{m_0} = (2\cos^5\delta)^{-\frac{i}{2}} \tag{3.22}$$

$$\frac{r_i}{r_0} = (2\cos\delta)^{-\frac{3i}{4}} = \left(\frac{L_i}{L_0}\right)^{\frac{3}{4}} \tag{3.23}$$

$$\frac{L_i}{L_0} = (2\cos\delta)^{-i} \tag{3.24}$$

$$\frac{L_i}{r_i} = \frac{L_0}{r_0}(2\cos\delta)^{-\frac{i}{4}} \tag{3.25}$$

$$F_i = \frac{E_0\pi r_i^4}{L_i^2} = \frac{E_0 m_i^2}{4^{2i}\rho_0^2 L_i^4} \tag{3.26}$$

$$m_i = 4^i\rho_0\pi r_i^2 L_i. \tag{3.27}$$

Note from (3.25) that the length to diameter ratio of the bars decreases with i if $\delta < 60°$.

Fig. 3.7 illustrates $C4T1^i$ structures for $i = 3, 4, 5, 6$. Taking the limit of (3.22) as $i \to \infty$ proves the following:

Theorem 1 *Suppose the compressive force which buckles a $C4T1^i$ system is a specified value, F. Then if $\delta < 29.477^o$, the total mass of the bars in the $C4T1^i$ system approaches zero as $i \to \infty$.*

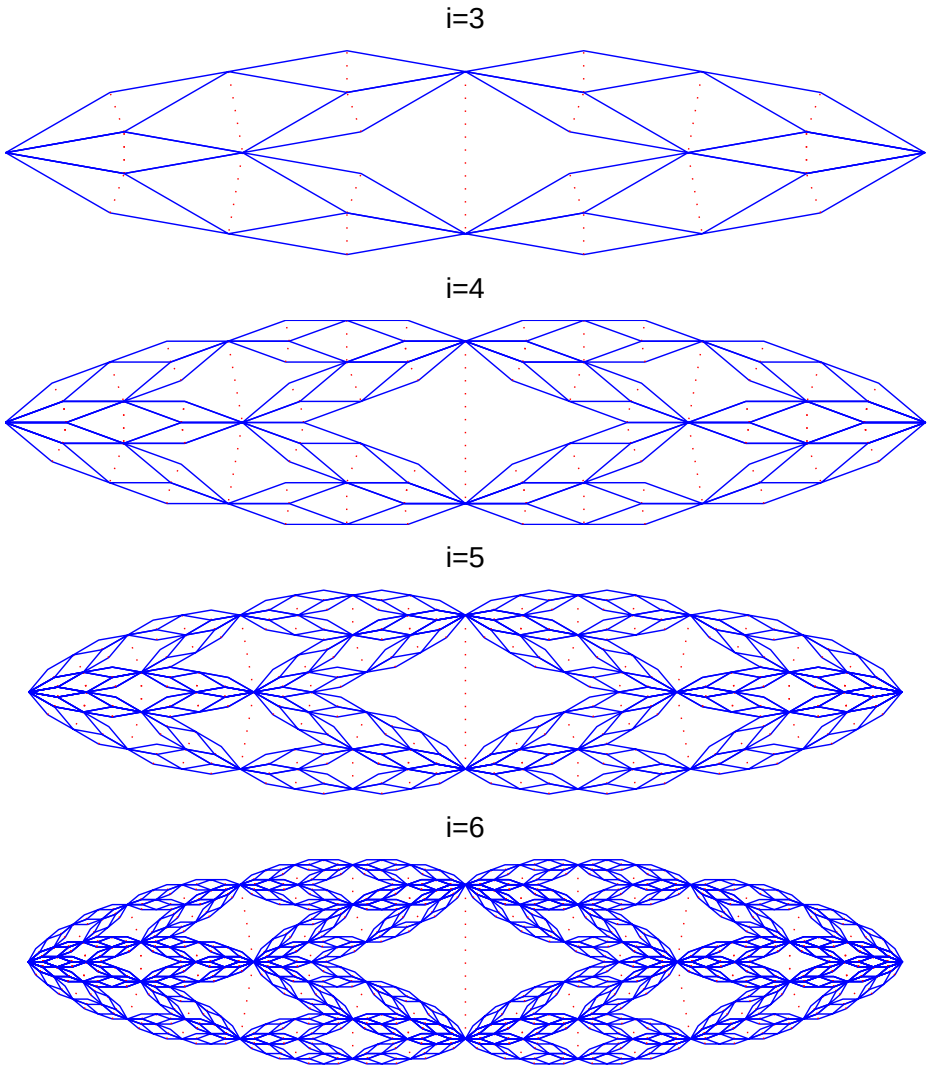

Fig. 3.7: A $C4T1^i$ Planar Tensegrity Structure for $i = 3, 4, 5, 6$.

Proof: Take i toward infinity in (3.22). □

Now suppose the number of self-similar iterations continue until the length of the bars are not longer than their diameters. Then, buckling cannot occur, and the structure is theoretically infinitely strong against buckling of the bars. But of course, the strings can still break. Therefore, ignoring the

obvious overlapping of material as the iterations become large, we cite this result which is more intriguing than practical.

Proposition 2 *The $C4T1^i$ structure is infinitely strong against buckling if i, δ satisfy*

$$(2\cos\delta)^i \geq \left(\frac{L_0}{2r_0}\right)^4 \tag{3.28}$$

Proof: The Euler buckling formula $F_B = \frac{\pi^2 EI}{L^2}$ applies to beams whose diameter is smaller than the length. Otherwise, buckling cannot occur. From Lemma 2, the diameter equals the length of the bar when $\frac{L_i}{2r_i} = \frac{L_0}{2r_0}(2\cos\delta)^{-\frac{i}{4}} = 1$. From (3.25) the i such that $\frac{L_i}{2r_i} = 1$, satisfies

$$\frac{L_0}{2r_0} = (2\cos\delta)^{\frac{i}{4}}. \tag{3.29}$$

□

As an example of (3.28) and (3.29), compared to a bar of length L_0 and radius r_0, the $C4T1^{18}$ structure with $\alpha = 10^o$ buckles at the same load as the original bar, has .39% of the mass of the original bar, and is infinitely stronger than the bar. For a given specified strength, this example suggests that solid materials are quite wasteful of mass. Of course, the above result has ignored the fact that the material overlaps, if one tried to place all elements in the same plane. However, multiple planar layers of elements can be pinned to give the desired planar effect mathematically described herein. A more important omission of the above analysis is the calculation of string mass. The string mass increases with self-similar iterations (increases with i) because strings are added in the process. The mass of the bars decrease with i, so obviously minimal mass of the system (bars plus strings) occurs at finite i. This calculation will be shown momentarily.

3.3.1 Robustness of the $C4T1$

In this section we mention briefly the issue of stability under a lateral force $F_L = 0$ in Fig. 3.2. We begin by mentioning two disastrous circumstances. Firstly, if the applied force F is small and F_L is big, then the $C4T1$ will collapse. Secondly, if the angle δ is very small and F is big, then a modest lateral force F_L will collapse the structure. Of course, a larger pretension in t_h will protect against larger F_L. Three important points on more general structures of this type: Firstly, big F always helps lateral robustness; secondly, larger δ helps lateral robustness; thirdly, increasing t_h helps robustness.

3.3.2 Mass and Tension of String in a $C4T1^1$ Structure

The mass m_{t1}, length L_{t1} and tension t_1 of string in the $C4T1^1$ structure are expressed as

$$m_{t1} = \rho_{t1} L_{t1} \pi r_{t1}^2, \tag{3.30}$$

$$L_{t1} = L_0 \tan\delta, \tag{3.31}$$

and

$$t_1 = F \tan\delta = \sigma_{t1} \pi r_{t1}^2. \tag{3.32}$$

respectively.
With (3.30) and (3.32),

$$t_1 = F \tan\delta = \sigma_{t1} \pi r_{t1}^2 = \sigma_{t1} \frac{m_{t1}}{\rho_{t1} L_{t1}}.$$

Hence,

$$\begin{aligned} m_{t1} &= \tfrac{\rho_{t1}}{\sigma_{t1}} L_{t1} F \tan\delta \\ &= \tfrac{\rho_{t1}}{\sigma_{t1}} (L_0 \tan\delta) \left(\tfrac{E_0 m_0^2}{\rho_0^2 L_0^4} \right) \tan\delta \\ &= \left(\tfrac{E_0 \tan^2\delta}{\sigma_{t1} L_0^3} \right) \left(\tfrac{\rho_{t1}}{\rho_0^2} \right) m_0^2 \\ &= \left(\tfrac{E_0 \tan^2\delta}{\sigma_{t1} L_0^3} \right) \left(\tfrac{\rho_{t1}}{\rho_0^2} \right) \rho_0 \pi r_0^2 L_0 m_0. \end{aligned}$$

So, the mass of string m_{t1} is

$$m_{t1} = \left(\frac{E_0 \tan^2 \delta}{4\sigma_{t1} l_0^2}\right)\left(\frac{\pi \rho_{t1}}{\rho_0}\right) m_0. \tag{3.33}$$

3.3.3 Total Mass of a $C4T1^1$ Structure

From (3.22) and (3.33), the total mass m_1 of the $C4T1^1$ structure is

$$m_1 = m_{t1} + m_{b1}$$

$$m_1 = \left[\left(\frac{E_0 \tan^2 \delta}{4\sigma_{t1} l_0^2}\right)\left(\frac{\pi \rho_{t1}}{\rho_0}\right) + \left(\frac{E_0}{E_1}\right)^{\frac{1}{2}}\left(\frac{\rho_1}{\rho_0}\right)\left(\frac{1}{2\cos^5 \delta}\right)^{\frac{1}{2}}\right] m_0. \tag{3.34}$$

For the same material of bar and string as that of the original structure, (3.34) is reduced to

$$m_1 = \left[\left(\frac{E_0 \pi \tan^2 \delta}{4\sigma_{t1} l_0^2}\right) + \left(\frac{1}{2\cos^5 \delta}\right)^{\frac{1}{2}}\right] m_0. \tag{3.35}$$

So, the minimal mass occurs at $\delta = 0°$, yielding $m_1 = \frac{1}{\sqrt{2}} m_0$. This configuration is shown in Fig. 3.8.

Figure 3.9 shows the plot of mass ratio $\frac{m_1}{m_0}$ versus δ for different l_0. It can be seen that the upper bound of δ is less than 29.477318° for mass reduction and also depends on the length to diameter ratio l_0.

3.3.4 $C4T1^i$ Structures

For bars, the Young's modulus, density and length to diameter ratio in $C4T1^i$ will be denoted as E_i, ρ_i and l_i respectively. For strings, the Young's modulus,

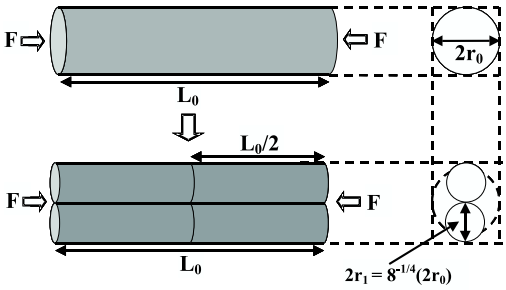

Fig. 3.8: The minimal mass of $C4T1^1$ structure (bottom) that replaces the $C4T1^0$ structure (top) with cross section area comparison (right)

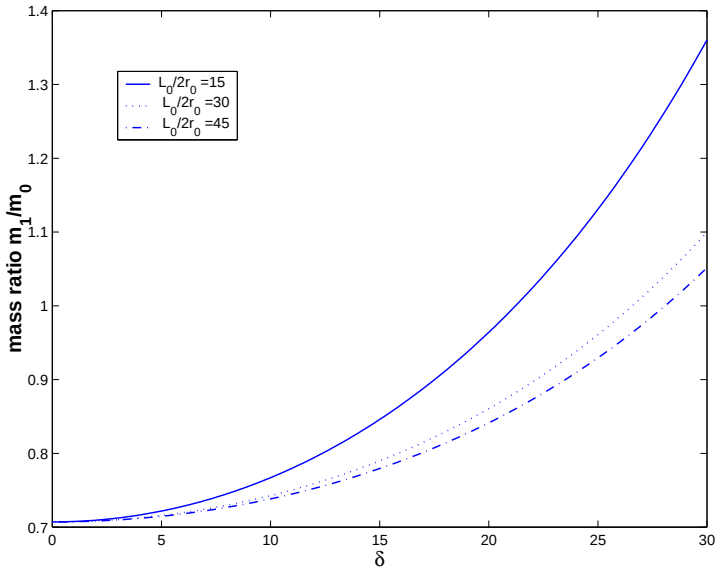

Fig. 3.9: mass ratio $\frac{m_1}{m_0}$ versus δ for different length to diameter ratio $l_0 = \frac{L_0}{2r_0}$

density and Yield strength in every stage j of $C4T1^i$ (where $j = 0, 1, 2...i-1, i$) will be denoted as E_{tj}, ρ_{tj} and σ_{tj} respectively. The extra subscript 't' is used to distinguish the string from bar. Applying the $C4T1^i$ operator to the original bar allows one to proceed from the $C4T1^0$ to $C4T1^i$ system. With

the similar analysis as before, the total mass of bars is

$$m_{bi} = 4^i \rho_i L_i \pi r_i^2. \tag{3.36}$$

The buckling load of each bar is

$$F_i = \frac{E_i \pi^2 r_i^4}{L_i^2} = \frac{E_i m_{bi}^2}{4^{2i} \rho_i^2 L_i^4}. \tag{3.37}$$

From the geometry of the structure, the length and load of each bar are

$$L_i = \frac{L_{i-1}}{2\cos\delta_i} = \frac{L_0}{\prod_{j=1}^{i} 2\cos\delta_j}, \tag{3.38}$$

and

$$F_i = \frac{F_{i-1}}{2\cos\delta_i} = \frac{F}{\prod_{j=1}^{i} 2\cos\delta_j}, \tag{3.39}$$

respectively, where δ_j is the angle described in the same way as in Fig. 3.6 and all δ_j might be equal, or might be different.

3.3.5 Mass of Bars in a $C4T1^i$ Structure

From (3.36),(3.37), (3.38) and (3.39), the total mass of the bars in $C4T1^i$ can be related to the mass of $C4T1^0$ through

$$F_i = \frac{E_i m_{bi}^2}{4^{2i} \rho_i^2 L_i^4} = \frac{F}{\prod_{j=1}^{i} 2\cos\delta_j} = \frac{E_0 m_0^2}{\rho_0^2 L_0^4 \prod_{j=1}^{i} 2\cos\delta_j}$$

$$m_{bi}^2 = \left(\frac{E_0}{E_i}\right)\left(\frac{\rho_i}{\rho_0}\right)^2 \frac{1}{\prod_{j=1}^{i} 2\cos^5\delta_j} m_0^2. \tag{3.40}$$

3.3.6 Length to Diameter Ratio of Bar in a $C4T1^i$ Structure

The length to diameter ratio of the bars in $C4T1^i$ will be l_i given by

$$l_i = \frac{L_i}{2r_i} = \left(\frac{E_i}{E_0}\right)^{\frac{1}{4}} \left(\frac{1}{\prod_{j=1}^{i} 2\cos\delta_j}\right)^{\frac{1}{4}} l_0. \tag{3.41}$$

3.3.7 Mass and Tension of Strings in a $C4T1^i$ Structure

Generalizing the concept from the previous section, the mass, length and tension of the strings in the j-th iteration ($j = 1, 2, 3, ...i-1, i$) of $C4T1^i$ will be

$$m_{tj} = 4^{j-1}\rho_{tj} L_{tj} \pi r_{tj}^2, \tag{3.42}$$

where (r_{tj}, L_{tj}) is the radius and length of the strings,

$$L_{tj} = 2L_j \sin\delta_j = \frac{2L_0 \sin\delta_j}{\prod_{r=1}^{j} 2\cos\delta_r}, \tag{3.43}$$

and

$$t_j = 2F_j \sin\delta_j = \frac{2F\sin\delta_j}{\prod_{r=1}^{j} 2\cos\delta_j} = \sigma_{tj}\pi r_{tj}^2, \tag{3.44}$$

where σ_{tj} is the yield stress of the string.
With (3.42), (3.43) and (3.44), the mass of the each string in the i-th iteration can be related to the mass of $C4T1^0$

$$t_j = \frac{2\sin\delta_j}{\prod_{r=1}^{j} 2\cos\delta_r}\left(\frac{E_0 m_0^2}{\rho_0^2 L_0^4}\right) = \sigma_{tj}\left(\frac{4}{4^j}\right)\left(\frac{m_{tj}\prod_{s=1}^{j} 2\cos\delta_s}{2\rho_{tj} L_0 \sin\delta_j}\right)$$

$$m_{tj} = \frac{E_0 \sin^2\delta_j}{4\sigma_{tj} l_0^2 \prod_{r=1}^{j}\cos^2\delta_r}\left(\frac{\pi\rho_{tj}}{\rho_0}\right) m_0. \tag{3.45}$$

3.3.8 Total Mass of $C4T1^i$ Structure

The total mass m_i of the $C4T1^i$ structure will be

$$m_i = m_{bi} + \sum_{j=1}^{i} m_{tj}.$$

With (3.40) and (3.45)
(3.46)

$$m_i = \left[\left(\frac{E_0}{E_i} \right)^{\frac{1}{2}} \left(\frac{\rho_i}{\rho_0} \right) \left(\frac{1}{\prod_{j=1}^{i} 2\cos^5 \delta_j} \right)^{\frac{1}{2}} + \sum_{j=1}^{i} \frac{E_0 \sin^2 \delta_j}{4\sigma_{tj} l_0^2 \prod_{r=1}^{j} \cos^2 \delta_j} \left(\frac{\pi \rho_{tj}}{\rho_0} \right) \right] m_0.$$

For the same angle $\delta_j = \delta$ and same material of bars and strings in every j-th stage, the total mass can be simplified to

$$m_i = \left[\left(\frac{1}{2\cos^5 \delta} \right)^{\frac{i}{2}} + \frac{E_0 \pi}{4\sigma_t l_0^2} \left(\frac{1}{\cos^{2i} \delta} - 1 \right) \right] m_0. \tag{3.47}$$

Figures 3.10 shows the plot of mass ratio $(\frac{m_i}{m_0})$ versus the number of iteration for different δ and $l_0 = 30$. From the figure, smaller angles δ will lead to larger mass reduction, and larger length to diameter ratio l_0 also enhances the mass reduction effect.

Figure 3.11 shows the plot of the mass ratio of bars to strings versus the angle δ for $l_0 = 30$. Bars will dominate the mass of structure at small δ and at a small number of iterations i.

Figure 3.12 shows the plot of δ versus the number of iterations for different length to diameter ratios such that $m_i = m_0$. Regions below each curve are the allowed regions for mass reduction.

Note that if $\delta \leq 29.477318°$ and the use of materials are the same for every iteration, from (3.40), the mass of bars decreases as the number of iterations increase. However, the mass reduction will be offset by the increase of string mass as can be seen from (3.47). Therefore, maximum mass reduction can be achieved in some finite number of iterations which depends on the angle δ and length to diameter ratio l_0.

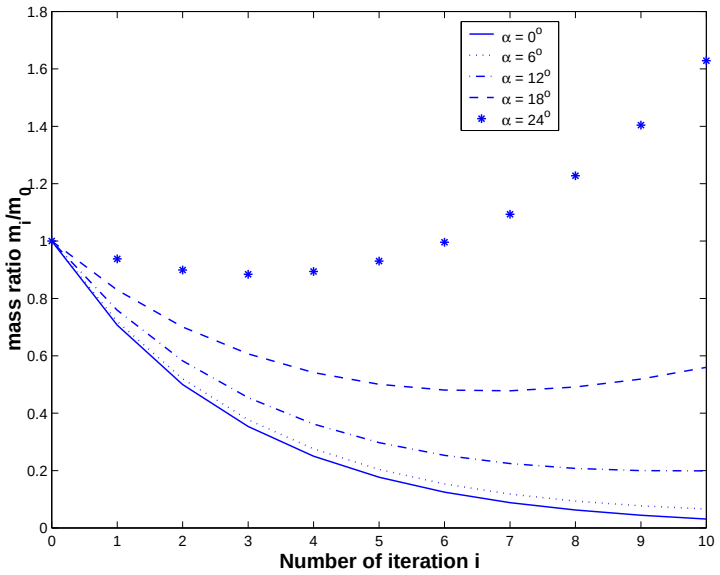

Fig. 3.10: mass ratio $\frac{m_i}{m_0}$ versus number of iteration for length to diameter ratio $l_0 = 30$

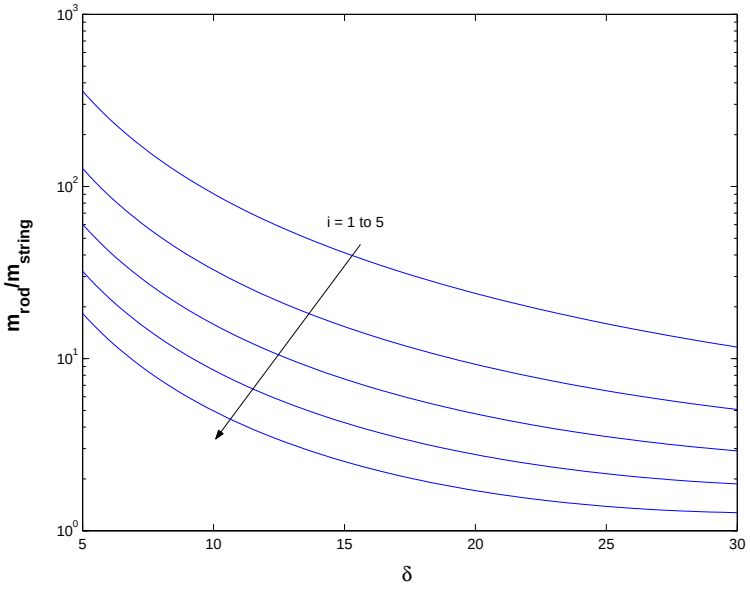

Fig. 3.11: mass ratio $\frac{m_{bar}}{m_{string}}$ versus δ of $C4T1^i$ with $l_0 = \frac{L_0}{2r_0} = 30$

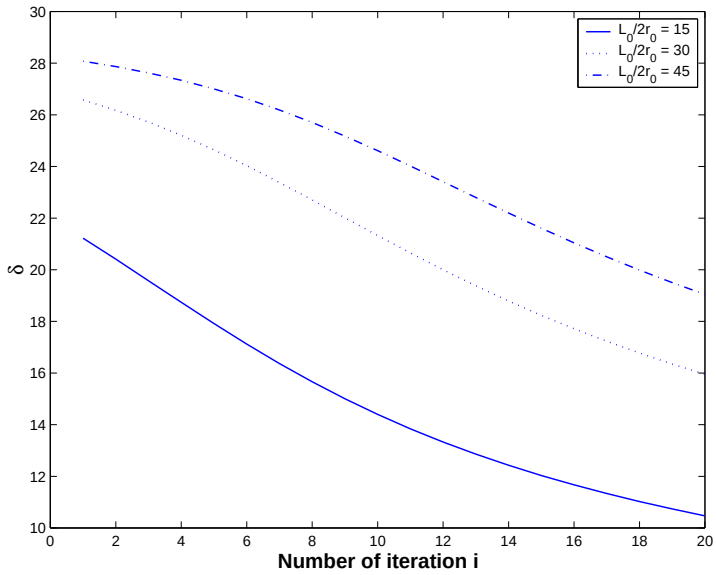

Fig. 3.12: δ versus number of iteration i for different for mass ratio $\frac{m_i}{m_0} = 1$ of iteration i

In fact, from (3.47), the mass reduction will be maximum when the number of iteration i, which is given by the following theorem:

Theorem 2 *Assume all bars and strings are composed of the same material. Let the $C4T1^i$ operator be applied to the original bar to get the $C4T1^i$ system, where the iterations are designed to preserve the buckling strength of the original bar. Minimum mass is achieved at a finite number of iterations and this number is given by either i_1 or i_2, where*

(3.48)

$$i_1 = \left\lceil \frac{2}{\ln\left(\frac{1}{2\cos\delta}\right)} \ln\left(\frac{E_0\pi}{\sigma_t l_0^2} \frac{\ln\cos\delta}{\ln\frac{1}{2\cos^5\delta}}\right) \right\rceil, \quad i_2 = \left\lfloor \frac{2}{\ln\left(\frac{1}{2\cos\delta}\right)} \ln\left(\frac{E_0\pi}{\sigma_t l_0^2} \frac{\ln\cos\delta}{\ln\frac{1}{2\cos^5\delta}}\right) \right\rfloor,$$

where $\lceil\ \rceil$ ($\lfloor\ \rfloor$) implies rounding up (down) to the closest integer. One must check the mass at both i_1 and i_2 to choose the smallest mass.

Proof: Let $\mu = \frac{m_i}{m_0}$, then, from (3.47),

$$\mu = \left(\frac{1}{2\cos^5\delta}\right)^{\frac{i}{2}} + \frac{E_0}{4\sigma_t l_0^2}\left(\frac{\pi\rho_t}{\rho_0}\right)\left(\frac{1}{\cos^{2i}\delta} - 1\right).$$

Take the derivative of μ w.r.t i by using the rule $\frac{da^x}{dx} = a^x \ln a$, and set it equal to zero to obtain

$$\frac{d\mu}{di} = \frac{1}{2}\left(\frac{1}{2\cos^5\delta}\right)^{\frac{i}{2}} \ln\left(\frac{1}{2\cos^5\delta}\right) + \frac{E_0}{4\sigma_t l_0^2}\left(\frac{\pi\rho_t}{\rho_0}\right)\frac{2}{\cos^{2i}\delta}\ln\left(\frac{1}{\cos\delta}\right) = 0.$$

Rearranging the equation gives

$$\left(\frac{1}{2\cos\delta}\right)^{\frac{i}{2}} = \frac{E_0}{\sigma_t l_0^2}\left(\frac{\pi\rho_t}{\rho_0}\right)\frac{\ln\cos\delta}{\ln\left(\frac{1}{2\cos^5\delta}\right)}.$$

Solving for i yields (3.48). □

Figure 3.13 shows the plot of the optimal iteration in (3.48) versus angle δ for maximum mass reduction given by (3.48).

Figure 3.14 shows the plot of the ratio of bar mass to string mass, versus δ at the optimal iteration given by (3.48). Note that at $\delta = 20°$ and $l_0 = 30$, the total bar mass and the total string mass are equal. Figure 3.15 shows the corresponding plot of total mass ratio.

3.4 Stiffness of the $C4T1^i$ Structure

3.4.1 Stiffness Definition

For the $C4T1i$, the structure will change it length (measured from 2 nodal points where external applied) in the same direction as the applied force.

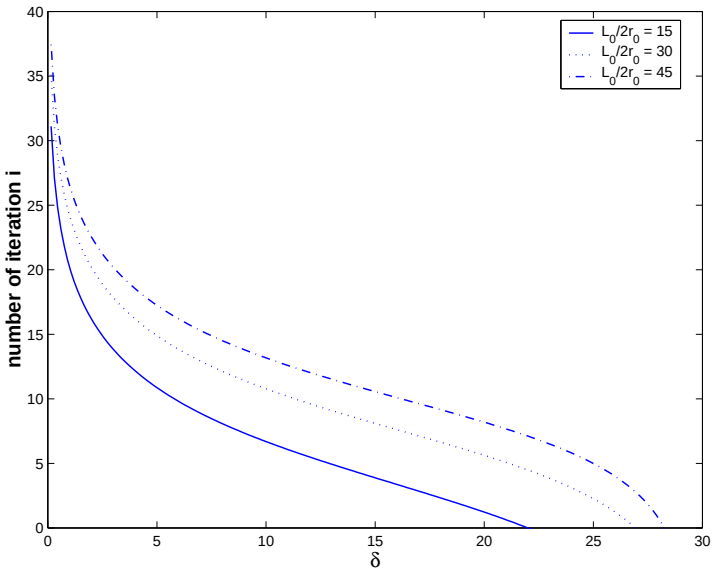

Fig. 3.13: optimal number of iteration i versus δ for maximum mass reduction

Therefore, the stiffness calculation is one-dimensional problem. For an external load F applied to the structure of length L, the stiffness K of the structure is defined as

$$K = -\frac{dF}{dL}, \tag{3.49}$$

where the negative sign means the length of the structure decreases as the applied load increases. Since the external load can be related to the potential energy of the structure U by

$$F = -\frac{dU}{dL},$$

the stiffness can also be calculated from the potential energy by

$$K = \frac{d^2U}{dL^2}. \tag{3.50}$$

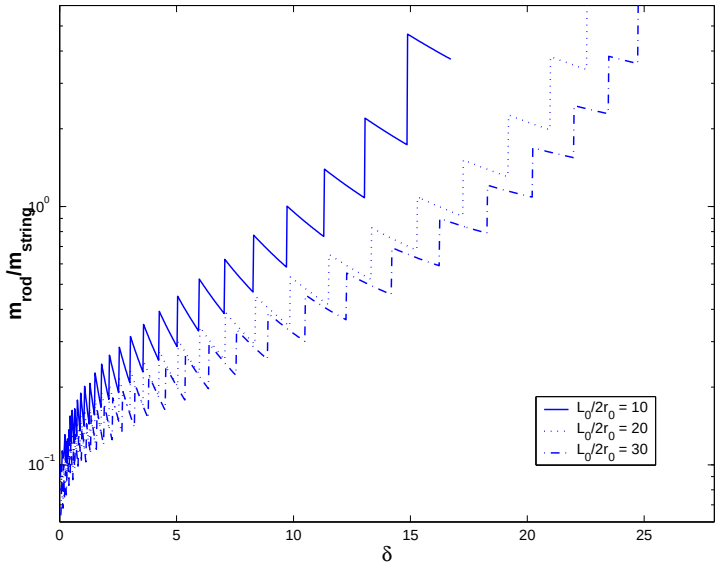

Fig. 3.14: mass ratio of bars to strings $\frac{m_{bar}}{m_{string}}$ versus δ at the optimal iteration

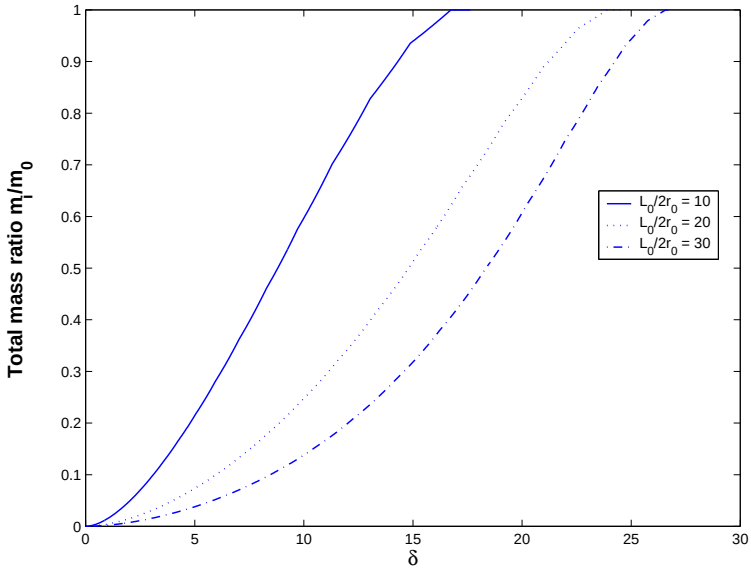

Fig. 3.15: Total mass ratio $\frac{m_i}{m_0}$ versus δ at the optimal iteration

3.4.2 The Stiffness Equation of a $C4T1^i$ Structure

In the calculations of stiffness (see Appendix C), it is assumed that the stiffness of bars k_{bi} and strings k_{tj}, where $1 \leq j \leq i$, are constant under deformation. This is not always a good assumption, but other string stiffness models, such as $k = \frac{EA}{L}$ can be analyzed in a straightforward manner. If L_{i0} and L_{tj0} are the rest lengths of bars in the i-th iteration and strings in the j-th iteration respectively, the stiffness of $C4T1^i$ is given by

(3.51)

$$K_i = k_{t1}\left\{\left(\frac{L_{t10}}{L_{t1}} - 1\right) + \left[4^i \frac{k_{t1}}{k_{bi}}\frac{L_i}{L_{i0}}\left(\frac{L_i}{L_0}\right)^2 + \sum_{j=1}^{i} 4^{j-1}\frac{k_{t1}}{k_{tj}}\frac{L_{tj}}{L_{tj0}}\left(\frac{L_{tj}}{L_0}\right)^2\right]^{-1}\right\},$$

where, in the buckling design (see Appendix B)

$$\begin{aligned}
L_0 &= L_i \textstyle\prod_{s=1}^{i} 2\cos\delta_s \\
L_{tj} &= 2L_i \sin\delta_j \textstyle\prod_{s=j+1}^{i} 2\cos\delta_s \\
\tfrac{k_{t1}}{k_{tj}} &= \tfrac{E_{t1}\sigma_{tj}}{E_{tj}\sigma_{t1}} \\
\tfrac{k_{t1}}{k_{bi}} &= \tfrac{E_{t1}\pi}{4\sigma_{t1}l_0^2}\sqrt{\tfrac{E_0}{E_i}}\left(\textstyle\prod_{s=1}^{i} 2\cos\delta_s\right)^{\frac{1}{2}} \\
\tfrac{L_{tj0}}{L_{tj}} &= 1 - \tfrac{\sigma_{tj}}{E_{tj}} \\
k_{t1} &= \tfrac{E_0 E_{t1}\pi^2 L_0}{16\sigma_{t1}l_0^4} \\
\tfrac{L_{i0}}{L_i} &= 1 + \tfrac{\pi}{4l_0^2}\left(\textstyle\prod_{s=1}^{i} 2\cos\delta_s\right)^{\frac{1}{2}}.
\end{aligned}$$

In particular, if the materials of bars and strings used are the same as that of original structure ($C4T1^0$) and $\delta_j = \delta$, the stiffness equation will be simplified to

$$K_i = k_{t1}\left\{-\frac{\sigma_t}{E_t} + \left[4^i \frac{k_{t1}}{k_{bi}}\frac{L_i}{L_{i0}}\left(\frac{L_i}{L_0}\right)^2 + \left(1 - \frac{\sigma_t}{E_t}\right)^{-1}\sum_{j=1}^{i} 4^{j-1}\left(\frac{L_{tj}}{L_0}\right)^2\right]^{-1}\right\}$$

(3.52)

$$K_i = k_{t1}\left\{-\frac{\sigma_t}{E_t} + \left[4^i \frac{k_{t1}}{k_{bi}}\frac{L_i}{L_{i0}}\left(\frac{L_i}{L_0}\right)^2 + \left(1 - \frac{\sigma_t}{E_t}\right)^{-1}\left(\frac{1}{\cos^{2i}\delta} - 1\right)\right]^{-1}\right\}$$

where

$$\begin{aligned} L_0 &= L_i(2\cos\delta)^i \\ \frac{k_{t1}}{k_{bi}} &= \frac{E_t\pi}{4\sigma_t l_0^2}\left(2\cos\delta\right)^{\frac{i}{2}} \\ k_{t1} &= \frac{E_0E_t\pi^2L_0}{16\sigma_t l_0^4} \\ \frac{L_{i0}}{L_i} &= 1+\frac{\pi}{4l_0^2}\left(2\cos\delta\right)^{\frac{i}{2}}. \end{aligned}$$

3.4.3 The Rigid Bar Case

If the bar has infinite rigidity (large compared to the stiffness of strings), this means

$$\frac{k_{ti}}{k_{bi}} \to 0,$$

then, the stiffness equation becomes

$$K_i = k_{t1}\left(\frac{\cos^{2i}\delta - \frac{\sigma_t}{E_t}}{1-\cos^{2i}\delta}\right), \tag{3.53}$$

where

$$k_{t1} = \frac{E_0E_t\pi^2L_0}{16\sigma_t l_0^4}.$$

Figure 3.16 shows the plot of stiffness to length ratio $\frac{K_i}{L_0}$ versus δ for length to diameter ratio $l_0 = 30$.

Figure 3.17 shows the plot of the stiffness ratio $\frac{K_i}{k_{t1}}$ versus δ for the infinite rigid bar $C4T1^i$ structure. Note that the ratio is independent of l_0.

Since the stiffness reduces with each iteration i, it is of interest to know how many iterations may be taken before the stiffness violates a desired lower bound $\underline{K}$.

Proposition 3 *Given δ and a desired lower bound stiffness $\underline{K}$ of $C4T1^i$, that is, $\underline{K} \leq K_i$, the number of iterations i which achieve this stiffness requirement*

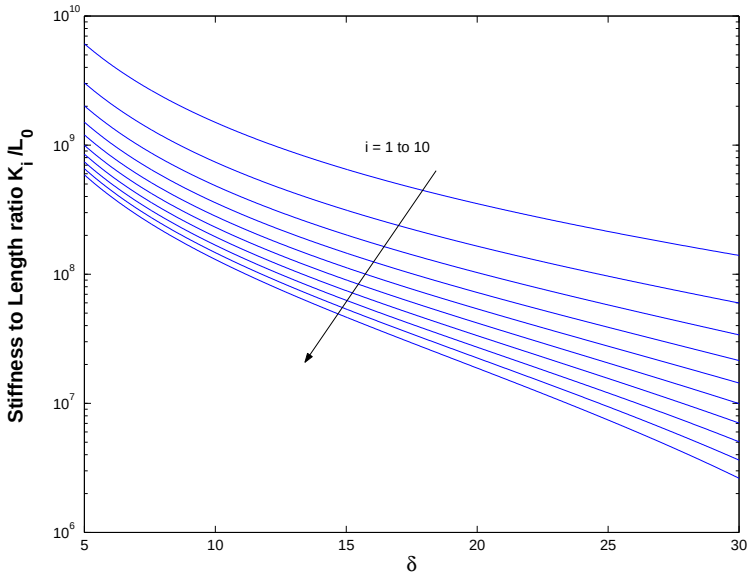

Fig. 3.16: Stiffness to length ratio $\frac{K_i}{L_0}$ of structure with rigid bars versus δ for $l_0 = 30$

is bounded by

$$i \leq \frac{\log \frac{\frac{\underline{K}}{k_{t1}} + \frac{\sigma_t}{E_t}}{1 + \frac{\underline{K}}{k_{t1}}}}{2 \log \cos \delta}. \tag{3.54}$$

Proof: From (3.53),

$$\begin{aligned} \underline{K} &\leq K_i \\ &\leq k_{t1} \left(\frac{\cos^{2i} \delta - \frac{\sigma_t}{E_t}}{1 - \cos^{2i} \delta} \right). \end{aligned}$$

Rearrange the inequality to expose $\cos^{2i} \delta$ on one side and then take the log of both sides to obtain (3.54). □

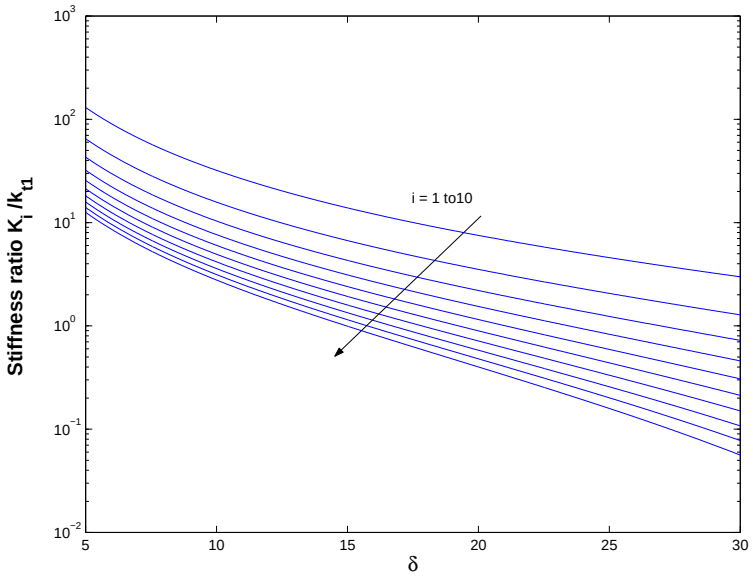

Fig. 3.17: Stiffness ratio $\frac{K_i}{k_{t1}}$ of $C4T1^i$ structure with rigid bars versus δ

3.4.4 The Elastic Bar Case

If the bars in the $C4T1^i$ structure is elastic,

$$\frac{k_{ti}}{k_{bi}} \neq 0,$$

and hence (3.52) will be used for numerical calculations.
Figure 3.18 shows the plot of stiffness to length ratio $\frac{K_i}{L_0}$ versus δ for length to diameter ratio $l_0 = 30$.

Figure 3.19 shows the corresponding plot of stiffness ratio $\frac{K_i}{k_{t1}}$ versus δ for Fig. 3.18. A comparison of Figs. 3.16 to 3.19 reveals that with elastic bars, the system stiffness is much less than for system made with rigid bars.

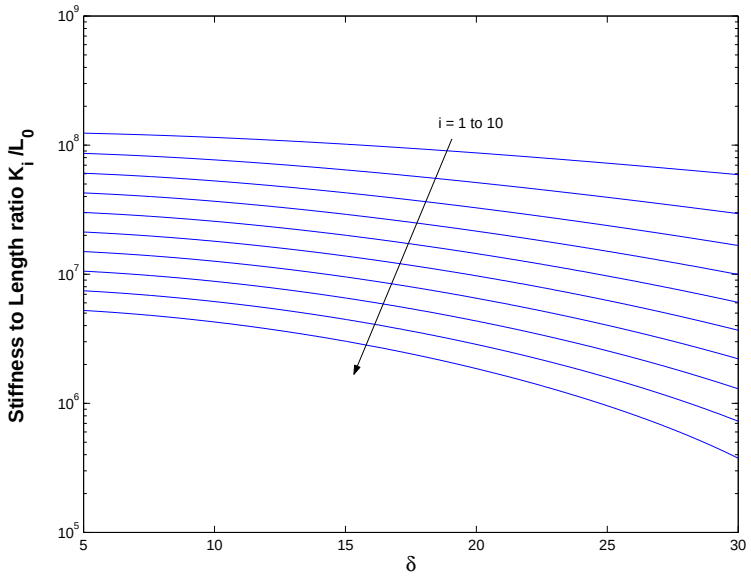

Fig. 3.18: Stiffness to length ratio $\frac{K_i}{L_0}$ versus δ for length to diameter ratio $l_0 = 30$, for elastic bars

Stiffness ratio $\frac{K_i}{K_0}$

The stiffness of $C4T1^0$ (a single bar) is

$$K_0 = \frac{E_0 \pi r_0^2}{L_0}. \tag{3.55}$$

With (3.52), the stiffness ratio $\frac{K_i}{K_0}$ is given by

$$\frac{K_i}{K_0} = \left(\frac{E_t \pi}{4\sigma_t l_0^2}\right) \left\{ -\frac{\sigma_t}{E_t} + \left[4^i \frac{k_{ti}}{k_{bi}} \frac{L_i}{L_{i0}} \left(\frac{L_i}{L_0}\right)^2 + \left(1 - \frac{\sigma_t}{E_t}\right)^{-1} \left(\frac{1}{\cos^{2i}\delta} - 1\right) \right]^{-1} \right\}, \tag{3.56}$$

where other physical quantities are the same as the that given in (3.52).

Figure 3.20 shows the plot of stiffness ratio $\frac{K_i}{K_0}$ versus δ for length to diameter ratio $l_0 = 30$.

Figures 3.17, 3.19 and 3.20 demonstrate that stiffness is much less sensitive to geometry (choice of δ) when bars are elastic than when the bars are rigid.

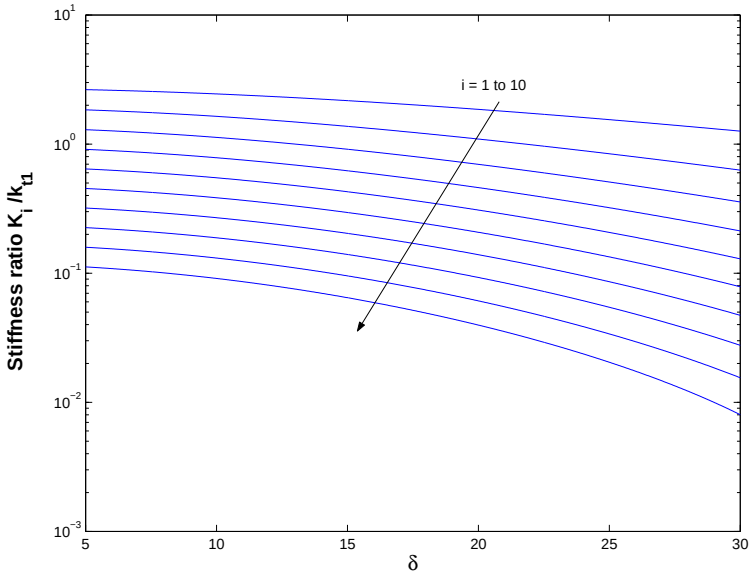

Fig. 3.19: Stiffness ratio $\frac{K_i}{k_{t1}}$ versus δ for length to diameter ratio $l_0 = 30$, for elastic bars

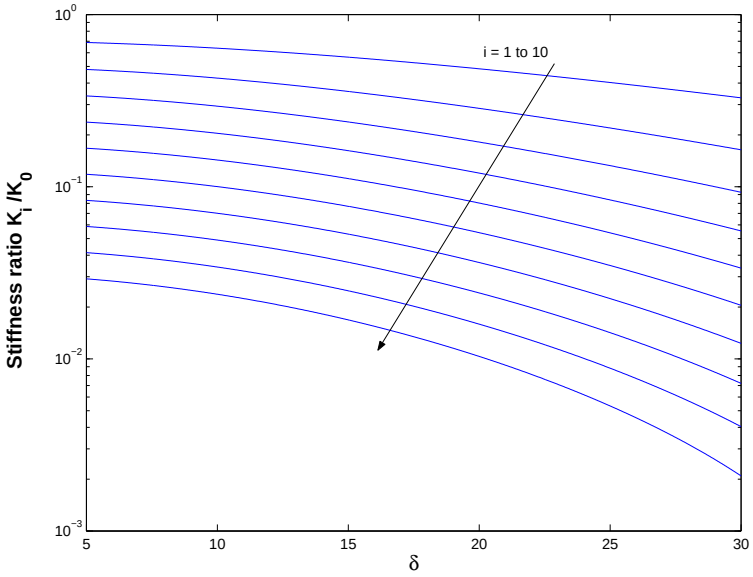

Fig. 3.20: Stiffness ratio $\frac{K_i}{K_0}$ versus δ for $l_0 = 30$, for elastic bars

Stiffness to Mass ratio

From (3.47) and (3.52), the stiffness to mass ratio is given by

(3.57)

$$\frac{K_i}{m_i} = \left(\frac{E_0 E_t \pi}{4\sigma_t \rho_0 l_0^2 L_0^2}\right) \left\{ \frac{-\frac{\sigma_t}{E_t} + \left[4^i \frac{k_{ti}}{k_{bi}} \frac{L_i}{L_{i0}} \left(\frac{L_i}{L_0}\right)^2 + \left(1 - \frac{\sigma_t}{E_t}\right)^{-1} \left(\frac{1}{\cos^{2i}\delta} - 1\right)\right]^{-1}}{\left(\frac{1}{2\cos^5\delta}\right)^{\frac{i}{2}} + \frac{E_0 \pi}{4\sigma_t l_0^2}\left(\frac{1}{\cos^{2i}\delta} - 1\right)} \right\},$$

where other physical quantities are the same as that given in (3.52).

Figures 3.21 and 3.22 show the corresponding plots of stiffness to mass ratio $\frac{K_i}{m_i}$, for 2 different choices of length to diameter ratio l_0. Note that for $\delta \leq (\geq) 14^\circ$ and $l_0 = 30$, the stiffness-to-mass ratio increases (decreases) with iteration i. For $\delta = 14^\circ$ and $l_0 = 45$, the stiffness-to mass ratio remains constant with self-similar iteration i.

3.5 $C4T1^i$ Structure with Elastic bars and Constant Stiffness

Given a bar of radius r_0 and length L_0 under applied force F (not buckling load), this section shows how to design the $C4T1^i$ structure to minimize the use of mass by replacing the bar with the $C4T1^i$ structure such that the stiffness of the structure is the same as that of bar under the same applied load F.

It is assumed that the stiffness of member bars and strings are constant and is given by

(3.58)
$$k = \frac{E\pi r^2}{L},$$

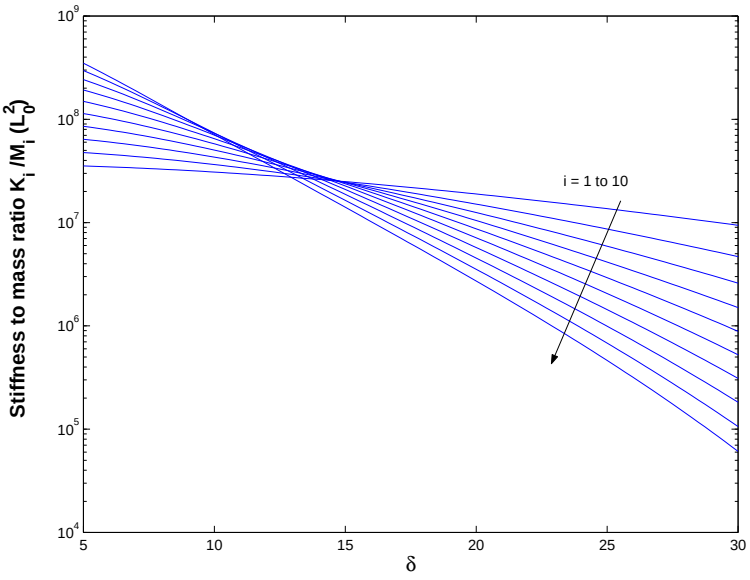

Fig. 3.21: Stiffness to mass ratio $\frac{K_i}{m_i}$ versus δ for $l_0 = 30$

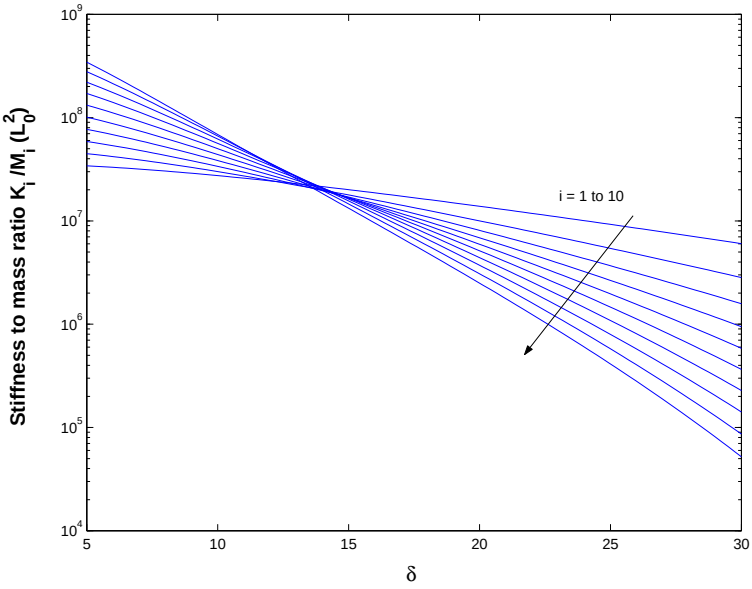

Fig. 3.22: Stiffness to mass ratio $\frac{K_i}{m_i}$ versus δ for $l_0 = 45$

where r and L are the cross section radius and length of bars or strings when the $C4T1^i$ structure is under external load F.

3.5.1 $C4T1^1$ at $\delta = 0°$

At $\delta = 0°$, it is known from the previous section that the use of mass is minimum while the stiffness is maximum. Therefore, a simple analysis of $C4T1^1$ at $\delta = 0$ will give the idea whether it is possible to reduce while preserving stiffness.

For the $C4T1^0$ structure, the stiffness is given by

$$K_0 = \frac{E\pi r_0^2}{L_0}. \tag{3.59}$$

For $C4T1^1$ structure at $\delta = 0°$, i.e. 2 pairs of parallel bars in series with each other, the length of each bar is $\frac{L_0}{2}$ and its stiffness is

$$k_b = \frac{E\pi r_1^2}{L_1} = \frac{2E\pi r_1^2}{L_0}. \tag{3.60}$$

For this 4 bars arrangement, the equivalent stiffness is same as the stiffness of each bar. i.e.

$$K_1 = \frac{2E\pi r_1^2}{L_0}. \tag{3.61}$$

To preserve stiffness, it is required that

$$K_1 = K_0$$

$$\frac{2E\pi r_1^2}{L_0} = \frac{E\pi r_0^2}{L_0}.$$

So,

$$r_0^2 = 2r_1^2. \tag{3.62}$$

Then, the mass of $C4T1^1$ at $\delta = 0^\circ$ for stiffness preserving design is

$$m_1 = 4\rho\pi r_1^2 L_1 = 4\rho\pi \frac{r_0^2}{2}\frac{L_0}{2} = \rho\pi r_0^2 L_0 = m_0, \tag{3.63}$$

which indicates, at $\delta = 0^\circ$, the mass of $C4T1^1$ is equal to that of $C4T1^0$ in a stiffness preserving design. Therefore, the mass reduction of $C4T1^i$ structure in a stiffness preserving design is unlikely to happen. However, if the horizontal string t_h is added in the $C4T1^1$ element to make it a $C4T2$ element, then stiffness can be improved, as shown in (3.11).

3.6 Summary of Chapter 3

This chapter illustrates the concept of self-similar tensegrity structures of class k. For the example of massless strings and rigid bars replacing a bar with a class 2 tensegrity structure $C4T1$ with specially chosen geometry, $\delta < 29^\circ$, the mass of the new system is less than the mass of the bar, the strength of the bar is matched, and a stiffness bound can be satisfied. Continuing this process for a finite member of iterations yields a system mass that is minimal for these stated constraints. This optimization problem is analytically solved and does not require complex numerical codes. For elastic bars, analytical expressions are derived for the stiffness, and choosing the parameters to achieve a specified stiffness is straightforward numerical work. It is also interesting to note that the *stiffness-to-mass* ratio can be improved with the number of self-similar iterations, whereas the *stiffness* always decreases.

Chapter 4

Statics of a 3–Bar Tensegrity

4.1 Classes of Tensegrity

The tensegrity unit studied here is the simplest three–dimensional tensegrity unit which comprises three bars held together in space by strings so as to form a tensegrity unit. A tensegrity unit comprising of three bars will be called a 3–bar tensegrity. A 3–bar tensegrity is constructed by using three bars in each stage which are twisted either in clockwise or in anti–clockwise direction. The top strings connecting the top of each bar support the next stage in which the bars are twisted in a direction opposite to the bars in the previous stage. In this way any number of stages can be constructed which will have an alternating clockwise and anti–clockwise rotation of the bars in each successive stage. This is the type of structure in Snelson's Needle Tower, Fig. 1.1. The strings that support the next stage are known as the "saddle strings (S)". The strings that connect the top of bars of one stage to the top of bars of the adjacent stages or the bottom of bars of one stage to the bottom of bars of the adjacent stages are known as the "diagonal strings (D)," whereas the strings that connect the top of the bars of one stage to the bottom of the bars of the same stage are known as the "vertical strings (V)."

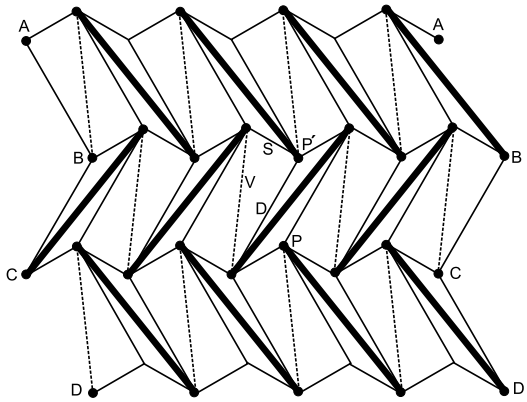

Fig. 4.1: Unfolded tensegrity architecture.

Figure 4.1 illustrates an unfolded tensegrity architecture where the dotted lines denote the "vertical" strings in Fig. 4.2 and thick lines denote bars. Closure of the structure by joining points A, B, C, D yield a tensegrity beam with four bars per stage as opposed to the example in Fig. 4.2 which employs only three bars per stage. Any number of bars per stage may be employed by increasing the number of bars laid in the lateral direction and any number of stages can be formed by increasing the rows in the vertical direction in

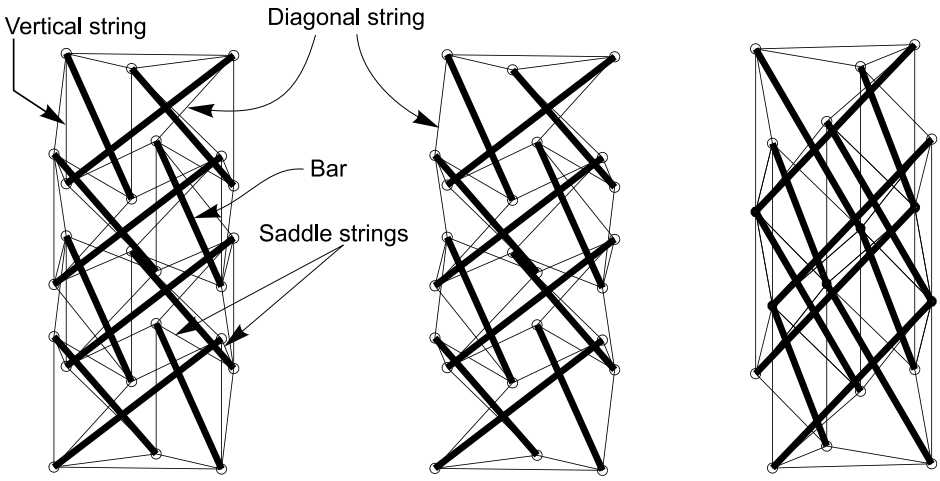

(a) 3–Bar SVD Tensegrity (b) 3–Bar SD Tensegrity (c) 3–Bar SS Tensegrity

Fig. 4.2: Types of structures with three bars in one stage.

Fig. 4.1.

Even with only three bars in one stage, which represents the simplest form of a three dimensional tensegrity unit, various types of tensegrities can be constructed depending on how these bars have been held in space to form a beam that satisfies the definition of tensegrity. Three variations of a 3–bar per stage structure are described below.

3–Bar SVD Class 1 Tensegrity: A typical two stage 3–bar SVD tensegrity is shown in Fig. 4.2(a) in which the bars of the bottom stage are twisted in the anti–clockwise direction. As is seen in Fig. 4.1 and Fig. 4.2(a), these tensegrities are constructed by using all three types of strings, viz. saddle strings (S), vertical strings (V), and the diagonal strings (D), hence the name SVD tensegrity.

3–Bar SD Class 1 Tensegrity: These types of tensegrities are constructed by eliminating the vertical strings to obtain a stable equilibrium with the minimal number of strings. Thus a SD type tensegrity only has saddle (S) and the diagonal strings (D), as shown in Fig. 4.1 and Fig. 4.2(b).

3–Bar SS Class 2 Tensegrity: It is natural to examine the case when the bars are connected with a ball joint. If one connects points P and P$'$ in Fig. 4.1, the resulting structure is shown in Fig. 4.2(c). The analysis of this class of structures is postponed to a later paper.

The static properties of a 3–bar SVD type tensegrity is studied in this chapter. A typical two stage 3–bar SVD type tensegrity is shown in Fig. 4.3 in which the bars of the bottom stage are twisted in the anti–clockwise direction. The coordinate system used is also shown in the same figure. The same configuration will be used for all subsequent studies on the statics of the tensegrity. The notations and symbols, along with the definition of angles α and δ, and overlap between the stages, used in the following discussions are

also shown in Fig. 4.3.

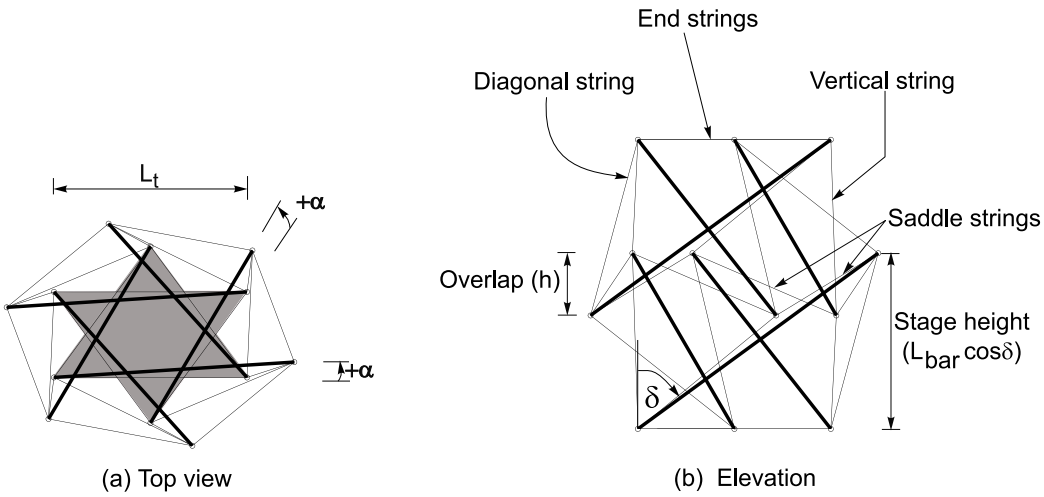

Fig. 4.3: Top view and elevation of a 2–Stage 3–Bar SVD tensegrity.

The assumptions related to the geometrical configuration of the tensegrity structure are listed below:

1. The projection of the top and the bottom triangles (vertices) on the horizontal plane make a regular hexagon.

2. The projection of bars on the horizontal plane make an angle α with the sides of the base triangle. The angle α is taken to be positive $(+)$ if the projection of the bar lies inside the base triangle, otherwise α is considered as negative $(-)$.

3. All of the bars are assumed to have the same declination angle δ.

4. All bars are of equal length, L.

4.2 Existence Conditions for 3–Bar SVD Tensegrity

The existence of a tensegrity structure requires that all bars be in compression and all strings be in tension in the absence of the external loads. Mathematically, the existence of a tensegrity system must satisfy the following set of equations.

$$\mathbf{A}(\bar{q})\mathbf{t}_0 = \mathbf{0}, \qquad \mathbf{t}_{0\_strings} > 0, \qquad \bar{q} : stable \quad equilibrium. \tag{4.1}$$

For our use, we shall define the conditions stated in 4.1 as the "tensegrity condition."

Note that $\mathbf{A}$ of 4.1 is now a function of α, δ and h, the generalized coordinates, labeled q generically. For a given q, the null space of $\mathbf{A}$ is computed from the singular value decomposition of $\mathbf{A}$ [36, 37]. Any singular value of $\mathbf{A}$ smaller than 1.0×10^{-10} was assumed to be zero and the null vector $\mathbf{t}_0$ belonging to the null space of $\mathbf{A}$ was then computed. The null vector was then checked against the requirement of all strings in tension. The values of α, δ and h that satisfy 4.1 yield a tensegrity structure. In this section, the existence conditions are explored for a two–stage 3–Bar SVD type tensegrity, as shown in Fig. 4.3, and are discussed below.

All of the possible configurations resulting in the self–stressed equilibrium conditions for a two stage 3–Bar SVD type tensegrity are shown in Fig. 4.4. While obtaining Fig. 4.4, the length of the bars was assumed to be 0.40 meter and L_t, as shown in Fig. 4.3, was taken to be 0.20 meter.

Figure 4.4 shows that out of various possible combinations of α–δ–h, there exists only a small domain of α–δ–h satisfying the existence condition for the two stage 3–Bar SVD type tensegrity studied here. It is interesting to explore the factors defining the boundaries of the domain of α–δ–h. For this, the relation between α and h, δ and h, and also the range of α and δ satisfying the existence condition for the two stage 3–Bar SVD type tensegrity

are shown in Figs. 4.4 (b), (c), and (d). Fig. 4.4 (b) shows that when $\alpha = 30^0$, there exists a unique value of overlap equal to 50% of the stage height. Note that $\alpha = 0^0$ results in a perfect hexagonal cylinder. For any value of α other than 0^0, there exists multiple values of overlap that satisfies the existence condition. These values of overlap for any given value of α depend on δ, as shown in Fig. 4.4 (c). It is also observed in Figs. 4.4 (b) and (c), that a larger value of negative alpha results in a large value of overlap and a larger value of positive alpha results in smaller value of overlap. Note that a large value of negative α means a "fat" or "beer–barrel" type structure whereas larger values of positive α give an "hour–glass" type of structure. It can be shown that a "fat" or "beer–barrel" type structure has greater compressive stiffness than an "hour–glass" type structure. Therefore, a tensegrity beam made of larger values of negative α can be expected to have greater compressive strength.

Figure 4.4 (d) shows that for any value of δ, the maximum values of positive or negative α is governed by overlap. The maximum value of positive α is limited by the overlap becoming 0% of the stage height, whereas the maximum value of negative α is limited by the overlap becoming 100% of the stage height. A larger value of negative α is expected to give greater vertical stiffness. Fig. 4.4 (d) shows that large negative α is possible when δ is small. However, as seen in Fig. 4.4 (d), there is a limit in the maximum value of negative α and on the minimum δ that would satisfy the existence conditions of the two–stage 3–Bar SVD type tensegrity. To understand this limit in the values of α and δ, the distribution of the internal pretensioning forces in each of the members are plotted as a function of α and δ, and are shown in Figs. 4.5 and 4.6.

Figure 4.5 shows the member forces as a function of α with $\delta = 35^0$, whereas Fig. 4.6 shows the member forces as a function of δ with $\alpha = -5^0$. Both of the figures are obtained for $K = 1/9$ and the prestressing force in the strings being equal to the force due to a maximum prestrain in the strings $\epsilon_0 = 0.05\%$ applied to the string which experiences maximum prestressing force. It is seen in both of the figures that for large negative α, the prestressing force in the saddle strings and the diagonal strings decrease with increase in the negative α. Finally, for α below certain values, the prestressing forces in the

saddle and diagonal strings become small enough to violate the definition of existence of tensegrity (i.e. all strings in tension and all bars in compression). Similar trend is noted in the case of the vertical strings also. As seen in Fig. 4.6, the force in the vertical strings decreases with decrease in δ for small δ. Finally, for δ below certain values, the prestressing forces in the vertical strings become small enough to violate the definition of existence of tensegrity. This explains the lower limits of the angles α and δ satisfying the tensegrity conditions.

Figures 4.5 and 4.6 show very remarkable change in the load–sharing mechanism between the members with increase in positive α and with increase in δ. It is seen in Fig. 4.5 that as α is gradually changed from a negative value towards a positive one, the prestressing force in the saddle strings increases, whereas the prestressing force in the vertical strings decreases. These trends continue up to $\alpha = 0^0$, when the prestressing force in both the diagonal strings and the saddle strings are equal and that in the vertical strings is small. For $\alpha < 0^0$, the force in the diagonal strings are always greater than that in the saddle strings. However, for $\alpha > 0^0$, the force in the diagonal strings decreases and is always less than the force in the saddle strings. The force in the vertical strings is greatest of all strings.

Figure 4.4 showing all the possible configurations of a two stage tensegrity can be quite useful in designing a deployable tensegrity beam made of many stages. The deployment of a beam with many stages can be achieved by deploying two stages at a time.

The existence conditions for a regular hexagonal cylinder (beam) made of two stages for which one of the end triangles is assumed to be rotated by an angle β about its mean position, as shown in Fig. 4.7, is next studied. The mean position of the triangle is defined as the configuration when $\beta = 0$ and all of the nodal points of the bars line up in a straight line to form a regular hexagon, as shown in Fig. 4.7. As it is seen in Fig. 4.8, it is possible to rotate the top triangle merely by satisfying the equilibrium conditions for the two stage tensegrity. It is also seen that the top triangle can be rotated merely by changing the overlap between the two stages. This information can be

quite useful in designing a Stewart platform type structure.

4.3 Load–deflection Curves and Axial Stiffness as a Function of the Geometrical Parameters

The load deflection characteristics of a two stage 3–Bar SVD type tensegrity is next studied and the corresponding stiffness properties are investigated.

Figure 4.9 depicts the load deflection curves and the axial stiffness as a function of prestress, drawn for the case of a two–stage 3–bar SVD type tensegrity subjected to axial loading. The axial stiffness is defined as the external force acting on the structure divided by the axial deformation of the structure. In another words, the stiffness considered here is the "secant stiffness".

Fig. 4.9 shows that the tensegrity under axial loading behaves like a nonlinear spring and the nonlinear properties depend much on the prestress. The nonlinearity is more prominent when the prestress is low and when the displacements are small. It is seen that the axial stiffness computed for both compressive and tensile loadings are practically equal to each other for this particular case of a two–stage 3–bar SVD type tensegrity. It is also seen that the axial stiffness is affected greatly by the prestress when the external forces are small (i.e. when the displacements are small), and the prestress has an important role in increasing the stiffness of the tensegrity in the region of small external load. However, as the external forces are increased, the effect of the prestress becomes negligible.

The characteristics of the axial stiffness of the tensegrity as a function of the geometrical parameters (i.e. α, δ) are next plotted in Fig. 4.10. The effect of the prestress on the axial stiffness is also shown in Fig. 4.10. In obtaining the Fig. 4.10, vertical loads were applied at the top nodes of the two–stage

tensegrity. The load was gradually increased until at least one of the strings exceeded its elastic limit. As the compressive stiffness and the tensile stiffness were observed to be nearly equal to each other in the present example, only the compressive stiffness as a function of the geometrical parameters, is plotted in Fig. 4.10. The change in the shape of the tensegrity structure from a "fat" profile to an "hour–glass" like profile with the change in α is also shown in Fig. 4.10(b).

The following conclusions can be drawn from Fig. 4.10:

1. Fig. 4.10(a) suggests that the axial stiffness increases with the decrease in the angle of declination δ (measured from the vertical axis).
2. Fig. 4.10(b) suggests that the axial stiffness increases with increase in the negative angle α. Negative α means a "fat" or "beer–barrel" type structure whereas a positive α means an "hour–glass" type structure, as shown in Fig. 4.10(b). Thus a "fat" tensegrity performs better than an "hour–glass" type tensegrity subjected to compressive loading.
3. Fig. 4.10(c) suggests that the prestress has an important role in increasing the stiffness of the tensegrity in the region of small external loading. However, as the external forces are increased, the effect of the prestress becomes practically negligible.

4.4 Load–deflection Curves and Bending Stiffness as a Function of the Geometrical Parameters

The bending characteristics of the Two–stage 3–Bar SVD tensegrity are presented in this section. The force is applied along the x–direction and then along the y–direction, as shown in Fig. 4.11. The force is gradually applied until at least one of the strings exceeds its elastic limit.

The load deflection curves for the load applied in the lateral are plotted in Fig. 4.11 as a function of the prestress. It was observed that as the load is gradually increased, one of the vertical strings goes slack and takes no load. Therefore, two distinct regions can be clearly identified in Fig. 4.11. The first region is the one when none of the strings is slack, whereas the second region, marked by the sudden change in the slope of the load–deflection curves, is the one when at least one string is slack. It is seen in Fig. 4.11 that in contrast to the response of the tensegrity subjected to the vertical axial loading, the bending response of the tensegrity is almost linear in the region of tensegrity without slack strings, whereas it is slightly nonlinear in the region of tensegrity with slack strings. The nonlinearity depends on the prestressing force. It is observed that the prestress plays an important role in delaying the onset of the slack strings.

The characteristics of the bending stiffness of the tensegrity as a function of the geometrical parameters (i.e. α, δ) are next plotted in Figs. 4.12 and 4.13. Fig. 4.12 is plotted for lateral force applied in the x–direction, as shown in Fig. 4.12, whereas Fig. 4.13 is plotted for lateral force applied in the y–direction, as shown in Fig. 4.13. The effect of the prestress on the bending stiffness is also shown in Figs. 4.12 and 4.13.

The following conclusions about the bending characteristics of the two–stage 3–Bar tensegrity could be drawn from Figs. 4.12 and 4.13:

1. It is seen in Figs. 4.12 and 4.13, that the bending stiffness of the tensegrity with no slack strings is practically equal in both the x– and y–directions. However, the bending stiffness of the tensegrity with slack string is greater along y–direction than along the x–direction.

2. The bending stiffness of a tensegrity is constant and is maximum for any given values of α, δ and prestress when none of the strings are slack. However, as soon as at least one string goes slack (marked by sudden drop in the stiffness curves in Figs. 4.12 and 4.13), the stiffness becomes a nonlinear function of the external loading and decreases monotonically with the increase in the external loading. As seen in

Figs. 4.12 and 4.13, the onset of strings becoming slack, and hence the range of constant bending stiffness, is a function of α, δ and prestress.

3. Figs. 4.12(a) and 4.13(a) suggest that the bending stiffness of a tensegrity with no slack strings increases with the increase in the angle of declination δ (measured from the vertical axis). The bending stiffness of a tensegrity with a slack string, in general, increases with increase in δ. However, as seen in Fig. 4.12(a), there exists a certain δ, beyond which the bending stiffness of a tensegrity with slack string decreases with increase in δ. Hence tensegrity structures have an *optimal* internal geometry with respect to the bending stiffness and other mechanical properties.

4. Figs. 4.12(b) and 4.13(b) suggest that the bending stiffness increases with the increase in the negative angle α. As negative α means a "fat" or "beer–barrel" type structure whereas a positive α means an "hour–glass" type structure, a "fat" tensegrity performs better than an "hour–glass" type tensegrity subjected to lateral loading.

5. Figs. 4.12(a,b) and 4.13(a,b) indicate that both α and δ play a very interesting and important role in not only affecting the magnitude of stiffness, but they also affect the onset of slackening of the strings (robustness to external disturbances). A large value of negative α and a large value of δ (in general) delay the onset of slackening of the strings, thereby increasing the range of constant bending stiffness. However, there exists a certain δ for which the onset of the slack strings is maximum.

6. Figs. 4.12(c) and 4.13(c) suggest that prestress does not affect the bending stiffness of a tensegrity with no slack strings. However, prestress has an important role in delaying the onset of slack strings and thus increasing the range of constant bending stiffness.

4.5 Summary of 3–Bar SVD Tensegrity Properties

The following conclusions could be drawn from the present study on the statics of a Two–stage 3–Bars SVD type tensegrities.

1. The tensegrity structure exhibits unique equilibrium characteristics. The self–stressed equilibrium condition exists only on a small subset of geometrical parameter values. This condition guarantees that the tensegrity is prestressable and that none of the strings is slack.

2. The stiffness (the axial and the bending) is a function of the geometrical parameters, the prestress and the externally applied load. However, the effect of the geometrical parameters on the stiffness are greater than the effect of the prestress. The external force, on the other hand, does not affect the bending stiffness of a tensegrity with no slack strings, whereas it does affect the axial stiffness. The axial stiffness shows a greater nonlinear behavior even up to the point when none of the strings are slack. The axial stiffness increases with the increase in the external loading, whereas the bending stiffness remains constant until at least one of the strings go slack, after which the bending stiffness decreases with increase in the external loading.

3. Both the axial and the bending stiffness increase by making α more negative. That is, both the axial and the bending stiffness are higher for a "beer–barrel" type tensegrity. The stiffness is small for an "hour–glass" type tensegrity.

4. The axial stiffness increases with the decrease in the vertical angle, whereas the bending stiffness increases with the increase in the vertical angle. This implies that the less the angle that the bars make with the line of action of the external force, the stiffer is the tensegrity.

5. Both the geometrical parameters α and δ, and the prestress play important role in delaying the onset of slack strings. A more negative α,

a more positive δ, and prestress, all delay the onset of slack strings, as more external forces are applied. Thus, both α and δ also work as a "hidden prestress". However, there lies a δ beyond which an increase in δ hastens the onset of slack strings, as more external force is applied.

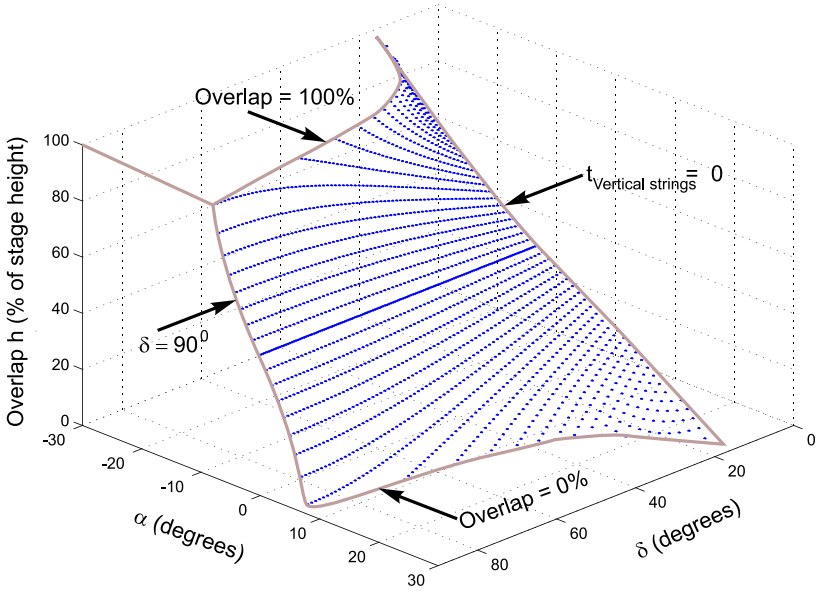

Fig. 4.4(a) (Cont.).

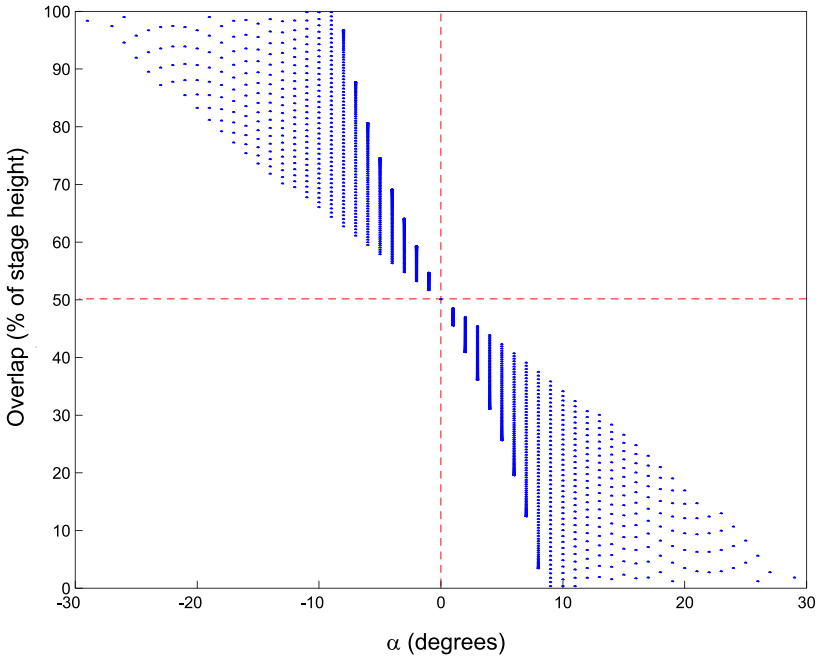

Fig. 4.4 (b) (Cont.).

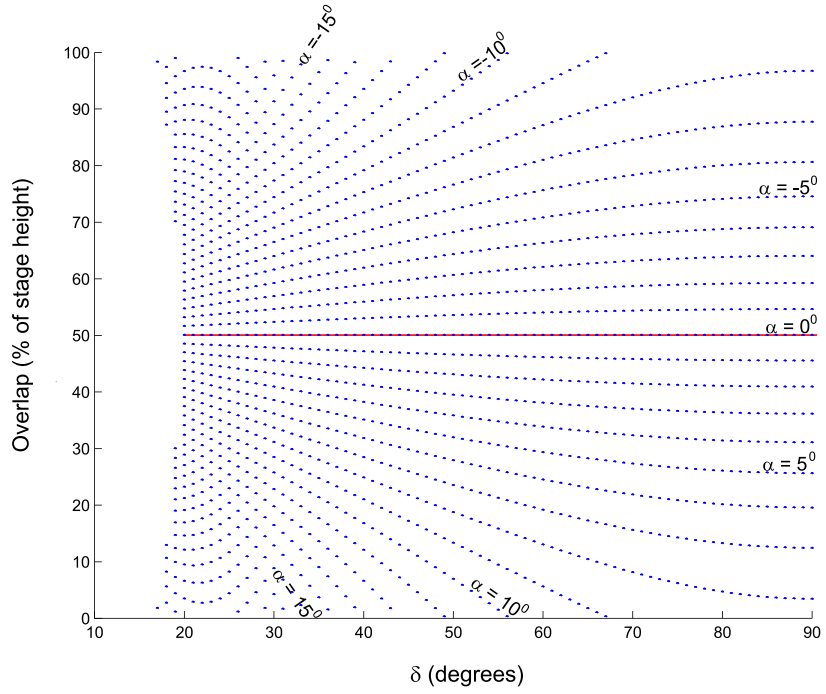

(c)

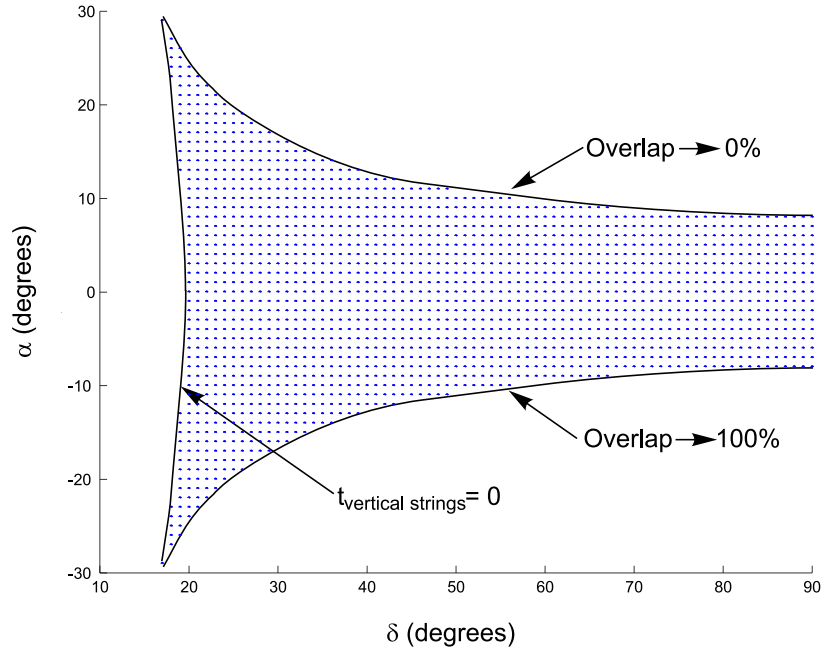

(d)

Fig. 4.4: Existence conditions for a two stage tensegrity. Relations between (a) α, δ and the overlap, (b) α and overlap, (c) δ and overlap, and (d) δ and α giving static equilibria.

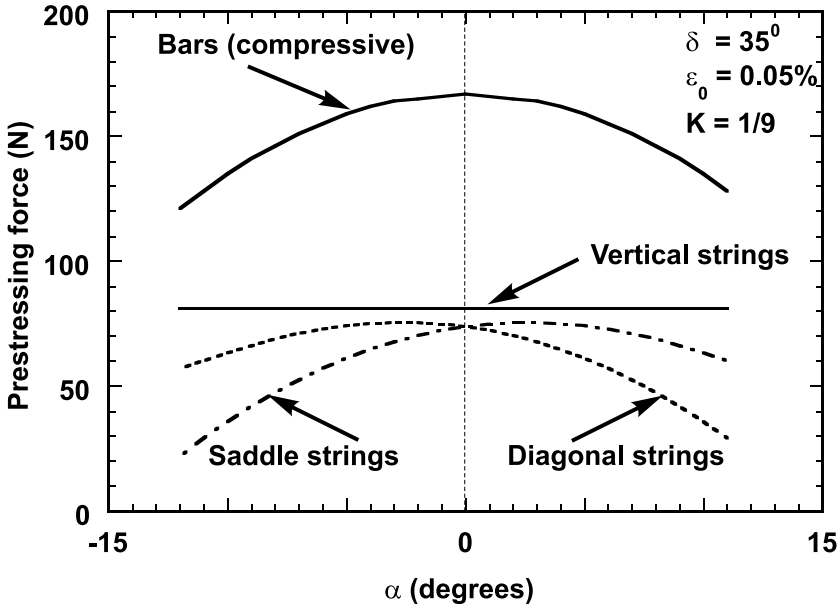

Fig. 4.5: Prestressing force in the members as a function of α.

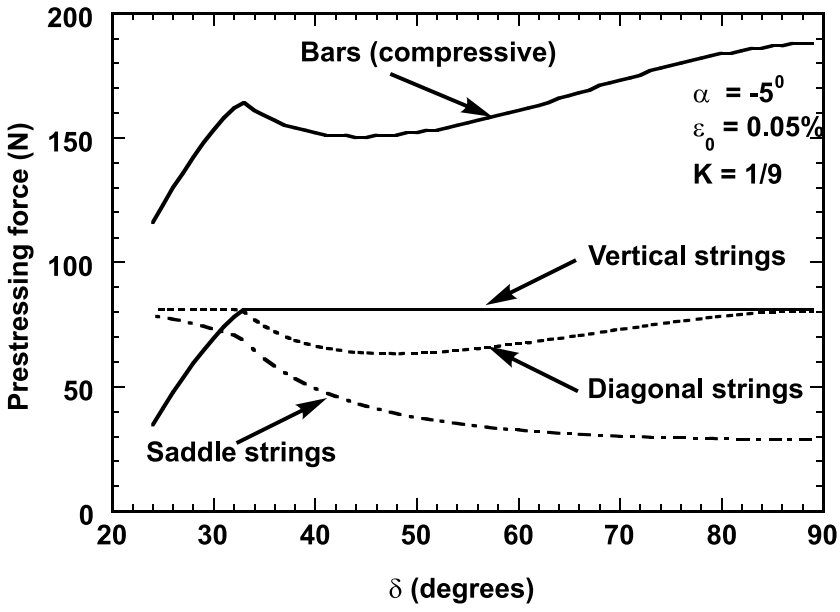

Fig. 4.6: Prestressing force in the members as a function of δ.

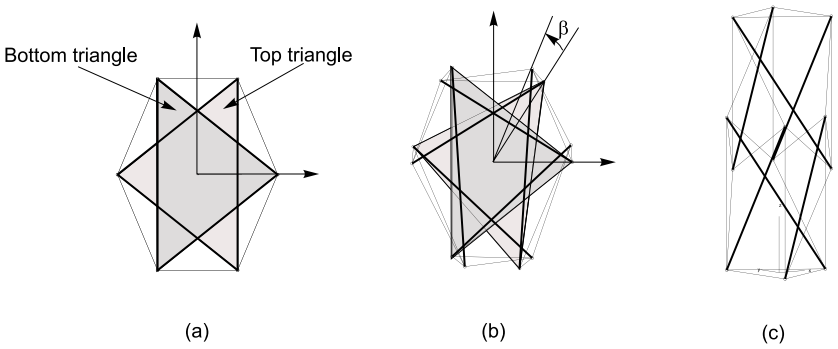

Fig. 4.7: Rotation of the top triangle with respect to the bottom triangle for a two stage cylindrical hexagonal 3–Bar SVD tensegrity. (a) Top view when $\beta = 0$, (b) top view with β and (c) elevation.

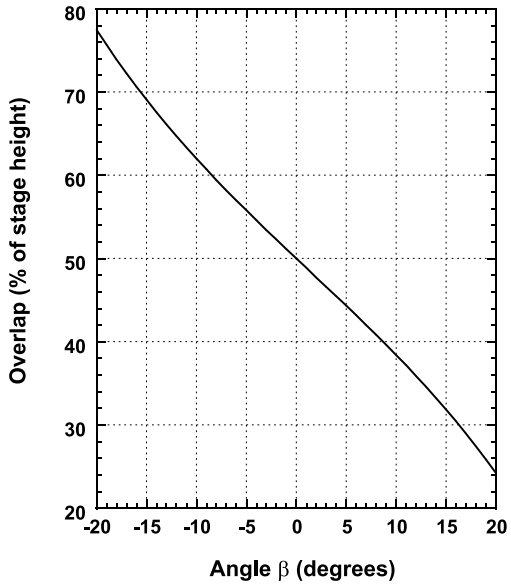

Fig. 4.8: Existence conditions for a cylindrical 2–Stage 3–Bars SVD tensegrity with respect to the rotation angle of the top triangle. (anticlockwise β is positive).

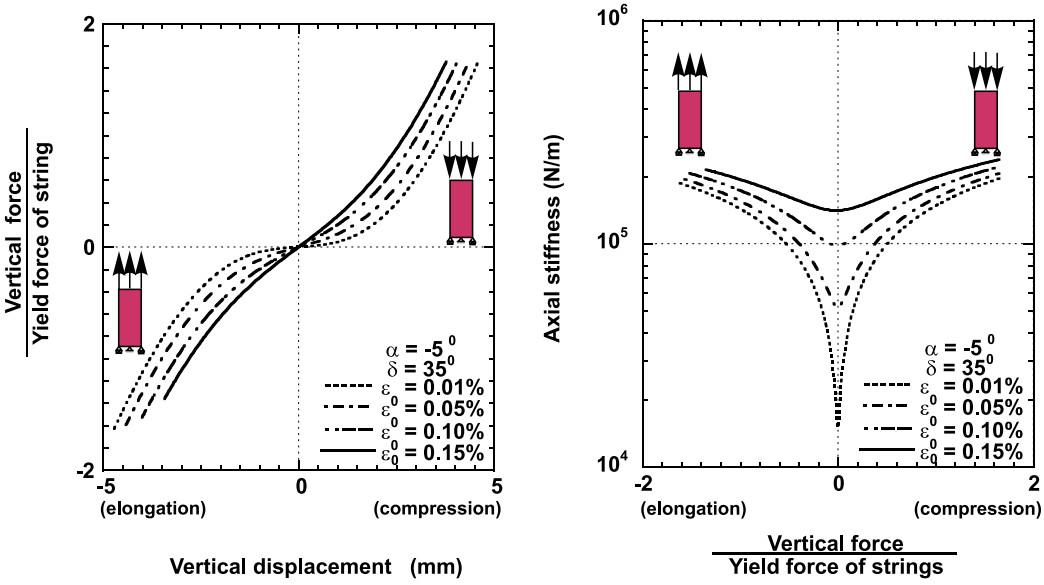

(a) (b)

Fig. 4.9: Load deflection curve and axial stiffness of a Two–Stage 3–bar SVD tensegrity subjected to axial loading.

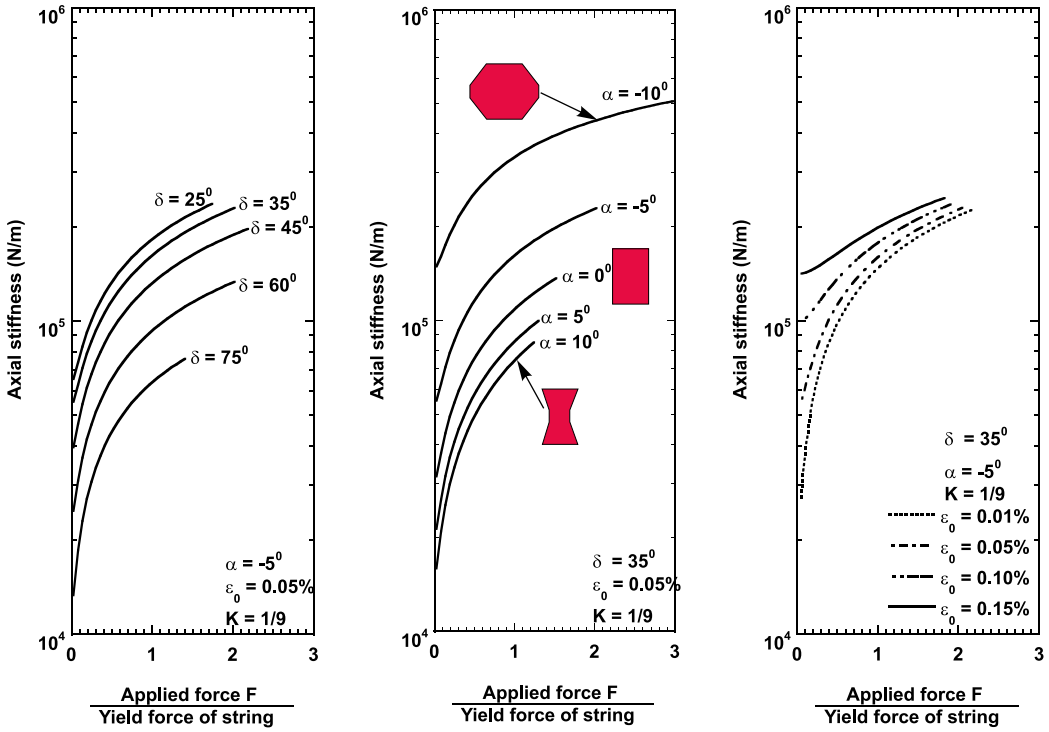

Fig. 4.10: Axial stiffness of a two–stage 3–Bar SVD tensegrity for (a) different δ with $\alpha = -5^0, \epsilon_0 = 0.05\%, K = 1/9$, (b) different angle α with $\delta = 35^0, \epsilon_0 = 0.05\%, K = 1/9$ and (c) different ϵ_0 with $\alpha = -5^0, \delta = 35^0, K = 1/9$. L_{bar} for all cases is 0.4m.

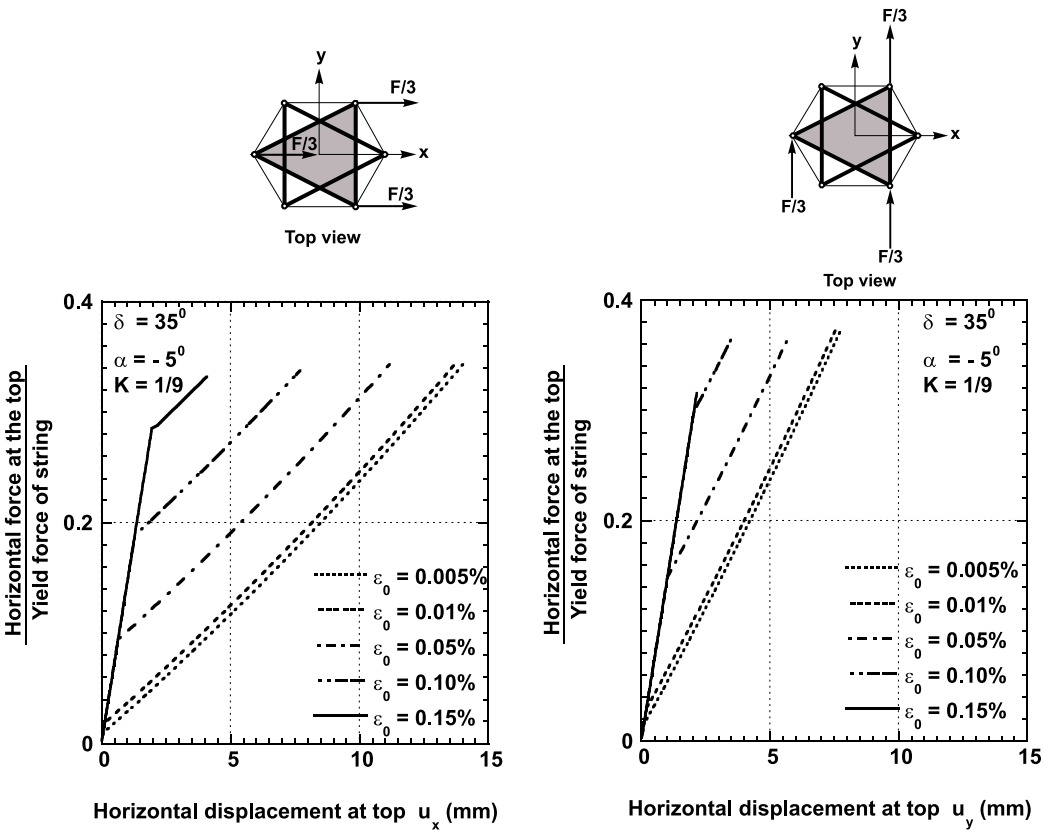

(a) (b)

Fig. 4.11: Load deflection curve of a Two–Stage 3–bar SVD tensegrity subjected to lateral loading. (a) Loading along X–direction, (b) Loading along Y–direction.

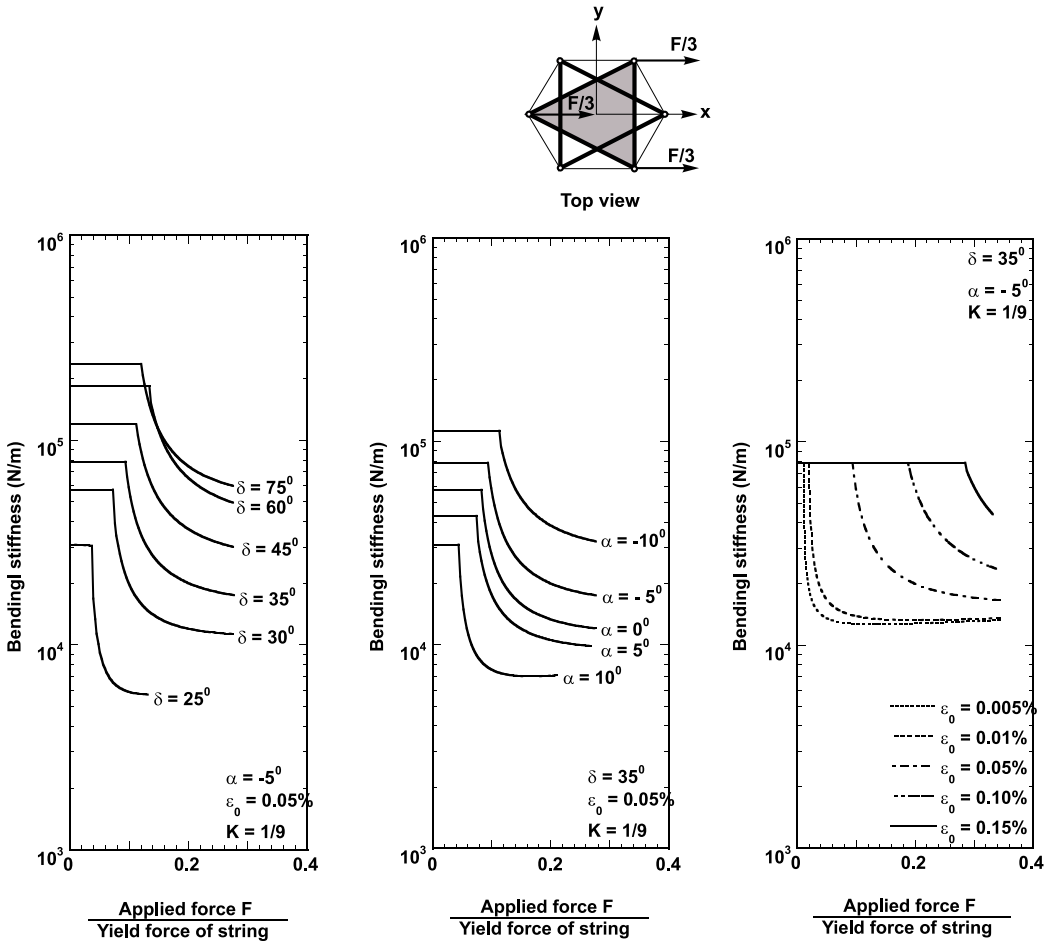

Fig. 4.12: Bending stiffness of a two–stage 3–Bar SVD tensegrity for (a) different δ with $\alpha = -5^0, \epsilon_0 = 0.05\%, K = 1/9$, (b) different angle α with $\delta = 35^0, \epsilon_0 = 0.05\%, K = 1/9$ and (c) different ϵ_0 with $\alpha = -5^0, \delta = 35^0, K = 1/9$. L_{bar} for all cases is 0.4m.

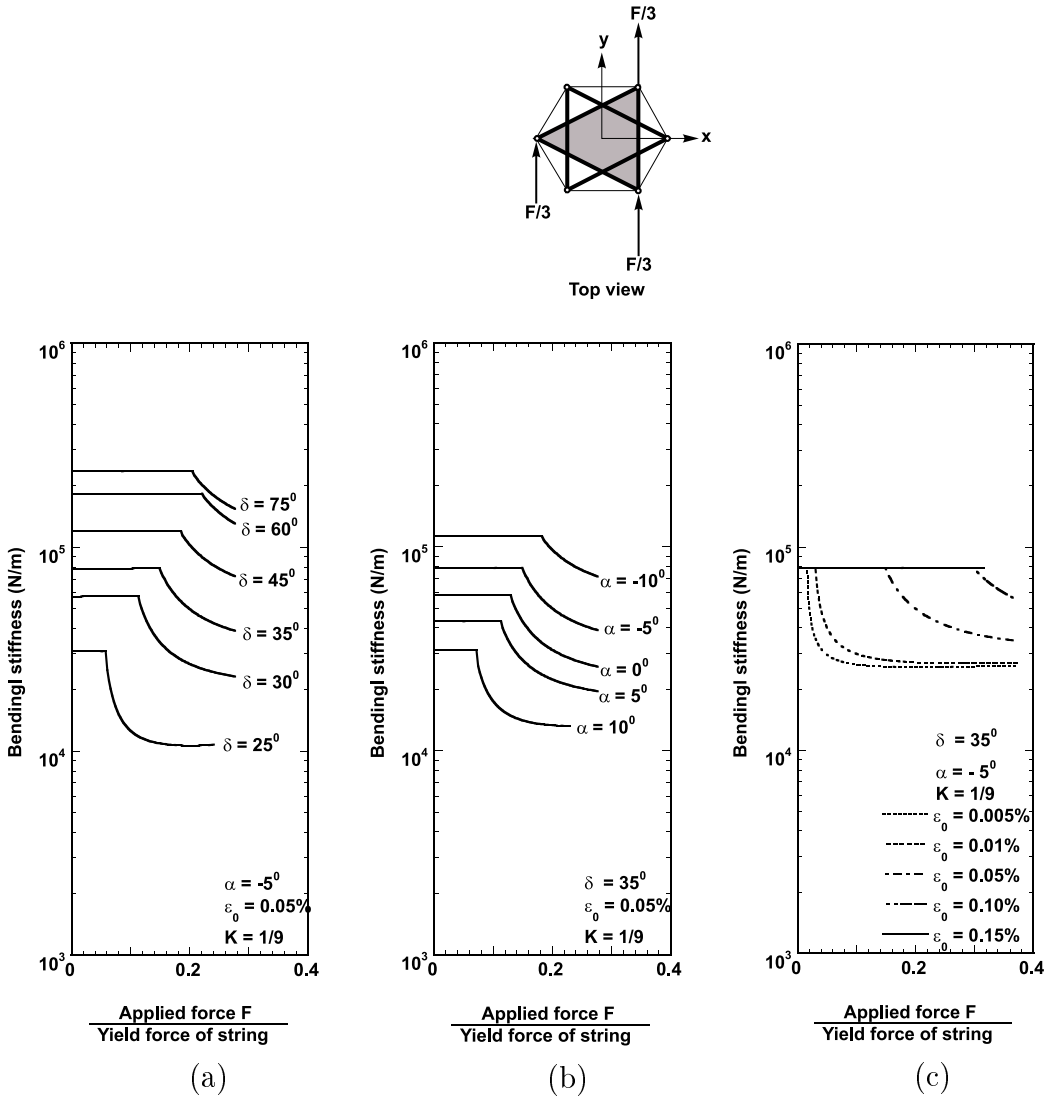

Fig. 4.13: Bending stiffness of a two–stage 3–Bar SVD tensegrity for (a) different δ with $\alpha = -5^0, \epsilon_0 = 0.05\%, K = 1/9$, (b) different angle α with $\delta = 35^0, \epsilon_0 = 0.05\%, K = 1/9$ and (c) different ϵ_0 with $\alpha = -5^0, \delta = 35^0, K = 1/9$. L_{bar} for all cases is 0.4m.

Chapter 5

Concluding Remarks

It is shown that tensegrity structures present a remarkable blend of geometry and mechanics. Out of various available combinations of geometrical parameters, there exists only a small subset that guarantees the existence of the tensegrity. The choice of these parameters dictate the mechanical properties of the structure. The choice of the geometrical parameters have a great influence on the stiffness. Pretension serves the important role of maintaining stiffness until a string goes slack. The geometrical parameters not only affect the magnitude of the stiffness either with or without slack strings, but they also affect the onset of slack strings. We now list the major findings of this paper.

Pretension vs. Stiffness Principle

This principle states that increased pretension increases robustness to uncertain disturbances. More precisely all situations we have seen(except for the $C4T2$):

> **When a load is applied to a tensegrity structure the stiffness does not decrease as the loading force increases unless a string goes slack.**

The effect of the pretension on the stiffness of a tensegrity without slack strings is practically negligible. The bending stiffness of a tensegrity without slack strings is not affected appreciably by the prestress.

Small Control Energy Principle

The second principle is that the shape of the structure can be changed with very small control energy. This is due to the fact that shape changes are achieved by changing the equilibrium of the structure. In this case, control energy is not required to hold the new shape. This is in contrast to the control of classical structures, where shape changes required control energy to work against the old equilibrium.

Mass vs. Strength

The paper also considered the issue of strength vs. mass of tensegrity structures. We found planar examples to be very informative. We considered two types of strength: the size of bending forces and the size of compressive forces required to break the object. We studied the ratio of **bending strength to mass** and **compression strength to mass**. We compared this for two planar structures, one called the $C2T4$ unit and the other called a $C4T1$ unit, to a solid rectangular bar of the same mass.

We find:

- Reasonably constructed $C2T4$ units are stronger in bending, than a rectangular bar, but they are weaker under compression.
- The C2T4 has worse strength under compression than a solid rectangular bar.
- The simple analysis we did indicates that $C4T2$ and $C4T1$ structures with reasonably chosen proportions have larger compression strength to mass ratio than a solid bar.
- On the other hand, a $C4T1$ while strong (not easily broken) need not be an extremely stiff structure.

- The $C4T2$ and $C4T1$ structure can be designed for minimal mass subjected to a constraint on both strength and stiffness.

It is possible to amplify the effects stated above by the use of self-similar constructions:

- **A 2D Tensegrity Beam.** After analyzing a $C2T4$ tensegrity unit, we lay n of them side by side to form a beam. In principle, we find that one can build beams with arbitrarily great bending strength. In practice this requires more study. However, the favorable bending properties found for $C2T4$ bode well for tensegrity beams.

- **A 2D Tensegrity Column.** We take the $C4T2$ structure and replace each bar with a smaller $C4T1$ structure, then we replace each bar of this new structure by a yet smaller $C4T1$ structure. In principle, such a self similar construction can be repeated to any level. Assuming that the strings do not fail and have significantly less mass than the bars, we find that we have a class of tensegrity structures with unlimited compression strength to mass ratio. Further issues of robustness to lateral and bending forces would have to be investigated to ensure practicality of such structures.

  The total mass including strings and bars (while preserving strength) can be minimized by a finite number of self-similar iterations, and the number of iterations to achieve minimal mass is usually quite small (less that 10). This provides an optimization of tensegrity structures that is analytically resolved and much easier and less complex than optimization of classical structures. We emphasize that the implications of overlapping of the bars is not seriously studied.

  For a special range of geometry, the stiffness to mass ratio increases with self-similar iterations. For the remaining range of geometry the stiffness to mass decreases with self-similar iterations. For a very specific choice of geometry the stiffness to mass ratio remains constant with self-similar iterations.

Self-similar steps can preserve strength while reducing mass, but cannot preserve stiffness while reducing mass. Hence a desired stiffness bound and reconciliation of overlapping bars will dictate the optimal number of iterations.

A Challenge for the Future

In the future, the grand challenge with tensegrity structures is to find ways to choose material and geometry, so that the thermal, electrical and mechanical properties are specified. The tensegrity structure paradigm is very promising for the integration of these disciplines with control, where either strings or bars can be controlled.

ACKNOWLEDGEMENT: This work received major support from a DARPA grant monitored by Leo Christodoulou. We are also grateful for support from DARPA, AFOSR, NSF, ONR, and the Ford Motor Company.

Appendix A

Nonlinear Analysis of Planar Tensegrity

A.1 Equations of Static Equilibrium

A.1.1 Static equilibrium under external forces

A planar tensegrity under external forces is shown in Fig. A.1, where F_i are the external forces and t_i represent the internal forces in the members of the tensegrity units. Note that $\mathbf{t}$ represents the net force in the members which includes the pretension and the force induced by the external forces. The sign convention adopted herein is also shown in Fig. A.1, where t_{ki} represents the member force t acting at the i–th node of the member k. We assume that $i < j$ and $t_{ki} = -t_{kj}$. With this convention, we write the force equilibrium equations for the planar tensegrity.

The equilibrium of forces in the x–direction acting on the joints yields the

following equations

$$
\begin{aligned}
t_{1i}\cos\delta_{x1} + t_{4i}\cos\delta_{x4} + t_{6i}\cos\delta_{x6} &= F_1,\\
t_{1j}\cos\delta_{x1} + t_{2i}\cos\delta_{x2} + t_{5i}\cos\delta_{x5} &= -F_2,\\
t_{2i}\cos\delta_{x2} + t_{3i}\cos\delta_{x3} + t_{6j}\cos\delta_{x6} &= -F_3,\\
t_{3j}\cos\delta_{x3} + t_{4j}\cos\delta_{x4} + t_{5j}\cos\delta_{x5} &= F_4.
\end{aligned}
\tag{A.1}
$$

Similarly, the equilibrium of forces in the y–direction acting on the joints yields the following equations

$$
\begin{aligned}
t_{1i}\cos\delta_{y1} + t_{4i}\cos\delta_{y4} + t_{6i}\cos\delta_{y6} &= 0,\\
t_{1j}\cos\delta_{y1} + t_{2i}\cos\delta_{y2} + t_{5i}\cos\delta_{y5} &= 0,\\
t_{2i}\cos\delta_{y2} + t_{3i}\cos\delta_{y3} + t_{6j}\cos\delta_{y6} &= 0,\\
t_{3j}\cos\delta_{y3} + t_{4j}\cos\delta_{y4} + t_{5j}\cos\delta_{y5} &= 0.
\end{aligned}
\tag{A.2}
$$

In the above equations $\cos\delta_{xk}$ represents the direction cosine of member k taken from the x–axis, whereas $\cos\delta_{yk}$ represents the direction cosine of member k taken from the y–axis.

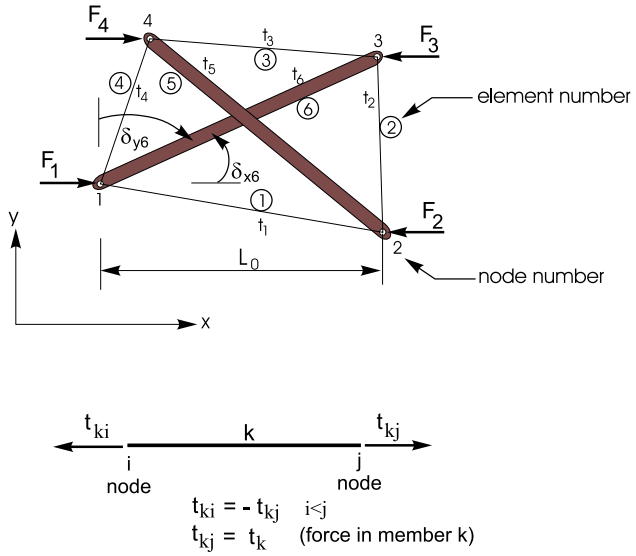

Fig. A.1: Forces acting on a planar tensegrity and the sign convention used.

The above equations can be rearranged in the following matrix form:

$$\mathbf{A}\mathbf{t} = \mathbf{f}, \tag{A.3}$$

where $\mathbf{t}$ is a vector of forces in the members and is given by $\mathbf{t}^T = [t_1\ t_2\ t_3\ t_4\ t_5\ t_6]$, matrix $\mathbf{A}$ (of size 8×6) is the equilibrium matrix, and $\mathbf{f}$ is a vector of nodal forces. For convenience, we arrange $\mathbf{t}$ such that the forces in the bars appear at the top of the vector, i.e.

$$\mathbf{t}^T = [\mathbf{t}_{bars}\ \ \mathbf{t}_{strings}] \ \ = [t_5\ t_6\ \ t_1\ t_2\ t_3\ t_4]. \tag{A.4}$$

Matrix $\mathbf{A}$ and vector $\mathbf{f}$ are given by

$$\mathbf{A} = \begin{bmatrix} \mathbf{C}^T & \vdots & \mathbf{0} \\ \cdots & \cdots & \cdots \\ \mathbf{0} & \vdots & \mathbf{C}^T \end{bmatrix} \begin{bmatrix} \mathbf{H}_x \\ \cdots \\ \mathbf{H}_y \end{bmatrix}, \qquad \mathbf{f} = \begin{Bmatrix} \mathbf{f}_x \\ \cdots \\ \mathbf{f}_y \end{Bmatrix}. \tag{A.5}$$

In the above equation, matrices $\mathbf{H}_x$ and $\mathbf{H}_y$ are diagonal matrices containing the direction cosines of each member taken from the x–axis or y–axis, respectively, i. e. $H_{x_{ii}} = \cos\delta_{x_i}$ and $H_{y_{ii}} = \cos\delta_{y_i}$. Similar to the arrangement of $\mathbf{t}$, H_x and H_y are also arranged such that the direction cosines of bars appear at the top of H_x and H_y whereas the direction cosines of strings appear at the bottom of H_x and H_y. Vectors $\mathbf{f}_x$ and $\mathbf{f}_y$ are the nodal forces acting on the nodes along x– and y–axes, respectively. Matrix $\mathbf{C}$ is a 6×4 (number of members $\times$ number of nodes) matrix. The k–th row of matrix $\mathbf{C}$ contains -1 (for i–th node of the k–th member), $+1$ (for j–th node of the k–th member) and 0. Matrix $\mathbf{C}$ for the present case is given as

$$\mathbf{C} = \begin{bmatrix} 0 & -1 & 0 & 1 \\ -1 & 0 & 1 & 0 \\ -1 & 1 & 0 & 0 \\ 0 & -1 & 1 & 0 \\ 0 & 0 & -1 & 1 \\ -1 & 0 & 0 & 1 \end{bmatrix} \begin{matrix} \} \longrightarrow \text{Bars} \\ \\ \\ \} \longrightarrow \text{Strings} \\ \\ \\ \end{matrix} \tag{A.6}$$

It should be noted here that matrix $\mathbf{A}$ is a nonlinear function of the geometry of the tensegrity unit, the nonlinearity being induced by the matrices $\mathbf{H}_x$ and $\mathbf{H}_y$ containing the direction cosines of the members.

A.2 Solution of the Nonlinear Equation of Static Equilibrium

Since the equilibrium equation given in (A.3) is a nonlinear equation and also since $\mathbf{A}$ (of size 8×6) is not a square matrix, we solve the problem in the following way.

Let $\tilde{\mathbf{t}}$ be the member forces induced by the external force $\mathbf{f}$, then from (A.3)

$$\begin{aligned} & \mathbf{At} = \mathbf{f} \\ \Rightarrow \quad & \mathbf{A}(\mathbf{t}_0 + \tilde{\mathbf{t}}) = \mathbf{f} \\ \Rightarrow \quad & \mathbf{A}\tilde{\mathbf{t}} = \mathbf{f} - \mathbf{At}_0 \\ \Rightarrow \quad & \mathbf{AKe} = \mathbf{f} - \mathbf{At}_0 \end{aligned} \tag{A.7}$$

where $\mathbf{e}$ is the deformation from the initial prestressed condition of each member, and from Hooke's law $\tilde{\mathbf{t}} = \mathbf{Ke}$, where $\mathbf{K}$ is a diagonal matrix of size 6×6, with $K_{ii} = (EA)_i/L_i$. $(EA)_i$ and L_i are the axial rigidity and the length of the i–th member. Note that $\mathbf{A}$ expressed above is composed of both the original $\mathbf{A}_0$ and the change in $\mathbf{A}_0$ caused by the external forces $\mathbf{f}$.

$$\mathbf{A} = \mathbf{A}_0 + \tilde{\mathbf{A}}, \tag{A.8}$$

where $\tilde{\mathbf{A}}$ is the change in $\mathbf{A}_0$ caused by the external forces $\mathbf{f}$.

The nonlinear equation given above can be linearized in the neighborhood of an equilibrium. In the neighborhood of the equilibrium, we have the linearized relationship,

$$\mathbf{e}_k = \mathbf{A}_k^T \mathbf{u}_k \tag{A.9}$$

Let the external force $\mathbf{f}$ be gradually increased in small increments ($\mathbf{f}_k = \mathbf{f}_{k-1} + \Delta\mathbf{f}$ at the k–th step), and the equilibrium of the planar tensegrity be satisfied for each incremental force, then (A.7) can be written as

$$\mathbf{A}(\mathbf{u}_k)\mathbf{K}\mathbf{A}(\mathbf{u}_k)^T\mathbf{u}_k = \mathbf{f}_k - \mathbf{A}(\mathbf{u}_k)\mathbf{t}_0 \tag{A.10}$$

The standard Newton–Raphson method can now be used to evaluate $\mathbf{u}_k$ of (A.10), for each incremental load step $\Delta\mathbf{f}_k$. The external force is gradually applied until it reaches its specific value and $\mathbf{u}_k$ is evaluated at every load step. Matrix $\mathbf{A}$, which is now a nonlinear function of $\mathbf{u}$, is updated during each load step.

In order to compute the external force that would be required to buckle the bars in the tensegrity unit, we must estimate the force being transferred to the bars. The estimation of the compressive force in the bars following full nonlinear analysis can be done numerically. However, in the following we seek to find an analytical expression for the compressive force in the bars. For this we adopt a linear and small displacement theory. Thus the results that follow are valid only for small displacement and small deformation.

Appendix B

Linear Analysis of Planar Tensegrity

B.1 EI of the Tensegrity Unit with Slack Top String

Forces in the Members A tensegrity with a slack top string does not have prestress. As mentioned earlier, we adopt the small displacement assumptions, which implies that the change in the angle δ due to the external forces, is negligible. Therefore, in the following, we assume that δ remains constant. The member forces in this case is obtained as

$$\begin{aligned} t_1 &= 2F, \\ t_2 &= F \tan\delta, \\ t_3 &= 0, \\ t_4 &= F \tan\delta, \\ t_5 &= -\frac{F}{\cos\delta}, \\ t_6 &= -\frac{F}{\cos\delta}. \end{aligned} \tag{B.1}$$

The strain energy in each of the members are computed as

$$
\begin{aligned}
U_1 &= \frac{1}{2}\frac{4L_0F^2}{(EA)_s},\\
U_2 &= \frac{1}{2}\frac{L_0F^2\tan^3\delta}{(EA)_s},\\
U_3 &= 0,\\
U_4 &= \frac{1}{2}\frac{L_0F^2\tan^3\delta}{(EA)_s},\\
U_5 &= \frac{1}{2}\frac{L_0F^2}{(EA)_b\cos^3\delta},\\
U_6 &= \frac{1}{2}\frac{L_0F^2}{(EA)_b\cos^3\delta}.
\end{aligned}
\tag{B.2}
$$

The total strain energy is then obtained as

$$
U = \sum_i U_i = \frac{1}{2}\frac{L_0}{(EA)_s}\frac{2F^2}{\cos^3\delta}\left[\sin^3\delta + 2\cos^3\delta + K\right], \tag{B.3}
$$

where K is defined as

$$
K = \frac{(EA)_s}{(EA)_b}. \tag{B.4}
$$

Thus, large value of K means that the strings are stiffer than the bars, whereas small value of K means that the bars are stiffer than the strings. $K \to 0$ means bars are rigid.

External Work and Displacement External work W is given by

$$
W = 4\frac{1}{2}Fu = 2Fu, \tag{B.5}
$$

where u is the displacement as shown in Fig. 2.1.

Equating the total strain energy given by (B.3) to the work done by the external forces given by (B.5), and then solving for u yields

$$
u = \frac{FL_0}{2(EA)_s\cos^3\delta}\left[\sin^3\delta + 2\cos^3\delta + K\right]. \tag{B.6}
$$

Effective EI Since $EI = M\rho$, we have,

$$EI = FL_0 \tan\delta \left(\frac{L_0}{2}\right)^2 \tan\delta \frac{1}{u}. \tag{B.7}$$

Substitution of $\tilde{u}$ from (B.6) into (B.7) yields

$$EI = \frac{1}{2} \frac{L_0^2 (EA)_s \sin^2\delta \cos\delta}{(\sin^3\delta + 2\cos^3\delta + K)}. \tag{B.8}$$

Substituting $L_0 = L_{bar} \cos\delta$ in (B.7) and (B.8) yields the following expressions for the equivalent bending rigidity of the planar section in terms of the length of the bars L_{bar},

$$EI = FL_{bar} \sin\delta \left(\frac{L_{bar}}{2}\right)^2 \cos\delta \sin\delta \frac{1}{u}. \tag{B.9}$$

or equivalently,

$$EI = \frac{1}{2} \frac{{L_{bar}}^2 (EA)_s \sin^2\delta \cos^3\delta}{(\sin^3\delta + 2\cos^3\delta + K)}. \tag{B.10}$$

Appendix C

Derivation of Stiffness of the $C4T1^i$ Structure

C.1 Derivation of Stiffness Equation

For a $C4T1^i$ structure under the buckling load F, the compressive load of bar in the i-th iteration is

$$F_i = \frac{F}{\prod_{j=1}^{i} 2\cos\delta_j}. \tag{C.1}$$

Similarly, the tension of strings in the i-th iteration is

$$t_j = \frac{2F\sin\delta_j}{\prod_{s=1}^{j} 2\cos\delta_s} \quad \text{for } j = 1, 2, 3, ..., i-1, i. \tag{C.2}$$

So, the buckling load F can be written in terms of any one of the compressive bar loads or tension of strings in i-th iteration

$$F = F_i \prod_{s=1}^{i} 2\cos\delta_s = \frac{t_j}{2\sin\delta_j} \prod_{p=1}^{j} 2\cos\delta_p \quad \text{for } j = 1, 2, 3, ..., i-1, i. \tag{C.3}$$

From the geometry of the structure,

$$\begin{aligned} \sin\delta_j &= \tfrac{L_{tj}}{2L_j}, \\ \cos\delta_j &= \tfrac{L_{j-1}}{2L_j}. \end{aligned} \tag{C.4}$$

Equation (C.3) can be simplified to

$$F = F_i \frac{L_0}{L_i} = t_j \frac{L_0}{L_{tj}}. \tag{C.5}$$

From this,

$$\frac{F}{L_0} = \frac{F_i}{L_i} = \frac{t_j}{L_{tj}} = \frac{t_1}{L_{t1}}. \tag{C.6}$$

This means the force to length ratio of every compressive or tensile members are the same. It is assumed that all the bars and strings have constant stiffness and hence are linear. With this assumption,

$$\begin{aligned} F_i &= k_{bi}\left(L_{i0} - L_i\right), \\ t_j &= k_{tj}\left(L_{tj} - L_{tj0}\right). \end{aligned} \tag{C.7}$$

So (C.6) becomes

$$k_{bi}\left(\frac{L_{i0}}{L_i} - 1\right) = k_{tj}\left(1 - \frac{L_{tj0}}{L_{tj}}\right) = k_{t1}\left(1 - \frac{L_{t10}}{L_{t1}}\right). \tag{C.8}$$

Taking the infinitesimal of all the length quantities yields

$$-k_{bi}\frac{L_{i0}}{L_i^2}dL_i = k_{tj}\frac{L_{tj0}}{L_{tj}^2}dL_{tj} = k_{t1}\frac{L_{t10}}{L_{t1}^2}dL_{t1},$$

and hence,

$$\begin{aligned} dL_i &= -\tfrac{k_{t1}L_{t10}}{k_{bi}L_{i0}}\tfrac{L_i^2}{L_{t1}^2}dL_{t1}, \\ dL_{tj} &= \tfrac{k_{t1}L_{t10}}{k_{tj}L_{tj0}}\tfrac{L_{tj}^2}{L_{t1}^2}dL_{t1}. \end{aligned} \tag{C.9}$$

From the geometry of the structure,

$$\begin{aligned} L_0^2 &= 4L_1^2 - L_{t1}^2 \\ &= 4\left(4L_2^2 - L_{t2}^2\right) - L_{t1}^2 \\ &= \ldots \\ &= 4^i L_i^2 - \textstyle\sum_{j=1}^{i} 4^{j-1} L_{tj}^2. \end{aligned} \tag{C.10}$$

Taking the infinitesimal of (C.10), noting that L_i is length of bars, yields

$$dL_0 = 4^i \frac{L_i}{L_0}dL_i - \frac{1}{L_0}\sum_{j=1}^{i} 4^{j-1} L_{tj}dL_{tj}. \tag{C.11}$$

Combining the (C.11) with (C.9) yields

$$\frac{dL_0}{dL_{t1}} = -\frac{k_{t1}L_{t10}}{L_0 L_{t1}^2}\left(4^i\frac{L_i^3}{k_{bi}L_{i0}} + \sum_{j=1}^{i} 4^{j-1}\frac{L_{tj}^3}{k_{tj}L_{tj0}}\right). \tag{C.12}$$

From (C.5), it is natural to choose F in term of the tension in the 1-st iteration, i.e.

$$F = t_1\frac{L_0}{L_{t1}} = k_{t1}\left(1 - \frac{L_{t10}}{L_{t1}}\right)L_0.$$

The derivative of F w.r.t. L_0 yields

$$\frac{dF}{dL_0} = k_{t1}\left(1 - \frac{L_{t10}}{L_{t1}}\right) + k_{t1}L_0\frac{L_{t10}}{L_{t1}^2}\frac{dL_{t1}}{dL_0}. \tag{C.13}$$

With (C.12), the stiffness of $C4T1^i$ will be

$$\begin{aligned} K_i &= -\frac{dF}{dL_0} = k_{t1}\left(\frac{L_{t10}}{L_{t1}} - 1\right) + L_0^2\left(4^i\frac{L_i^3}{k_{bi}L_{i0}} + \sum_{j=1}^{i} 4^{j-1}\frac{L_{tj}^3}{k_{tj}L_{tj0}}\right)^{-1} \\ &= k_{t1}\left\{\left(\frac{L_{t10}}{L_{t1}} - 1\right) + \left[4^i\frac{k_{t1}}{k_{bi}}\frac{L_i}{L_{i0}}\left(\frac{L_i}{L_0}\right)^2 + \sum_{j=1}^{i} 4^{j-1}\frac{k_{t1}}{k_{tj}}\frac{L_{tj}}{L_{tj0}}\left(\frac{L_{tj}}{L_0}\right)^2\right]^{-1}\right\}. \end{aligned} \tag{C.14}$$

C.2 Some Mathematical Relations in Buckling Design

In the strength preserving design, the $C4T1^i$ system is designed to buckle at the same load as the original bar $C4T1^0$. The angles δ_j where $j = 1, 2, ..., i-1, i$ are free variables to to be specified to fix the geometry. Therefore, it is important to find out all the lengths, ratio quantities in terms of these angles.

C.2.1 Length of Structure and Strings

From the geometry of the structure, it can be shown that

$$\begin{aligned} L_0 &= L_i \prod_{s=1}^{i} 2\cos\delta_s, \\ L_{tj} &= 2L_i \sin\delta_j \prod_{s=j+1}^{i} 2\cos\delta_s. \end{aligned} \tag{C.15}$$

C.2.2 Computing the Stiffness Ratio of Strings, $\frac{k_{ts}}{k_{tj}}$ for $s, j = 1, 2, 3, ..., i-1, i$

Consider the ratio

$$\begin{aligned} \frac{k_{t(j+1)}}{k_{tj}} &= \frac{E_{t(j+1)}A_{t(j+1)}}{L_{t(j+1)}} \frac{L_{tj}}{E_{tj}A_{tj}} \\ &= \frac{E_{t(j+1)}}{E_{tj}} \left(\frac{\pi r_{t(j+1)}^2}{\pi r_{tj}^2}\right) \left(\frac{L_{tj}}{L_{t(j+1)}}\right). \end{aligned}$$

From (3.44)

$$\frac{k_{t(j+1)}}{k_{tj}} = \frac{E_{t(j+1)}}{E_{tj}} \left(\frac{\sigma_{tj} t_{j+1}}{\sigma_{t(j+1)} t_j}\right) \left(\frac{L_{tj}}{L_{t(j+1)}}\right).$$

With (C.2) and (C.15), the ratio can be simplified to

$$\frac{k_{t(j+1)}}{k_{tj}} = \frac{E_{t(j+1)}}{E_{tj}} \left(\frac{\sigma_{tj}}{\sigma_{t(j+1)}}\right).$$

From this,

$$\frac{k_{ts}}{k_{tj}} = \frac{E_{ts}\sigma_{tj}}{E_{tj}\sigma_{ts}}. \tag{C.16}$$

In particular, if $E_{tj} = E_t$ and $\sigma_{tj} = \sigma_t$, then

$$\frac{k_{ts}}{k_{tj}} = 1. \tag{C.17}$$

So, in the strength preserving design, if the same material is used, then all strings have the same stiffness.

C.2.3 Computing the Stiffness Ratio of String to bar, $\frac{k_{tj}}{k_{bi}}$ where $j = 1, 2, ..., i-1, i$

The stiffness of bar and strings are defined by

$$k = \frac{EA}{L},$$

where E is the Young's modulus, A is the cross section area and L is the length of bar or strings at the buckling load. With this definition and (C.16),

$$\begin{aligned}\frac{k_{tj}}{k_{bi}} &= \frac{k_{tj}}{k_{ti}}\frac{k_{ti}}{k_{bi}} = \frac{E_{tj}\sigma_{ti}}{E_{ti}\sigma_{tj}}\frac{E_{ti}\pi r_{ti}^2}{L_{ti}}\frac{L_i}{E_i\pi r_i^2} \\ &= \frac{E_{tj}\sigma_{ti}}{E_i\sigma_{tj}}\left(\frac{1}{L_{ti}L_i}\right)\frac{L_i^2}{r_i^2}r_{ti}^2.\end{aligned}$$

From (3.41), (3.44) and (C.15),

$$\begin{aligned}\frac{k_{tj}}{k_{bi}} &= \frac{E_{tj}\sigma_{ti}}{E_i\sigma_{tj}}\left(\frac{t_i}{\pi\sigma_{ti}}\right)\left(\frac{4l_i^2}{2L_i^2\sin\delta_i}\right) \\ &= \frac{E_{tj}\sigma_{ti}}{E_i\sigma_{tj}}\left(\frac{2F\sin\delta_i}{\pi\sigma_{ti}\prod_{s=1}^{i}2\cos\delta_s}\right)\left(\frac{2}{L_i^2\sin\delta_i}\right)\left(\frac{E_i}{E_0}\right)^{\frac{1}{2}}\left(\frac{1}{\prod_{p=1}^{i}2\cos\delta_p}\right)^{\frac{1}{2}}l_0^2.\end{aligned}$$

Substitute F from (3.1) into the above equation to obtain

$$\frac{k_{tj}}{k_{bi}} = \frac{E_{tj}\pi}{4\sigma_{tj}l_0^2}\sqrt{\frac{E_0}{E_i}}\left(\prod_{s=1}^{i}2\cos\delta_s\right)^{\frac{1}{2}}. \tag{C.18}$$

If $E_0 = E_i$, (C.18) reduces to

$$\frac{k_{tj}}{k_{bi}} = \frac{E_{tj}\pi}{4\sigma_{tj}l_0^2}\left(\prod_{s=1}^{i}2\cos\delta_s\right)^{\frac{1}{2}}. \tag{C.19}$$

C.2.4 Computing the Rest Length to Length Ratio of Strings, $\frac{L_{tj0}}{L_{tj}}$

The tension in the strings is given by

$$\begin{aligned}t_j &= k_{tj}\left(L_{tj} - L_{tj0}\right), \\ t_j &= \frac{E_{tj}\pi r_{tj}^2}{L_{tj}}\left(L_{tj} - L_{tj0}\right).\end{aligned}$$

From (3.44),

$$t_j = \frac{E_{tj} t_j}{L_{tj} \sigma_{tj}} \left(L_{tj} - L_{tj0} \right).$$

So,

$$\frac{L_{tj0}}{L_{tj}} = 1 - \frac{\sigma_{tj}}{E_{tj}}. \tag{C.20}$$

C.2.5 Computing the Rest Length to Length Ratio of Bars $\frac{L_{i0}}{L_i}$

From (C.6),

$$\frac{F_i}{L_i} = \frac{t_1}{L_{t1}}$$

Hence,

$$k_{bi} \left(\frac{L_{i0}}{L_i} - 1 \right) = k_{t1} \left(1 - \frac{L_{t10}}{L_{t1}} \right)$$

leading to

$$\frac{L_{i0}}{L_i} = 1 + \frac{k_{t1}}{k_{bi}} \left(1 - \frac{L_{t10}}{L_{t1}} \right). \tag{C.21}$$

Using (C.20) and (C.21) reduces to

$$\frac{L_{i0}}{L_i} = 1 + \frac{k_{t1}}{k_{bi}} \frac{\sigma_{t1}}{E_{t1}}. \tag{C.22}$$

C.2.6 Computing the String Stiffness, k_{t1}

Recall that the string stiffness is given by

$$k_{t1} = \frac{E_{t1} \pi r_{t1}^2}{L_{t1}}.$$

Using (3.1), (3.43) and (3.44), the string stiffness becomes

$$\begin{aligned} k_{t1} &= \frac{E_{t1}}{L_{t1}} \frac{t_1}{\sigma_{t1}} \\ &= \frac{E_{t1}}{\sigma_{t1}} \frac{F \tan \delta_1}{L_0 \tan \delta_1} \\ &= \frac{E_{t1}}{\sigma_{t1}} \frac{E_0 \pi^2 r_0^4}{L_0^3} \\ &= \frac{E_0 E_{t1} \pi^2 L_0}{16 \sigma_{t1} l_0^4}. \end{aligned} \tag{C.23}$$

References

[1] K. Snelson. Continuous tension, discontinous compression structures. *U.S. Patent 3,169,611*, 1965.

[2] R. Buckminister Fuller. *Tensile–integrity structures.* US Patent, 3,063,521, 1962.

[3] R. Adhikari, R. E. Skelton, and W. J. Helton. *Mechanics of Tensegrity Beams.* UCSD, Structural System and Control Lab., Report No. 1998–1, 1998.

[4] D. M. Campbell, D. Chen, P. A. Gossen, and K. P. Hamilton. *Effects of spatial triangulation on the behavior of "Tensegrity" domes*, pages 652–663. IASS–ASCE International Symposium, Apr. 24∼28, Atlanta, GA, USA, 1994.

[5] R. Chu. Tensegrity. *Journal of Synergetics*, 2(1), 1988.

[6] M. F. Coughlin and D. Stamenović. A tensegrity structure with buckling compression elements: Application to cell mechanics. *Trans. of ASME, Journal of Applied Mechanics*, 64:480–486, 1997.

[7] D. E. Ingber. Tensegrity: The architectural basis of cellular mechanotransduction. *Annual Review of Physiology*, 59:575–599, 1997.

[8] I. J. Oppenheim and W. J. Williams. Tensegrity prisms as adaptive structures. *ASME Annual meeting, Dallas, Nov. 1997*, 1997.

[9] A. Pugh. *An Introduction to Tensegrity.* University of California Press, Berkeley, 1976.

[10] R. Motro, N. Vassart, and Chercheur. *Form finding numerical methods for tensegrity systems*, pages 706–713. IASS–ASCE International Symposium, Apr. 24∼28, Atlanta, GA, USA, 1994.

[11] H. Furuya. Concept of deployable tensegrity structures in space applications. *International Journal of Space Structures*, 7(2):143–151, 1992.

[12] S. Pellegrino. Analysis of prestressed mechanisms. *International Journal of Solids and Structures*, 26 (12):1329–1350, 1989.

[13] S. Pellegrino. A class of tensegrity domes. *International Journal of Space Structures*, 7 (2), 1992.

[14] A. Hanaor. Double-layer tensegrity grids as deployable structures. *International Journal of Space Structures*, 8, 1992.

[15] S. Pellegrino. Foldable bar structures. *International Journal of Solids and Structures*, 34 (15):1825–1847, 1996.

[16] D. Williamson and R.E. Skelton. A general class of tensegrity systems: Equilibrium analysis. In *Engineering Mechanics for the 21st Century, ASCE Conference*, La Jolla, 1998.

[17] R.E. Skelton, J.P. Pinaud, and D.L. Mingori. Dynamics of the shell class of tensegrity structures. *Journal of the Franklin Institute.*, 338/2-3:255–320, 2001.

[18] H. Murakami and Y. Nishimura. Static and dynamic characterization of regular truncated icosahedral and dodecahedral tensegrity modules. *to appear in International Journal of Solids and Structures.*, 2001.

[19] B. de Jager and R.E. Skelton. Optimizing stiffness properties of tensegrity structures. In *Proceedings of International Mechanical Engineering Congress and Exposition 2001*, volume 3330, New York, 2001.

[20] C. Sultan. *Modeling, design, and control of tensegrity structures with applications.* Ph.D. Dissertation, Purdue University, School of Aeronautics and Astronautics, West Lafayette, 1999.

[21] C. Sultan, M. Corless, and R.E. Skelton. The prestressability problem of tensegrity structures. some analytical solutions. *to appear in International Jounal of Solids and Structures*, 2001.

[22] C. Sultan, M. Corless, and R.E. Skelton. Tensegrity flight simulator. *Journal of Guidance, Control, and Dynamics*, 23(6):1055–1064, 2000.

[23] C. Sultan, M. Corless, and R.E. Skelton. Linear dynamics of tensegrity structures. *to appear in Engineering Structures*, 2001.

[24] C. Sultan, M. Corless, and R.E. Skelton. Symmetrical reconfiguration of tensegrity structures. *to appear in International Journal of Solids and Structures*, 2001.

[25] L. Caviglione. Modellazione statica e dinamica di una tensegrity nell'ambito di una strategia di controllo attivo. *Laurea Thesis, School of Engineering of the University of Genoa*, 1999.

[26] M. Pedretti. Smart tensegrity structures for the swiss expo. In *Smart Structures and Materials*, volume 3330, San Diego, 1998.

[27] L. Caviglione, Andrea Del Grosso, and Mauro Pedretti. Stabilisation and control of large tensegrity structures. *private communication.*

[28] A.G.M. Michell. The limits of economy in frame structures. *Philosophical Magazine*, 8:589–597, 1904.

[29] M. P. Bendsoe and N. Kikuchi. Generating optimal topologies in structural design using a homozenization method. *Computer Methods in Applied Mechanics and Engineering*, 71:197–224, 1988.

[30] F. Jarre, M. Kocvara, and Zowe J. Optimal truss design by interior-point methods. *SIAM Journal on Optimization*, 8(4):1084–1107, 1998.

[31] J. Lu and R.E. Skelton. Optimal hybrid control for structures. *Computer-Aided Civil and Infrastructure Engineering*, 13:405–414, 1998.

[32] A. H. Simmons, C. A. Michal, and L. W. Jelinski. Molecular orientation and two–component nature of the crystalline fraction of dragline silk. *Science*, 271:84–87, 1996.

[33] Y. Termonia. Molecular modeling of spider silk elasticity. *Macromolecules*, 27:7378–7381, 94.

[34] D. E. Ingber. Architecture of life. *Scientific American*, January:48–57, 1998.

[35] D. E. Ingber. Cellular tensegrity: Defining new rules of biological design that govern the cytoskeleton. *Journal of Cell Science*, 104(3):613–627, 1993.

[36] R. E. Skelton. *Dynamic Systems Control – Linear Systems Analysis and Synthesis*. John Wiley & Sons, 1988.

[37] S. Pellegrino and C.R. Calladine. Matrix analysis of statistically and kinematically indeterminate frameworks. *International Journal of Solids and Structures*, 22(4):409–428, 1985.